MIXING OF LIQUIDS IN LARGE TANKS

A Thesis Submitted for the Degree of Doctor of Philosophy to the Chemical Engineering Department of the University of Aston in Birmingham by Keith Gilbert Doyle.

January 1974.

Summary

A 1.2 m diameter tank has been used to model the mixing process in large storage tanks equipped with side-entry mixers. Terminal mixing times have been measured as a function of impeller speed, impeller diameter, liquid depth and impeller angle. It is shown that the indicator method for measuring mixing times yields results which are dependent upon the molecular diffusivity of the materials employed. A mathematical model is presented which accounts for this effect, and some of its predictions have been tested using a 70 mm diameter tank. It is shown that the conductivity method for measuring mixing times gives results which can be used for scale-up using the rule $NTD^2/T^2 = \text{const.}$, and this has been tested on a 31 m diameter tank. Measurements have also been made of fluid velocities using a hot film anemometer, and these are shown to be consistent with a simple boundary layer theory.

Contents

List of Figures

List of Tables

Acknowledgements

This work was sponsored by the British Petroleum Company Ltd., and supported by a Science Research Council industrial studentship. I should like to thank the staff at Britannic House, the B.P. Research Centre, and Grangemouth and Llandarcy Refineries who gave advice and assistance, particularly Mr. R. Turner, research coordinator, for his constant support and invaluable administrative work. My thanks are also due to the academic and technical staff and postgraduate students of the University of Aston Chemical Engineering Department for their generous help, and above all to my supervisor, Professor G. V. Jeffreys for his continual encouragement and assistance.

1. Introduction

The object of this work is to study the feasibility of using hydrodynamic modelling to provide information about the effectiveness of mixers in storage tanks, with particular reference to the very large storage tanks used in the petroleum industry. These range in size up to 88m diameter by 20m high, and are normally fitted with from one to four side-entry propeller mixers mounted horizontally about 1m above the base. These mixers are used for blending materials from different sources to ensure that dip samples are fully representative of the material in the tank, before sale or processing, and in the case of crude oil storage tanks they are also used to disperse sludge, which would otherwise collect on the floor of the tank reducing its capacity. Very little is known concerning the length of time for which these mixers must be run to achieve the desired effect, and it is likely that considerable amounts of power are wasted by running them for longer than necessary. There is, moreover, no satisfactory design basis for new types of mixing systems, resulting in a reluctance to try other, possibly more efficient, systems. Although some tests have been carried out on full-scale tanks (1,2), experimentation on this

scale is subject to considerable restriction on the experimental methods available. Measurements are consequently exceedingly time-consuming and can generally be carried out only when suitable conditions occur during normal production. Changes to the mixing system can be made only at considerable expense, and with possible loss of production, and their effect is difficult to estimate since the fluctuating material properties introduce further uncertainties. It is therefore advantageous to use a hydrodynamic model to study the effect of such changes under controlled conditions, provided that suitable scaling laws can be obtained to enable the results to be transferred to the full scale. This has the advantages that large numbers of measurements can be made in a relatively short time, the system can be modified quickly and easily, and the use of transparent material for the model tank allows the flow pattern and the progress of the mixing process to be observed visually using dyes, as well as being monitored by instruments. The use of water as the working fluid allows a much wider variety of experimental techniques to be used, and contaminated material can be discarded after the measurements have been carried out.

The scale-up factor from a laboratory model to a

full-size tank is considerable, amounting to a factor of up to 74:1 in the linear dimensions, corresponding to 4×10^5:1 in the volume, and consequently it is necessary to determine the scale-up rules to a good degree of accuracy if the results are to be applied over this range. The majority of this work is therefore concerned with determining the correct scaling law for terminal mixing, which has been tested by comparison of the model results with those obtained from a tank 25 times larger in linear dimensions. Some measurements have also been made of the flow velocity in the boundary layer on the floor of the tank in which sludge tends to accumulate.

2. Literature Survey

2.1. Introduction

This survey of existing literature on fluid mixing is intended to cover experimental and theoretical work aimed at providing a means of predicting the mixing efficiency and the flow pattern in a batch operated stirred tank. It is not limited to any specific agitator geometry, since it seems probable that similar general principles will apply to all systems. Experimental work on the power consumption of impellers is not included since no power measurements have been carried out in the present study. This aspect has been well reviewed by Voncken (3).

2.2. Mixing Time Measurements

2.2.1. Experimental Methods

The first systematic measurements of mixing times in a stirred tank were carried out by Wood, Whittemore & Badger (4). They used a paddle stirrer in a wooden tank, drawing off samples through a set of conductivity cells, and monitoring the change in conductivity as a

solution of sodium chloride was blended into the water in the tank. The conductivity cells were connected in series, with the result that there was considerable interaction between them, making it difficult to define the terminal mixing time unambiguously. The authors in fact determined terminal mixing times by a graphical method which allows considerable latitude, so that their results cannot be regarded as very reliable. The conductivity method was subsequently used by Fossett & Prosser (5) to study mixing by jets, and by Kramers, Baars & Knoll (6) for propellers and turbines in both baffled and unbaffled tanks. These authors used conductivity cells placed in the tank, thereby eliminating any lag in the sampling tubes.

In the thermal impulse method, used by Gluz & Pavluschenko (7), the electrolyte is replaced by a small quantity of warm liquid, and the conductivity cells by thermocouples. This has the advantage that the method can be used in liquids of very high or very low conductivity, and does not require contamination of the system. The results, however, are rather dubious since they may be affected by both thermal conduction and convection. A similar method was used by Oldshue, Hirschland & Gretton (8) to measure mixing times in tanks up to 6m in diameter.

In this case, the warm liquid was placed as a layer above the cold, to simulate the blending of two different liquids.

In systems where continuous monitoring is not possible, it is necessary to take samples for subsequent analysis of, for example, density (Rushton (1)). This method can be used in systems where any other measurement would be impractical, but is extremely tedious as a very large number of samples must be taken and analysed to achieve reasonable accuracy.

All these methods have the disadvantage that concentrations are measured only over one or two small volumes, so that there is a tendency to underestimate the mixing time. The position of the regions measured is also rather critical in those cases where stagnant regions are formed. These objections can be overcome by methods in which the whole tank is observed visually, at the cost of changing from an objective measurement of conductivity to a rather more subjective estimate of the moment when terminal mixing has occurred. The simplest such method is to add a dye solution and estimate when the colour is uniform. This method was introduced by Macdonald & Piret (9) and has been used mainly with highly viscous materials, where it has the advantage

of giving a good picture of the flow pattern (Gray (10)). However it is incapable of detecting stagnant regions, and the times measured depend greatly on the visual acuity of the observer, so it should not be regarded as a valid means of measuring mixing times.

An improvement on the dye method is the decolorisation method originated by Stead, Page & Denbigh (11) in which the tank is filled with a coloured solution which is then decolorised by the tracer material. Fox & Gex (12) used an alkaline solution of phenolphthalein, decolorised by the addition of a small amount of acid, and this method has since been widely used. The method has been criticised by Landau & Prochazka (13) on the grounds that reaction times for some indicators are of the order of minutes. The reference they cite (Tomicek (14)), however, appears to apply only to dried indicators on indicator papers. Rice, Toor & Manning (15) have shown that reaction times for phenolphthalein are of the order of a millisecond or less. The criticism may well apply, though, to starch-iodine-thiosulphate systems as used by Nagata, Yokoyama & Yamagimoto (16), where iodine bound to colloidal starch particles may react more slowly. The decolorisation method does have the disadvantage that, since mixing must be completed down

to the molecular level, the results may depend on the diffusivities of the materials involved. This possibility was ignored by Fox & Gex (12), but Sykes & Gomez-plata (17) suggested corrections to be applied to results obtained in this way, and applied them to the data of Norwood & Metzner (18).

Another method relying on visual observation of the whole tank is the Schlieren method originated by Dodd(19), and used by Van de Vusse (20) in an extensive study on the mixing of fluids of different densities. In this method, a Schlieren image of the tank is produced in the usual way, and liquids of differing refractive indices are used, so that striations appear on the image. The terminal mixing time is defined as the time elapsing between the moment the stirrer starts mixing and the moment of disappearance of the striations. This method suffers from the same disadvantages as the indicator method in that it requires a subjective visual judgement, and that the results may depend on the diffusivities of the materials involved. It also requires an elaborate optical set-up with the mixing vessel contained in an outer vessel with plane-parallel walls.

The repeatability of all these methods is similar, the standard error in a single reading being about 15%.

This suggests that the variation in measurements of mixing time for a given set of parameters arises from the nature of the mixing mechanism rather than of the experimental method used.

2.2.2. Results

The first set of mixing time measurements in which several factors were varied independently were obtained by Kramers, Baars & Knoll (6) using the conductivity method. They found that mixing time varied inversely with the impeller speed for all the systems they studied. The influences of different impeller types and locations and of baffling were also studied but it was not found possible to summarize these results in a general correlation.

Van de Vusse (20) attempted to produce a general correlation for systems with liquids of different density. Although he lists six dimensionless groups to be correlated, these are lumped together into a Reynolds number, ND^2/ν, a dimensionless mixing time $\tau ND^3/T^2Y$, a modified Froude number $\rho^2 N^2 D/\Delta\rho gY$, and a geometrical group $D^3/T^{2.5}Y^{0.5}$. In determining the group for the dimensionless mixing time it is assumed that mixing is governed by the pumping capacity of the impeller, whereas in the modified Froude

number it is the dynamic head that is considered important. No justification is given for the last grouping which was presumably determined empirically. The correlation given for large Reynolds numbers is

$$\frac{\tau N D^3}{T^3} \propto \left(\frac{\rho N^2 D^2}{\Delta\rho\, gY}\right)^{-0.3}$$

which implies that for $\Delta\rho=0$ the mixing time becomes zero. This correlation is therefore evidently unsuitable for liquids of equal density.

The next attempt at a general correlation is that of Fox & Gex (12), using the indicator method to measure mixing times for both jets and propellers. They assumed in their dimensional analysis that the dimensionless mixing time was a function of Reynolds and Froude numbers only, ignoring the effect of Schmidt number. This gave the results $Ho \propto Re^{-1/6} Fr^{1/6} (Y/T)^{1/2}$ for high Reynolds numbers ($>10^4$) and $Ho \propto Re^{-1} Fr^{1/6} (Y/T)^{1/2}$ for $10^3 < Re < 10^4$. Similar results were obtained for jet mixing.

These results show several interesting features. It is seen that there are two distinct regimes termed "incipient laminar" and "turbulent" in which the effect of Reynolds number is respectively large, and unimportant. The scaling law for different impeller sizes is found to be such that the

quantity ND^2 determines the mixing capacity of the impeller, rather than ND^3 as assumed by Van de Vusse (20). The apparent dependence of the mixing times on the gravitational field appears curious, since the tracer is of the same density as the bulk liquid. The authors do not comment on this, but the inclusion of g in the dimensional parameters is justified by Norwood & Metzner (18) on the grounds that vortexing can change the shape of the liquid and therefore the flow pattern. Their conclusions, using the same method, are very similar to those of Fox & Gex (12) but their correlation for turbines indicates that the mixing capacity for these is determined by the quantity $ND^{2.75}$ rather than ND^2.

Landau & Prochazka (21) measured mixing times for propellers, paddles and turbines in the turbulent regime using the conductivity method. Like Kramers, Baars & Knoll (6) they found $\tau \propto N^{-1}$, and found the mixing capacity to depend on $ND^{2.05}$ for propellers, $ND^{2.20}$ for inclined-blade paddles, and $ND^{2.57}$ for turbines, in quite good agreement with the results mentioned above. They also introduced a "degree of homogeneity" determined from a number of concentration measurements, and correlated the mixing time with this.

Marr & Johnson (22) carried out a series of measurements on a batch stirred tank as a special case of a

continuous flow stirred tank. Although they did not carry out sufficient measurements to enable any useful conclusions to be drawn regarding scaling rules, they did show that the curve of mixing time against liquid depth can change rapidly, with apparent discontinuities. They were unable to account for these changes except in a general way, as being due to a change in the flow pattern.

Further non-linear effects were found by Landau et al. (23) for mixing times at rather low Reynolds numbers (300 -2000). The mixing times here varied with the position of measurement, the position of tracer addition, and the density of the tracer. These results emphasise that the effect of changing geometry is complex and unpredictable, so that it is necessary to model any particular physical arrangement.

Various later papers (Gray (10) , Hoogendoorn & den Hartog (24) and Moo-Young et al. (25)) are concerned with different impeller types, particularly for use at low Reynolds numbers, but throw little light on the correct scale-up rules.

2.2.3. Theory

There is no theory of single phase blending capable of making any predictions beyond those obtained from

simple dimensional considerations. Corrsin (26) presented an idealised theory based on the assumption of local isotropy, using approximate relationships for the Taylor microscale of turbulence and for a corresponding scale of mixing. This theory leads to the conclusion that the concentration fluctuations decrease exponentially with time, at a rate which is independent of the molecular diffusivity.

A similar theory was used by Sykes & Gomezplata (17) to estimate the effect of molecular diffusivity on mixing times, but the time they calculated for diffusion to occur is small compared with the measured mixing time.

The principle drawback to this approach arises from the necessary assumption of locally isotropic turbulence, in which the rate of homogenation depends only upon the rate of dissipation of energy, ε, in the region concerned. It has been shown experimentally (27) that for a stirred tank, ε is distributed in a highly non-uniform way, falling off rapidly away from the impeller. Any fluid element will therefore be carried through regions of varying ε, so that a knowledge both of the distribution of ε and of the large-scale flow pattern is necessary. The treatments mentioned evade this problem by assuming that ε is constant throughout the tank. This

over-simplification leads to the conclusion that scale-up can be carried out on the basis of equal power per unit volume, giving a scaling law for impeller diameter which is in disagreement with experiment (28).

Landau & Prochazka (21) presented a model of the mixing process based on the concept of an eddy diffusivity applied to an idealised system. They introduced a degree of homogeneity $\overline{X}$ defined by

$$\overline{X} = \frac{1}{V}\int_T \left|\frac{C - C_F}{C_F - C_I}\right| dV$$

where C is the tracer concentration having initial and final values C_I and C_F. According to their theory, $\overline{X}$ should decrease exponentially from an initial value , $\overline{X}_o$ of 2.09. This result is confirmed by experiment, but cannot be regarded as evidence of the correctness of the model since the value of $\overline{X}_o$ is implicit in the definition of $\overline{X}$. Thus for a tracer of volume V_T and concentration C_T

$$\overline{X}_o = \frac{1}{V}\left(\left|\frac{C_I - C_F}{C_F - C_I}\right| V + \left|\frac{C_T - C_F}{C_F - C_I}\right| V_T\right)$$

and from mass conservation

$$C_I V + C_T V_T = C_F(V + V_T)$$

so $$(C_T - C_F)V_T = (C_F - C_I)V$$

Hence $$\overline{X}_o = 2$$

Another approach to the treatment of mixing is consideration of the physical deformation of the surface surrounding the tracer material by the flow field. This was considered by Batchelor (29) and Reid (30) who concluded that material lines and surfaces in isotropic turbulence would be extended exponentially with time. Rosenhouse (31) attempted to verify this conclusion, by observing the behaviour of a stream of fluorescent dye in turbulent pipe flow, using an optical probe. The data, however, are not sufficiently extensive to distinguish between exponential and linear extension. Corrsin (32) showed how the scale of concentration fluctuations could be related to the interfacial area per unit volume.

2.3. Flow Patterns and Turbulence Measurements

2.3.1. Experimental Methods

In the absence of a complete theory for turbulent flow processes, it is necessary to determine the flow patterns and turbulence parameters for a stirred tank empirically. The earliest studies were carried out by Sachs & Rushton (33) using the 'streak' method. This relies upon photography of small particles in the tank using an exposure time sufficient to show each particle

as a streak of light on the photograph. Providing the particles are small enough, so that they follow the movement of the fluid exactly, the trace of each particle provides an indication of the velocity of the fluid at that point. The method was later modified by Schwartzberg & Treybal (34) who used a strobe lamp so that each trace was a series of dots, to allow more accurate measurement of velocities. The method has the advantage that no specialised equipment is required, and interference with the flow is minimal, but it is extremely tedious, requiring the measurement of many thousands of traces for an even moderate spatial resolution.

Aiba (35) measured flow rates with an apparatus in which the deflection of a steel sphere suspended by a wire was determined using a Geiger counter to monitor the intensity of radiation from a radio-isotope placed in the sphere. The Geiger tube, which was immersed in the liquid, was large enough to produce disturbance of the flow, at least in the vicinity of the sphere, and it is not clear why this equipment was preferred to measurement of the deflection directly by means of a protractor or a cathetometer; these were in any case used to determine the flow direction and thelocation of the sphere in the tank. The results are presented as radial, tangential

and vertical velocity components, although the apparatus described does not appear to be capable of measuring vertical velocities, and no information is given on how these were determined.

Various forms of pressure-measuring tubes have been used for the measurement of fluid velocities. Rao & Brodkey (36) point out that the simple type of Pitot tube such as that used by Kim & Manning (37) gives incorrect results if used in turbulent flows, but more elaborate probes such as the three-hole probe used by Fort et al. (38) or the five-hole type used by Blasinski & Tyczkowski (39) seem capable of providing good results. Limitations on the speed of differential pressure measurement make it impossible to measure turbulence levels with these probes, and it is uncertain whether the results obtained represent a true mean velocity at high turbulence levels, since this requires that the turbulent velocity fluctuations should be normally distributed, which has been shown by Mujumdar (40) to be a poor assumption for the region near the impeller.

The most detailed information on velocity distributions has been obtained by means of various forms of heated probes, in which the rate of loss of heat from the probe provides a measurement of the fluid velocity.

These probes require individual calibration, but are capable of sufficiently fast response to measure the most rapid turbulent fluctuations with an accuracy of around 1%. The earliest measurements were made with the thermistor probe, developed by Norwood & Metzner (18), which was subsequently displaced by the hot wire anemometer used by Bowers (41) and Mujumdar et al. (40), and in the most recent form, the hot film anemometer used by Rao & Brodkey (36). The probes are only a few millimetres in diameter, so that they produce little disturbance of the flow, and the principal source of error appears to be the requirement for accurate alignment with the flow. Rao & Brodkey (36) recommend the use of an auxiliary Pitot tube for this purpose, the hot film being used to measure only the magnitude of the flow.

2.3.2. Impeller Pumping Capacities

The earliest measurements of velocities in stirred tanks were made in order to determine the impeller pumping capacity, defined as the total flux of liquid through the impeller. This was measured by Rushton, Mack & Everett (42) in a system in which the impeller pumped water over a weir, and the volume of water pumped was measured directly.

Since the geometry differed considerably from that of a simple stirred tank the results cannot be regarded as valid for this situation. Sachs & Rushton (33) measured velocities in the discharge stream from a turbine by the streak method, and found these to be proportional to impeller speed, but since they did not vary the impeller diameter they could not provide a general expression for the pumping capacity. Norwood & Metzner (18) measured the total flow rate by integrating the velocity across the impeller discharge stream, and obtained the result

$$Q = 9.0 \times 10^{-4} N D^{2.2} w \nu^{-0.5} (1-q^2)^{0.5}$$

where q is the ratio of fluid velocity to impeller velocity at the blade tip. They state that the term $(1-q^2)^{0.5}$ was found to be negligibly different from unity under almost all conditions. As it stands, the correlation is dimensionally inconsistent, though it could possibly be made consistent over a limited range of Reynolds numbers by treating q as a function of D and ν.

All subsequent work has shown that the pumping capacity is independent of both ν and T, so that dimensional considerations require

$$Q = KND^3$$

and measurements of pumping capacity can be expressed solely in terms of K. This parameter has been measured

for various impellers by integrating velocities obtained by streak photography (Fort (43)), Pitot tube (Blasinski & Tyczkowski (39)), and hot film anemometry (Rao & Brodkey (36)). K has also been estimated by a method devised by Porcelli & Marr (44) in which a single tracer particle of neutral buoyancy is used, and the frequency with which the particle passes through the impeller is measured by visual observation. Fort (43) has shown that the results obtained in this way agree well with those obtained by more complex methods, although the spread in measured values is rather greater.

2.3.3. Flow Patterns

The next step in determining the total flow pattern in the tank is concerned with the behaviour of the discharge stream from the impeller. Sachs & Rushton (33) showed that the stream broadens out and entrains liquid from the surrounding region, with a resultant decrease in radial velocity. The variation in radial velocity with distance was studied for a wide range of impeller diameters by Blasinski & Tyczkowski (39). There do not appear to be any published data on flow and entrainment from propeller mixers, but it seems likely that this will follow the same law as that for jets determined by

Folsom & Ferguson (45).

The complete flow pattern at all points in the tank is likely to be peculiar to the particular geometrical configuration studied. It has been measured for a turbine-stirred, unbaffled tank by Nagata et al. (46), and by Fort (38) for a baffled tank in the region below the impeller only. Schwartzberg & Treybal (34) showed that in a region remote from the impeller in a baffled tank the fluid velocity is proportional to ND^2, rather than to ND as is the case in the impeller stream. This result was confirmed by Holmes, Voncken & Dekker (47), who measured circulation times for a slug of tracer material.

2.3.4. Turbulence Parameters

Although the mean velocities measured in the work mentioned above govern the bulk transfer of material around the tank, the later stages of mixing will be governed by the smaller scale details of the flow, and particularly by the spectrum of the turbulence in the tank. This was first studied indirectly by Manning & Wilhelm (48) who used a small conductivity probe to measure concentration fluctuations in an electrolyte tracer, on the assumption that the spectrum obtained

would be similar to the velocity spectrum. The spectra had slopes of around -5/3, corresponding to the Kolmogoroff inertial-convective subrange, and showed peaks at the impeller blade frequency. Concentration microscales were also measured and found to be larger than expected- around 10 mm. This was attributed to lack of resolution and bandwidth in the probe system, although the equipment appears to be capable of detecting fluctuations on a smaller scale than this. More direct measurements of the spectrum were made by Kim & Manning (37) using a probe with a piezoelectric transducer to measure pressure fluctuations, and they confirmed the existence of a region at high wavenumber where the turbulence intensity spectrum has a slope of -5/3. Mujumdar et al. (40) in a study of various turbulence parameters using hot wire anemometry failed to find such a region, probably because of the rather low Reynolds number arising from the use of air as the working fluid. Rao & Brodkey (36), using a similar method in water, found an extensive -5/3 region working at a Reynolds number of 5×10^4.

Attempts to utilise Kolmogoroff's theory of locally isotropic turbulence (49) have given rise to attempts at measuring the distribution of the rate of dissipation of energy, as this is then sufficient to define the

turbulence completely. Cutter (27) found that this quantity, ε, decreases roughly as the cube of the distance from the centre of the impeller on the centreline, and varies by a factor of 270 from the region near the blade tip to that outside the impeller stream. Rao & Brodkey (36) presented their results as a correlation involving the local fluid velocity, giving similar wide variations in ε from one part of the tank to another.

It can be seen from this survey that there are a number of different methods of measuring mixing times, from which different scaling laws have been derived . The different experimental methods, criteria for terminal mixing, and correlations used, make it impossible to compare the results of different studies. Velocity measurements have been used to determine impeller pumping capacities, and flow patterns have been determined for a few systems. No information is available on flow patterns in tanks equipped with side-entry mixers.

3. Theory

3.1. Mixing Times

It will be shown in Section 5.2.1 that mixing time measured by the indicator method is a function of the molecular diffusivity. The identification of a term involving the molecular diffusivity in the correlation for mixing times under fully turbulent conditions is surprising, since all previous theoretical work indicates that such a term should be negligible, as mentioned in Section 2.2.3. There appear to be two doubtful assumptions in this work. The first is that the scale of the concentration fluctuations, in the absence of molecular diffusion, will be of the same order of magnitude as the turbulence microscale given by $(\nu^3/\varepsilon)^{1/4}$ (28). However since the spectrum of the concentrations decreases with slope -5/3, as shown by Batchelor (50), the greatest contribution to the concentration fluctuations will come from the lowest, rather than the highest wavenumber, and it is the turbulence macroscale, rather than the microscale, which must be considered. This macroscale, of the order of the dimensions of the impeller, corresponds to the size of the largest eddies. It is this quantity which was measured by Manning & Wilhelm (48), who found it to be of the order of 10mm for an impeller

diameter of 50mm.

The second assumption is that fluid motion can be neglected in considering the diffusion process. Rice, Toor & Manning (15), calculating concentration scales from measured reaction rates for a diffusion-controlled reaction on this assumption, obtained values of 10^{-5} -10^{-6} mm, 30 times smaller even than the turbulence microscale, as noted by Sykes & Gomezplata (17).

Toor (51) has shown that for a diffusion-controlled bimolecular reaction between materials of equal diffusivities, the situation is analogous to the transport of a single substance without reaction whose concentration C is equal to $C_A - C_B$, where C_A and C_B are the concentrations of the two species. Although the materials used in practice generally have different diffusivities, this simplification will be used, and it can be expected that the results will be substantially the same, with some average value being used for the diffusivity. Reid (30) has shown that a blob of tracer material will be stretched into a ribbon, so that the diffusion will nearly all be in a direction normal to this surface. It is therefore convenient to use a one-dimensional equation, the distance parameter x being measured normal to the surface of such a ribbon in any region of the tank. This is

equivalent to considering diffusion in a stratified medium. For such a stratified medium the concentration C of diffusing material will obey the equation

$$\left(\frac{\partial C}{\partial t}\right)_x = D\left(\frac{\partial^2 C}{\partial x^2}\right)_t - u_x\left(\frac{\partial C}{\partial x}\right)_t$$

where x is the distance normal to the stratified surfaces, and u_x is the component of velocity parallel to the x-direction. For a uniform rate-of-strain tensor, $u_x = kx$, where k is a function of time only.

Making the substitutions

$$x' = x \exp\left(-\int_o^t k\, dt\right)$$

and

$$t' = \int_o^t \exp\left(-2\int_o^t k\, dt\right) dt$$

we have $\left(\frac{\partial C}{\partial x}\right)_t = \left(\frac{\partial C}{\partial x'}\right)_t \left(\frac{\partial x'}{\partial x}\right)_t = \exp\left(-\int_o^t k\, dt\right)\left(\frac{\partial C}{\partial x'}\right)_t$

and $\left(\frac{\partial^2 C}{\partial x^2}\right)_t = \exp\left(-2\int_o^t k\, dt\right)\left(\frac{\partial^2 C}{\partial x'^2}\right)_t$

and also $\left(\frac{\partial C}{\partial t'}\right)_{x'} = \left(\frac{\partial C}{\partial t}\right)_{x'}\left(\frac{\partial t}{\partial t'}\right)_{x'} = \left(\frac{\partial C}{\partial t}\right)_{x'} \exp\left(2\int_o^t k\, dt\right)$

We can now use the identity

$$\left(\frac{\partial C}{\partial t}\right)_x = \left(\frac{\partial C}{\partial t}\right)_{x'} - \left(\frac{\partial C}{\partial x}\right)_t \left(\frac{\partial x}{\partial t}\right)_{x'}$$

$$\left(\frac{\partial C}{\partial t}\right)_x = \exp\left(-2\int_o^t k\, dt\right)\left(\frac{\partial C}{\partial t'}\right)_{x'} - \left(\frac{\partial C}{\partial x}\right)_t . kx$$

Comparing this with the original diffusion equation, we have

$$\exp(-2\int_0^t k\,dt)\left(\frac{\partial C}{\partial t'}\right)_{x'} = \mathcal{D}\left(\frac{\partial^2 C}{\partial x^2}\right)_t = \mathcal{D}\exp(-2\int_0^t k\,dt)\left(\frac{\partial^2 C}{\partial x'^2}\right)_t$$

Since t' is a function of t only,

$$\left(\frac{\partial^2 C}{\partial x'^2}\right)_t = \left(\frac{\partial^2 C}{\partial x'^2}\right)_{t'}$$

So $$\left(\frac{\partial C}{\partial t'}\right)_{x'} = \mathcal{D}\left(\frac{\partial^2 C}{\partial x'^2}\right)_{t'}$$

This is an ordinary diffusion equation whose solutions are known. Since at t=0, $x'=x$ and $t'=0$, the initial conditions are identical to those for the original situation.

The question then arises of the correct form for the function k(t). This governs the rate at which the surfaces of constant concentration move closer together as the surfaces are extended by the flow. Batchelor (29) showed that in homogeneous turbulence, an infinitesimal line segment will grow exponentially, so that by the argument of Corrsin (32), distances in the x-direction will follow a decaying exponential law, such that u_x is proportional to x. This is equivalent to a pure straining motion, so we can write $k=\sigma_{11}$ where this is the component of the rate-of-strain tensor acting in the x-direction, and will be negative.

This gives $$t' = \int_0^t \exp(-2\int_0^t \sigma_{11}\,dt)\,dt$$

$$t' = \int_0^t \exp(-2\sigma_{\parallel} t)\, dt$$
$$= \left[\frac{-1}{2\sigma_{\parallel}} \exp(-2\sigma_{\parallel} t)\right]_0^t$$
$$= \frac{1}{2\sigma_{\parallel}}(1-\exp(-2\sigma_{\parallel} t))$$
$$\exp(-2\sigma_{\parallel} t) = 1-2\sigma_{\parallel} t'$$
$$t = \frac{-1}{2\sigma_{\parallel}} \ln(1-2\sigma_{\parallel} t')$$

It should be noted that since $\sigma_{\parallel}$ is negative, both t and the term in brackets will always be positive. Terminal mixing occurs at $t=\tau$ when the concentration fluctuations have fallen to some arbitrarily defined level, corresponding to the solution of the reduced equation at $t'=\tau'$ For such a solution we have

$$\tau' = k_1/D$$
$$\frac{\partial \tau'}{\partial D} = -k_1/D^2 = -\tau'/D$$
$$\frac{\partial(\ln\tau)}{\partial(\ln D)} = \frac{D}{\tau}\frac{\partial\tau}{\partial D} = \frac{D}{\tau}\frac{\partial\tau'}{\partial D}\frac{\partial\tau}{\partial\tau'} = -\frac{\tau'}{\tau}\frac{\partial\tau}{\partial\tau'}$$

And $$\tau = \frac{-1}{2\sigma_{\parallel}} \ln(1-2\sigma_{\parallel}\tau')$$

So $$\frac{\partial\tau}{\partial\tau'} = \frac{-1}{2\sigma_{\parallel}} \cdot \frac{-2\sigma_{\parallel}}{1-2\sigma_{\parallel}\tau'}$$
$$= \frac{1}{1-2\sigma_{\parallel}\tau'}$$
$$\frac{\partial(\ln\tau)}{\partial(\ln D)} = -\frac{\tau'}{\tau} \cdot \frac{1}{1-2\sigma_{\parallel}\tau'}$$
$$= \frac{1}{2\sigma_{\parallel}}(1-\exp(-2\sigma_{\parallel}\tau)) \cdot -\frac{1}{\tau} \cdot \exp(2\sigma_{\parallel}\tau)$$
$$= \frac{-1}{2\sigma_{\parallel}\tau}(\exp(2\sigma_{\parallel}\tau)-1)$$

Since $\sigma_{\parallel} \sim -N$, $\sigma_{\parallel}\tau \ll 1$, so $\frac{\partial(\ln\tau)}{\partial(\ln D)} \simeq \frac{1}{2\sigma_{\parallel}\tau}$ which is very small ($\sim 10^{-3}$). This implies that the diffusivity has negligible influence on the mixing time, so the original

assumption of homogeneous turbulence appears inadequate to account for the observed dependence. This can be accounted for by the fact that since the mean velocity in homogeneous turbulence is everywhere zero, this assumption ignores the effect of bulk shearing on the tracer material.

Since we are concerned with concentration fluctuations on the scale of the tank dimensions, it seems reasonable to consider the mean flow pattern alone as being responsible for the extension of the surfaces of constant concentration. Turbulent eddies will produce local convolutions, but these will be rapidly smoothed out by the diffusive process, so that it is the rate of destruction of the concentration fluctuations of lowest wavenumber that is the rate-determining factor. Since the flow pattern can be represented by a hypothetical streamline flow pattern corresponding to the mean velocities, on which turbulent fluctuations are superimposed, the mixing process can be regarded as a two-stage process in which the turbulence serves to transport packets of material across the streamlines, and these packets are then stretched by the streamline flow, while molecular diffusion occurs in a direction normal to the streamlines.

The rate of stretching of a line element in such a streamline flow can be found by considering two points

A and B, separated by a short vector $\underline{\delta l}$, in a region where the velocity is $\underline{v}$ (See Fig. 1). If the points are allowed to move with the fluid, A will return to its starting point after a time t, having traversed a closed path. B will follow an adjacent path of slightly different length, taking a time $t+\delta t$, so that it will return to a point $\underline{\delta l} - \underline{v}\delta t$ away from A. After a time 2t, B will be $\underline{\delta l} - 2\underline{v}\delta t$ from A and so on. Over several cycles, therefore, A and B will move apart as if there were a uniform shearing motion in that region. This is equivalent to a steady uniform shear applied to a stratified medium. It can be shown (See Appendix 1) that for such a shear, the distance x obeys the equation

$$\frac{x_0^2}{x^2} = 1+2\alpha\sigma_{12}t+\beta\sigma_{12}^2t^2$$

where α and β depend on the initial orientation of the surfaces of constant concentration to the shear. This can now be used to find the value of k(t), since $k=\frac{1}{x}\cdot\frac{dx}{dt}$.

The quantity we in fact need is

$$\int_0^t k\,dt = \int_0^t \frac{1}{x}\frac{dx}{dt}\,dt = \int_{x_0}^{x}\frac{1}{x}\,dx = \ln\left(\frac{x}{x_0}\right)$$

$$t' = \int_0^t \exp(-2\ln(x/x_0))\,dt = \int_0^t \frac{x_0^2}{x^2}dt$$

$$= \int_0^t (1+2\alpha\sigma_{12}t+\beta\sigma_{12}^2t^2)\,dt$$

$$= t+\alpha\sigma_{12}t^2+\frac{\beta}{3}\sigma_{12}^2t^3$$

Since α and β are of order unity except for special initial

Figure 1.

Streamline Flow

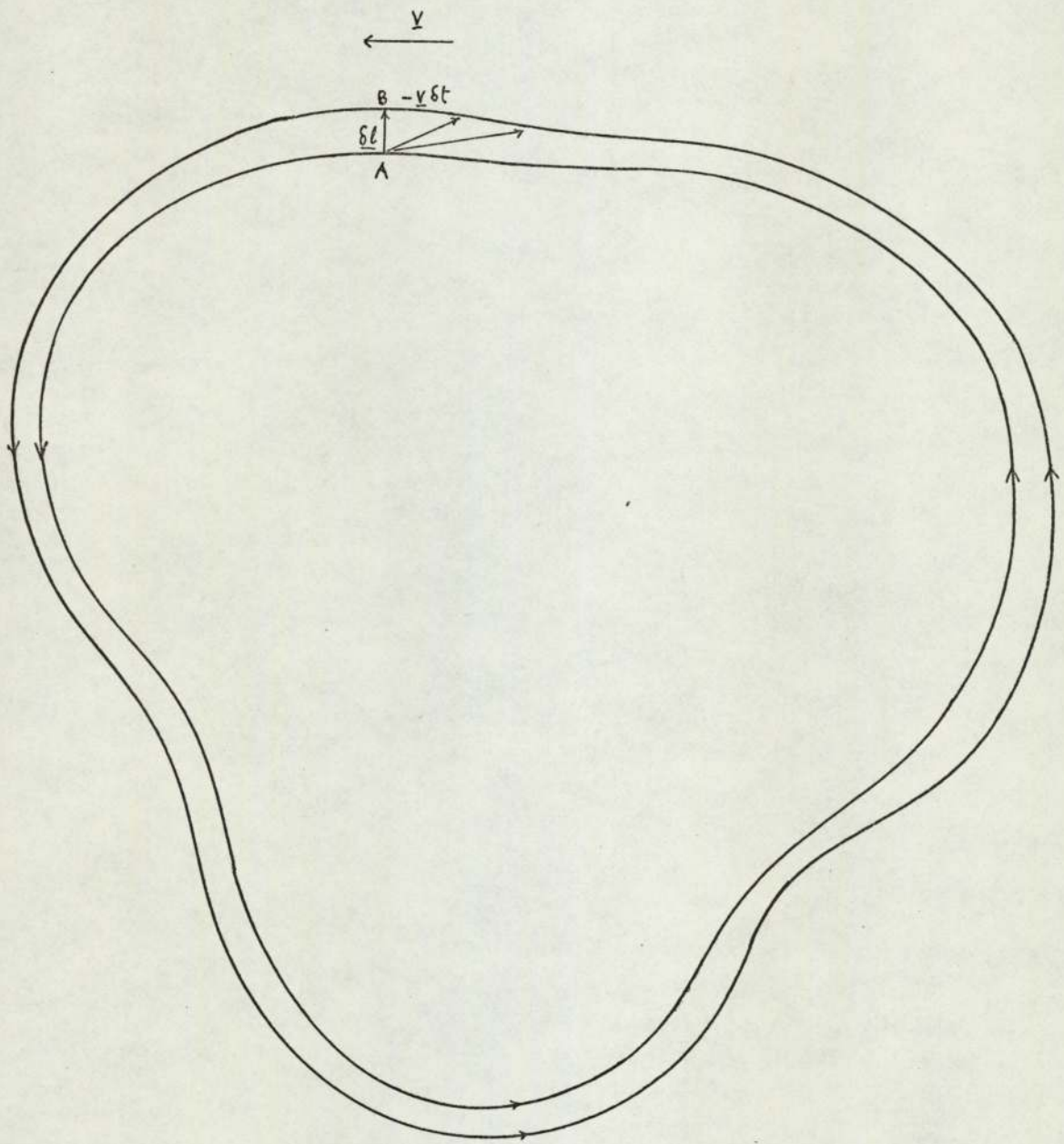

orientations, and $\sigma_{12}\tau$ is large, we have

$$\tau' \simeq \frac{\beta}{3}\sigma_{12}^2\tau^3$$

$$\tau = \left(\frac{3\tau'}{\beta\sigma_{12}^2}\right)^{1/3}$$

This can be used to obtain an order-of-magnitude estimate of τ, taking $\beta=1$, $\sigma_{12}=N=30\ s^{-1}$, $l_c=D=50mm$, $\mathcal{D}=2\times10^{-9}\ m^2\ s^{-1}$ giving $\tau' \sim \frac{l_c^2}{\mathcal{D}}=5\times10^6\ s$

$$\tau \sim \left(\frac{3\times5\times10^6}{30\times30}\right)^{1/3}=25s$$

The mixing time calculated in this way is thus of the same order of magnitude as the observed value (40s). Since l_c depends on the impeller and tank dimensions only, and σ_{12} is proportional to N, this gives

$$\tau \propto N^{-\frac{2}{3}}\mathcal{D}^{-\frac{1}{3}}D^{\frac{2}{3}}$$

or writing this in dimensionless form

$$N\tau \propto \left(\frac{ND^2}{\mathcal{D}}\right)^{1/3}$$

Under fully turbulent conditions the first step in the mixing process, dispersal of the tracer across the streamlines, will take a time τ_T which will be independent of the viscosity, so on dimensional grounds we can write $N\tau_T=A$, a constant. The total mixing time should therefore be given by

$$N\tau = A + B\left(\frac{ND^2}{\mathcal{D}}\right)^{1/3}$$

The quantity A will be of the same order of magnitude as the dimensionless mixing time measured by the conductivity method, as this also is a measure of the time required for turbulent fluctuations to transport material across the streamlines of the time-averaged flow without diffusion. This is of the same order of magnitude as the estimated time for the second step in the mixing process, so the two terms in this expression will be roughly equal. The second term will dominate at high Péclet numbers, and the first term at low Péclet numbers, although this effect may be masked by the influence of viscosity at low Péclet, and consequently low Reynolds number. A graph of mixing time against impeller speed should have a slope tending towards -1 at low impeller speed, and towards $-\frac{2}{3}$ at high impeller speed. This accounts for the value of $-\frac{5}{6}$ obtained by Fox & Gex (12) by fitting a straight line to values obtained over a range of impeller speeds. Norwood & Metzner (18) present their results as a plot in which $\tau N^{\frac{2}{3}}$ is plotted against N, if other variables are excluded. This shows a slope of around -0.2 (corresponding to $\tau \propto N^{-0.87}$) at the point where the turbulent region starts, changing to zero ($\tau \propto N^{-\frac{2}{3}}$) at very high Péclet number. This behaviour agrees well with that expected from this model. The data

of Fox & Gex (12) are too widely scattered, and cover too short a range of Péclet number to enable this variation in slope to be seen, but they are not inconsistent with such a variation.

3.2. Effect of Impeller Diameter

The pumping capacity of a propeller is proportional to ND^3, but since the jet from a small propeller entrains fluid more efficiently than that from a large one, the fluid velocity at a distance from the propeller depends on the momentum transferred to the liquid. This is equal to the product of the pumping capacity and the velocity of the fluid leaving the impeller.

Momentum Transfer $\propto ND^3.ND = N^2D^4$

Similarly the angular momentum transfer is equal to the shaft torque.

Angular Momentum Transfer = Torque = Power / Angular Velocity

$\propto N^3D^5/N \propto N^2D^5$

For a sufficiently small impeller, nearly all the tank can be considered as being distant, so the impeller has an effect only through its momentum transfer. For a small propeller, angular momentum will become negligible compared with linear momentum. Since the index of D is twice that of N in the expression for momentum transfer, this relation

must also hold in the expression for mixing time, as stated by Fox & Gex (12). For measurements made by the conductivity method, therefore, we should have

$$\frac{ND^2\tau_c}{T^2} = \text{const.}$$

Landau & Prochazka (21) obtained the result

$$N\left(\frac{D}{T}\right)^{2.02}\tau_c = \text{const.}$$

from experiments with propellers with D/T ratio of 1/3 to 1/10. The requirement that the impeller should be small is therefore evidently valid for typical petroleum storage tanks with D/T ~ 1/100 and so this correlation can be used confidently. For unbaffled turbines the flow is predominantly tangential, so angular momentum transfer is the important parameter, and the index of D is 5/2 that of N. Landau & Prochazka (21) found

$$N\left(\frac{D}{T}\right)^{2.57}\tau_c = \text{const.}$$

for turbine impellers. For impellers providing both axial and radial pumping, the index of D/T will lie in the range 2 to 2.5. Thus for angled paddles Landau & Prochazka (21) obtained a value of 2.20, and for baffled turbines in a continuous flow system Biggs (52) found an index of D which was 2.29 times the index of N. Applying this principle to the expression for mixing times by the indicator method gives

$$\frac{ND^2}{T^2}\tau = A + B\left(\frac{ND^2}{D}\right)^{1/3}.$$

3.3. Application of Boundary Layer Theory

It is well known that, except at very low Reynolds numbers, the effect of viscosity is confined to a thin boundary layer on the walls of the vessel. Although the full behaviour of such a boundary layer cannot be predicted without detailed knowledge of the flow pattern in the body of the tank, some useful results can be obtained if it is assumed that for regions of the tank distant from the impeller, the flow pattern can be considered as a simple circulation with velocity u, with a boundary layer of thickness δ on the roof, walls and floor of the tank. Although the main flow is turbulent except at very low Reynolds numbers, the question of whether the boundary layer is laminar or turbulent will be determined by the boundary layer Reynolds number defined by

$$Re_\delta = \frac{u\delta}{\nu}$$

rather than by the impeller Reynolds number Re. It is thus possible for a laminar boundary layer to exist where the flow as a whole is turbulent, and although velocities parallel to the floor will fluctuate in such a boundary layer as the mean flow fluctuates, the vertical velocity will remain zero, so that sludge particles entering such a boundary layer may settle out unless their settling

velocity is so low that they are carried into a region where the boundary layer is turbulent before reaching the floor. For a laminar boundary layer with uniform velocity, Blasius' solution for a flat plate (53) can be applied with the tank diameter inserted as the appropriate linear dimension.

$$\frac{\delta}{T} \propto \left(\frac{uT}{\nu}\right)^{-\frac{1}{2}}$$

The circulation velocity u will be governed by the balance between the thrust on the impeller shaft and the drag on the walls

$$\rho N^2 D^4 \propto \eta \frac{u}{\delta} T^2$$

Eliminating δ from these equations and putting $\eta/\rho = \nu$ gives

$$\left(\frac{\nu}{uT}\right)^{\frac{1}{2}} T \propto \frac{\nu u T^2}{N^2 D^4}$$

$$u \propto \nu^{-\frac{1}{3}} T^{-1} N^{4/3} D^{8/3}$$

or in dimensionless form

$$\left(\frac{uT}{ND^2}\right) \propto \left(\frac{ND^2}{\nu}\right)^{1/3}$$

and also $$\delta \propto \nu^{2/3} T N^{-\frac{2}{3}} D^{-4/3}$$

$$\left(\frac{\delta}{T}\right) \propto \left(\frac{ND^2}{\nu}\right)^{-2/3}$$

so $$Re_\beta = \frac{u\delta}{\nu} \propto \nu^{-\frac{2}{3}} N^{\frac{2}{3}} D^{4/3} = \left(\frac{ND^2}{\nu}\right)^{\frac{2}{3}} = Re^{2/3}$$

For a more complicated flow pattern than that considered, the constant of proportionality will be a function of

position, so that for a given value of Re, there will be some regions in which Re_δ is above the critical value for turbulent flow, and others in which it is not. Increasing Re will increase the value of Re_δ everywhere, so that the critical value will be exceeded over a greater area, and sludge will settle in fewer regions. At a sufficiently high value of Re, the boundary layer will be turbulent everywhere, δ and $\frac{uT}{ND^2}$ will become independent of viscosity, and no sludge settlement will occur.

4. Experimental Work

4.1 Introduction

A model tank was used to simulate a large oil storage tank, and it was intended to use this to determine the correct scale-up rules, and the effect of varying such parameters as the liquid depth and the impeller angle. The typical crude oil storage tank selected for modelling purposes is 67 m in diameter by 17 m high with a 0.7 m diameter impeller rotating at 360 r.p.m. In order that the same flow pattern should be obtained in the model as in the full-size tank, it is necessary to operate at the same impeller Reynolds number (around 2×10^5). For a 1.2 m diameter model tank, the diameter of a correctly scaled impeller is 12.5 mm, and using water as the working fluid, the impeller speed would then have to be 80,000 r.p.m. Since this is clearly impractical, it is necessary to use a larger impeller, and to determine the correct scaling law for impeller diameter.

In order to simulate the mixing of liquids of different densities, it is necessary for the buoyancy number $\frac{\Delta\rho g}{\rho N^2 D}$ to be the same in both systems as well as the Reynolds number $\frac{ND^2}{\nu}$. This implies

$$\frac{\Delta\rho}{\rho} \propto \frac{N^2 D}{g} \propto \frac{\nu^2}{gD^3}$$

Since D for the model tank is very much less (~1/50) that for the full-scale one, and ν can be reduced only by a factor of about 10, $\frac{\Delta\rho}{\rho}$ becomes impossibly large in the model tank for even quite a small density difference in the full-scale one. It has therefore been necessary to confine the study to measurements on liquids of equal density. Of the tracer materials used, the one of highest density was 2N sodium hydroxide solution of specific gravity 1.08. Visual observation of dyed material showed no tendency for this to sink to the bottom of the tank under the conditions encountered in this tank.

4.2. Equipment- Tank and Fittings

The model tank used is shown in Figs. 2 & 3, and was 1.2 m in diameter by 0.6 m high, fabricated from $\frac{1}{4}$" acrylic sheet, and reinforced with bands of the same material. The base of the tank was painted externally with white emulsion paint, and a 100 mm grid was scribed through the paint to provide a reference for positioning probes. A self-adhesive scale was used to indicate the liquid depth. A floating roof was also included, constructed of the same material as the tank, with a 75 mm high rim around the edge. This was made to fit inside the main tank with a clearance of about

Figure 2.
1.2 m Diameter Tank (Scale 1:10)

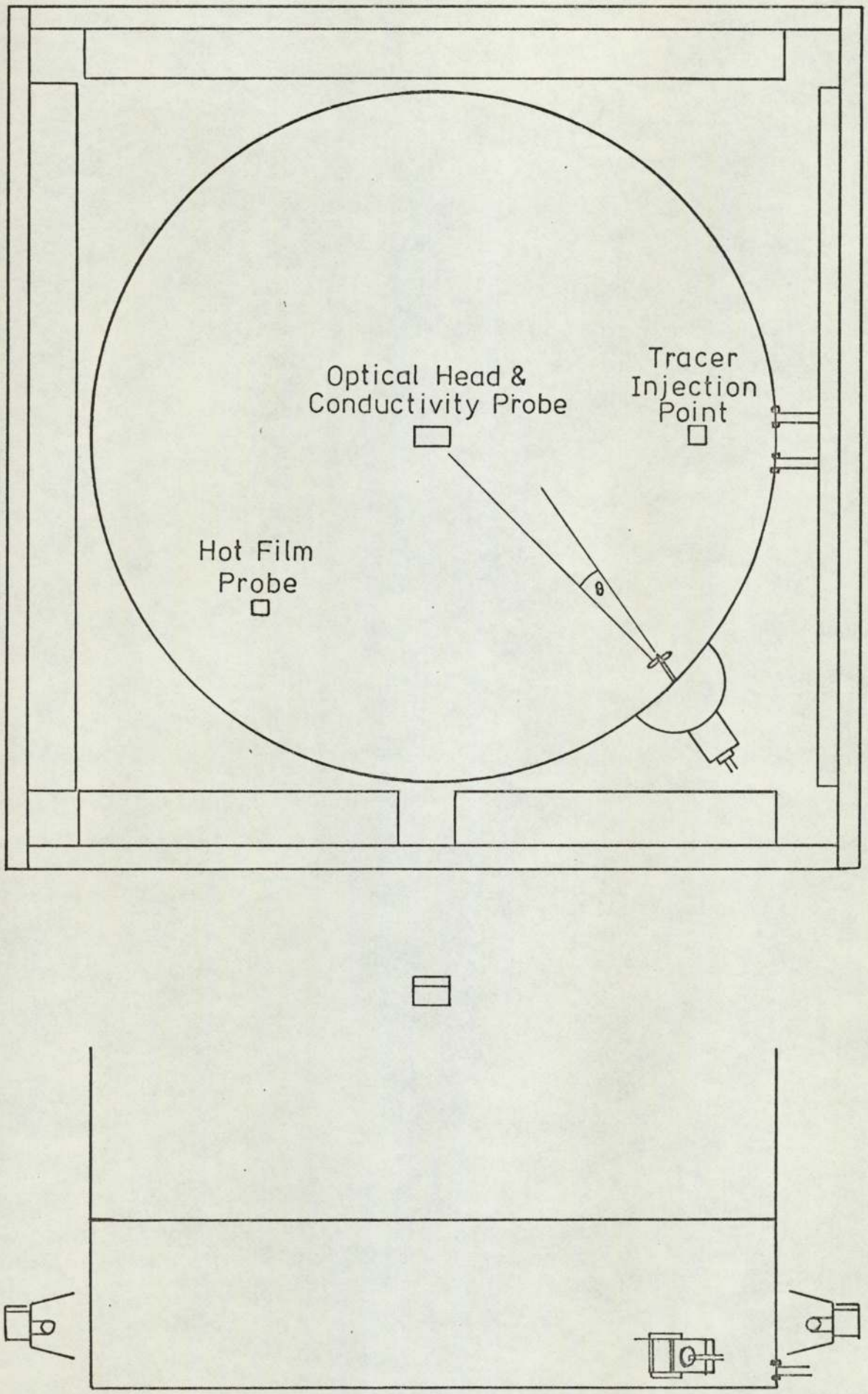

Figure 3

1.2 m Diameter Tank

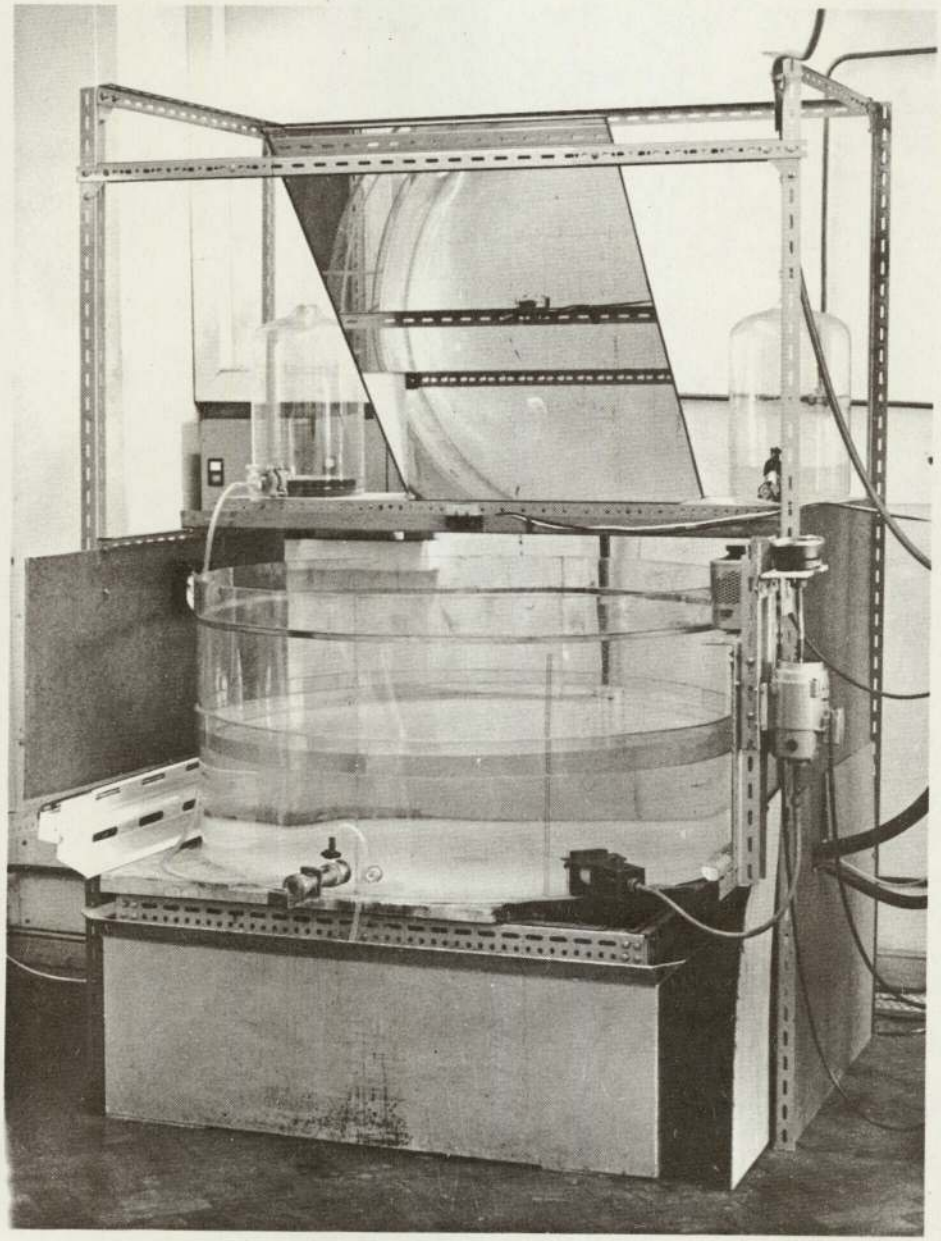

10 mm, and could be wedged to prevent it from rotating during use. The tank was mounted over a steel catch-tank to prevent spillage in the event of the acrylic tank bursting, and was surrounded by a slotted angle framework which carried various pieces of ancillary equipment. A mirror mounted at an angle of 45° above the tank enabled photographs to be taken as if from a point 4 metres above the base of the tank, avoiding the distortion inherent in the use of a wide-angle lens. The tank was illuminated by a set of fluorescent tubes arranged so as to light the tank through the walls below the waterline. Repeated reflection at the surface and diffusion by the white base of the tank ensured very even lighting over the whole area. The sides of the framework were boxed in, and a large black polythene sheet could be used to exclude light from external sources during colorimetric meaurements. A small axial fan was used to circulate room air through the enclosure and prevent heat from the lights from increasing the temperature. The framework was also used to support the impeller motor, the reservoirs of tracer material, and the various probes used.

A swivelling shaft seal assembly shown in Figs. 4 & 5 was used to provide a means whereby the impeller shaft could be swivelled about a vertical axis while preventing leakage of liquid from inside the tank. A mechanical shaft

Figure 4

Swivelling Shaft Seal Assembly Cross-Section (Full Scale)

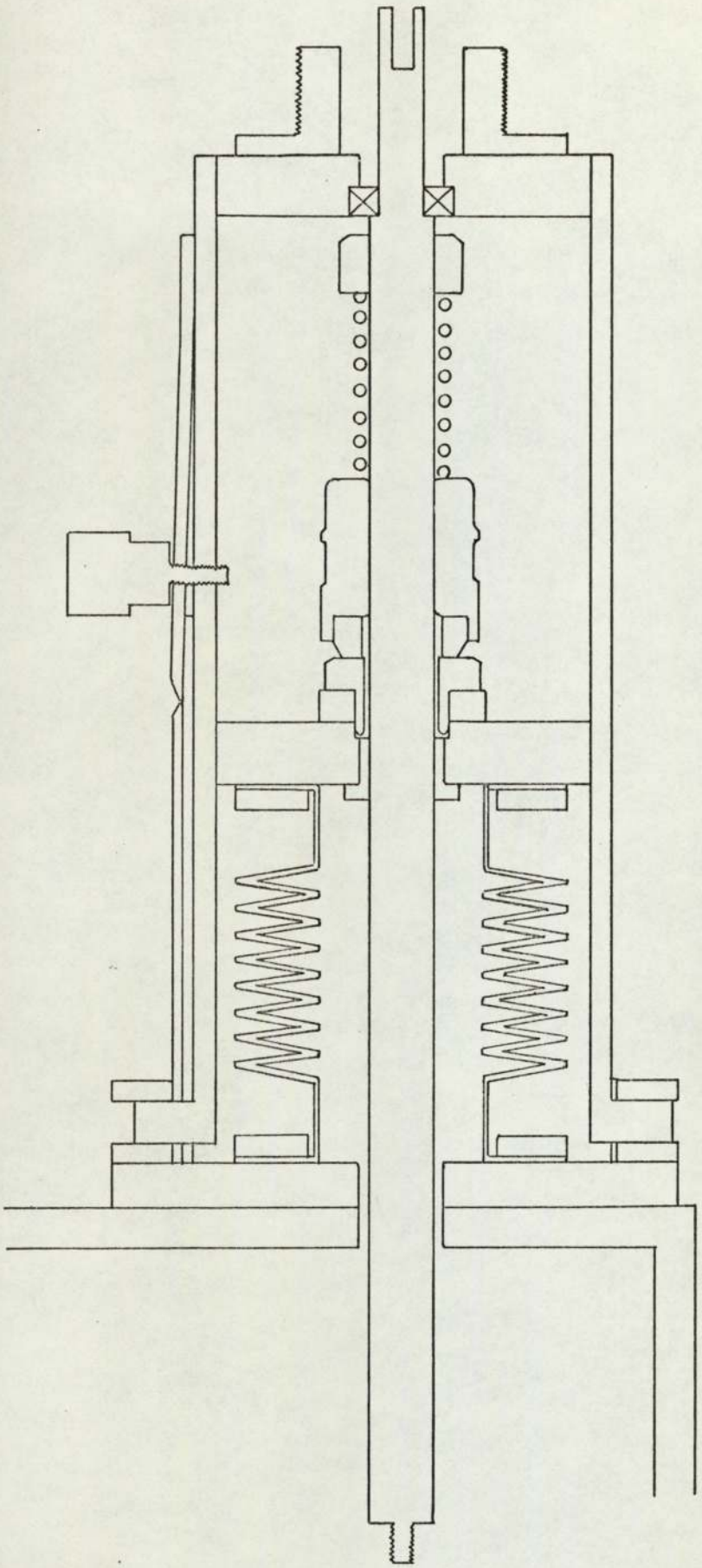

Figure 5

Swivelling Shaft Seal

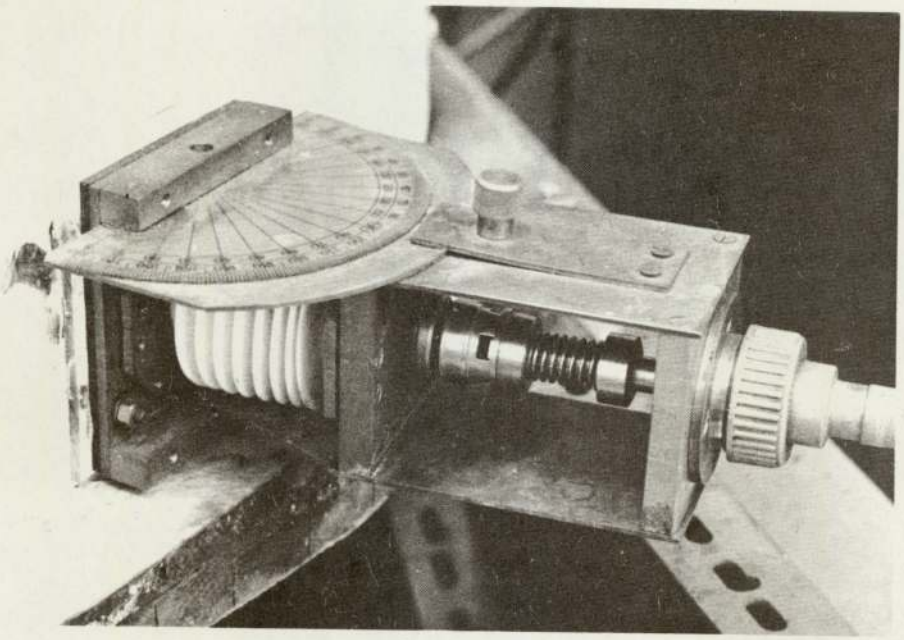

seal was mounted in a brass housing pivoted, at a point as close as possible to the tank wall, to a brass plate secured to the tank and sealed by a rubber gasket. One end of a P.T.F.E. bellows was fixed to this plate, and the other end to the seal housing, so that the impeller shaft passed through the bellows, and through a slot in the wall of the tank. This shaft was supported by a plastic bush located next to the seal, and a miniature ball bearing which took up the thrust from the seal spring and the impeller. One end of the shaft was screwed to allow a variety of impellers to be fitted, and the other end was slotted to accept a flexible drive connected to a $\frac{1}{8}$ H.P. D.C. motor. The other end of the motor shaft was connected by a second flexible drive to a mechanical tachometer reading 0-3000 r.p.m. A protractor fitted to the front plate enabled the impeller to be set to any desired angle, using a knurled clamping screw.

The impellers used were either plastic marine propellers (Ripmax), or a set of geometrically similar brass impellers constructed as shown in Fig. 6. These are in fact inclined blade paddles rather than propellers, as the pitch decreases towards the centre, but the flow pattern produced is very similar. Perfect geometrical similarity is not maintained as the material thickness and the hub diameter are identical for all these impellers, but it can be shown that the effect

Figure 6

Brass Impellers (Scale 2:1)

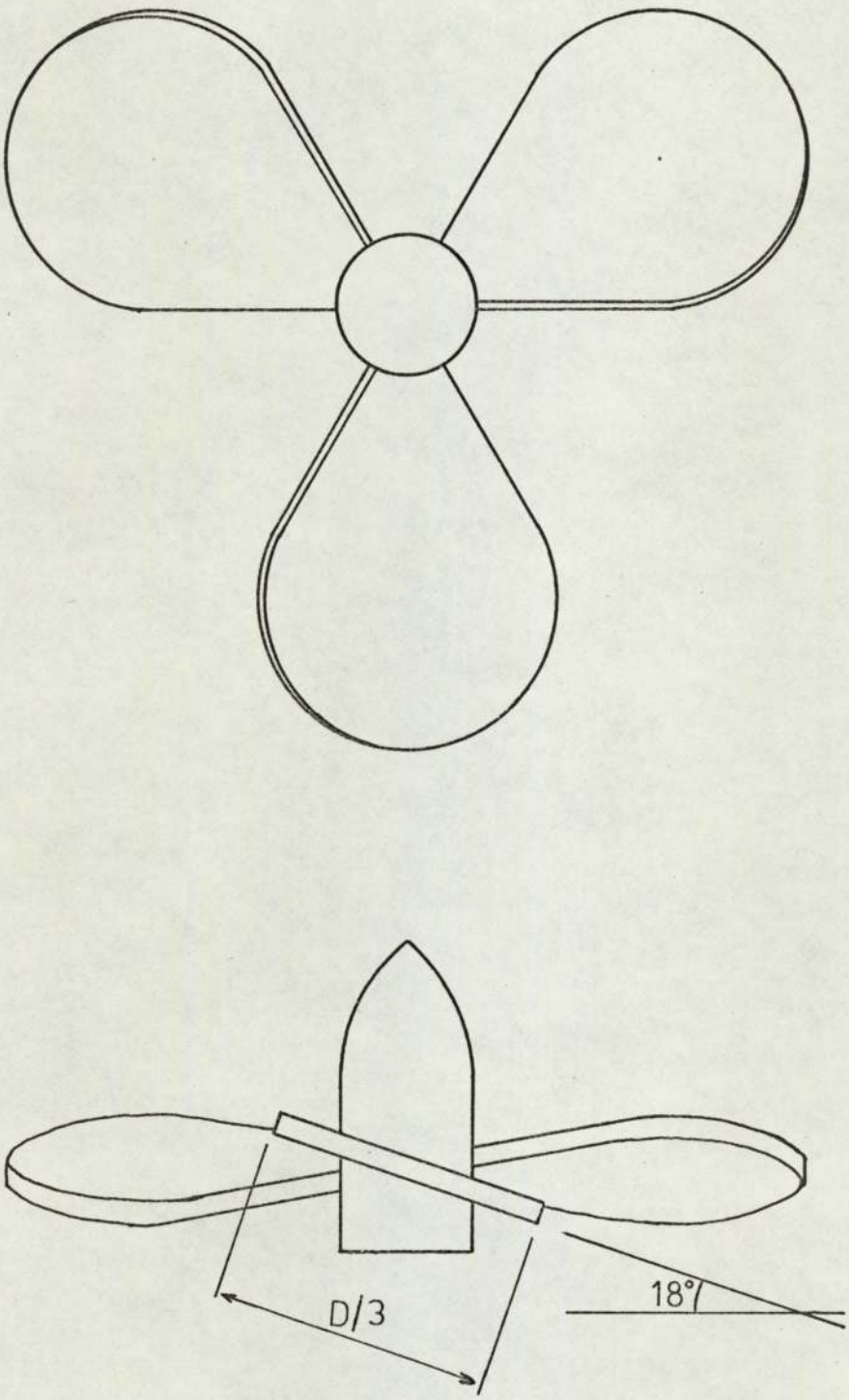

of this is small (Appendix 2).

An injector illustrated in Figs. 7 & 8 was used to add tracer material beneath the floating roof. A 50 ml glass syringe with the end removed was mounted in a brass holder equipped with adjustable stops. This screwed onto a body mounted into a hole in the tank wall, with O-rings providing liquid seals. Brass stopcocks mounted into the body were used for filling the injector and venting air, care having been taken in the design to prevent air from being trapped. The tracer material was injected into the tank through a P.T.F.E. poppet valve ground into a conical seat, and held in place by a phosphor-bronze spring. The injector was tested before installation by squirting water into a beaker and weighing it, and the repeatability was found to be better than 0.1 ml in 25 ml, with an operating time of less then 0.5 sec.

4.3. Measurement of Mixing Times by the Indicator Method

4.3.1. Equipment

Of the various methods for measuring terminal mixing times, the indicator method was selected as the principal method for studying the effect of changing physical parameters, as it is the only method capable of detecting

Figure 7

Injector Cross-Section (Scale 1:1)

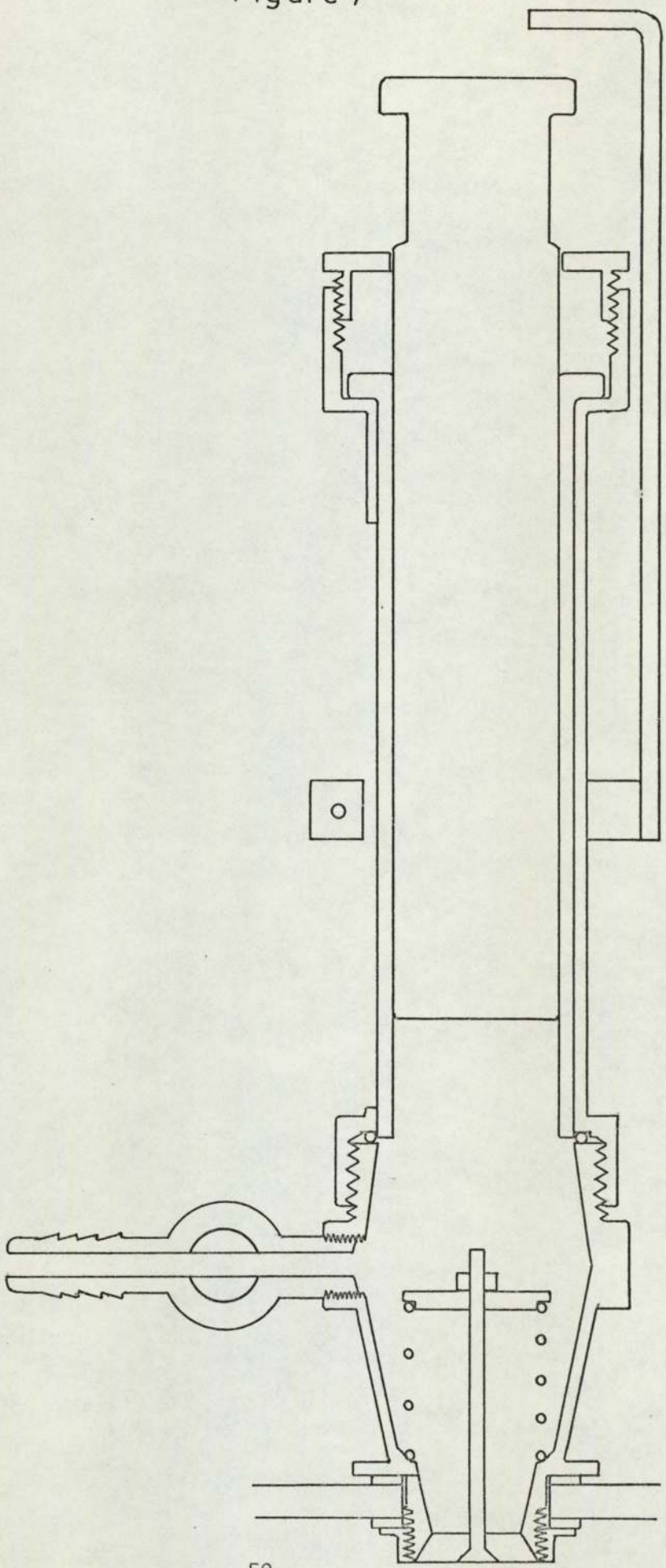

Figure 8

Injector

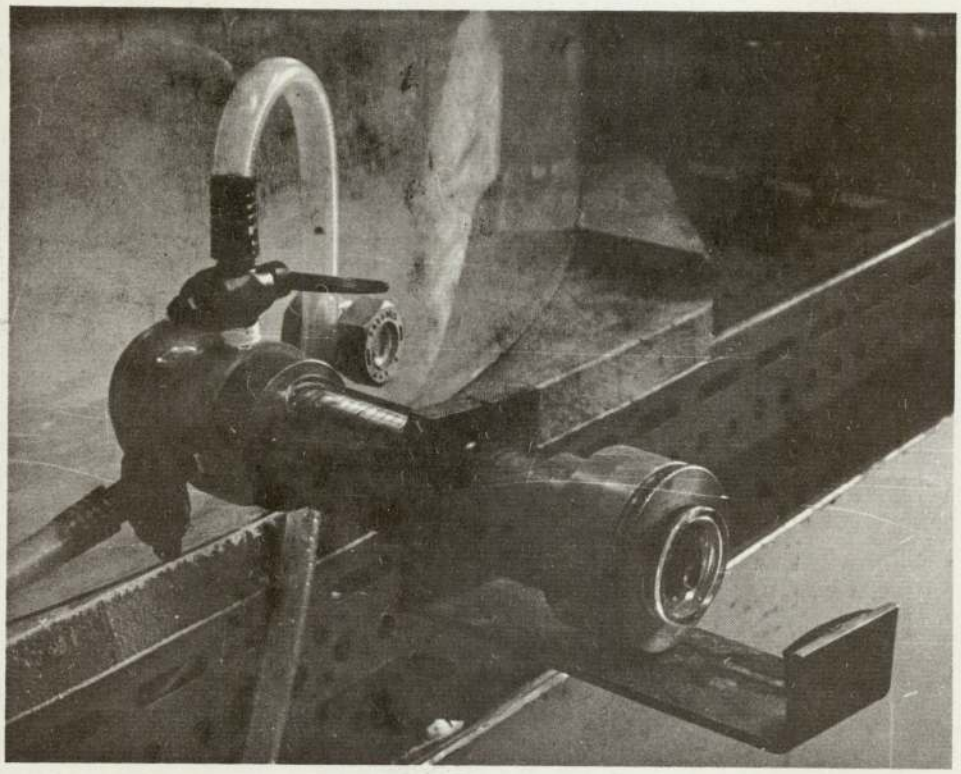

an unmixed region in the tank except for the Schlieren method, which is impractical on this scale.

It was found that phenolphthalein as used by Fox & Gex (12) was unsatisfactory, as the colour change occurred under alkaline conditions, and was therefore affected by absorption of carbon dioxide from the atmosphere. Moreover it was impossible to use sucrose to increase the liquid viscosity as this had a buffering effect at high pH, and methyl red, which has a colour change from red at pH 4.4 to yellow at pH 6.0 was used instead. The acid and base used were 2N solutions of hydrochloric acid and sodium hydroxide standardised by titrating against one another using the same 25 ml pipettes as were to be used for measuring the amounts to be added to the tank. In order to avoid making a subjective estimate of the terminal mixing time by visual observation, a photoelectric colorimeter was constructed capable of giving an objective indication of the colour of the material in the tank. The sensing head contained a pair of phototransistors of type BPY 65, fitted with red and green filters, mounted so as to accept light from the central region of the tank, with adjustable shutters to compensate for inequalities in the filters and transistors as shown in Fig. 9. These transistors have a small sensitive area, so that

Figure 9

Photoelectric Head (Scale 2:1)

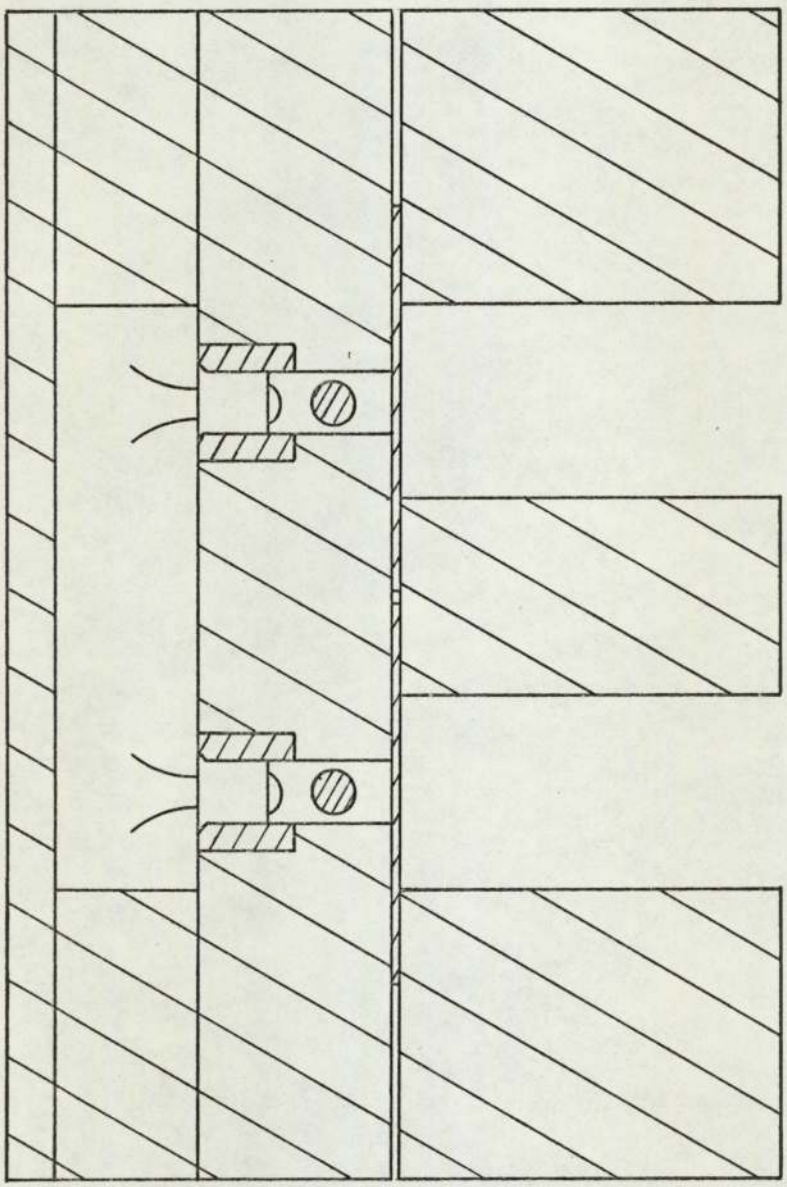

the field of view is easily controlled, but they have poor sensitivity in the green region of the spectrum. To obtain roughly equal signals from the two phototransistors it was necessary to make the red filter very dense, and the photocurrents produced were consequently small (~ 100 nA)

The circuit diagram of the associated electronics is shown in Fig. 10. The photocurrents are fed in opposition to the summing junction of a virtual earth amplifier. Changes due to thermal leakage in the transistors or variation in light level are compensated for by this arrangement, so that only difference signals due to colour changes are detected. It was found necessary to use low-noise screened lead to connect the phototransistors to the amplifier to eliminate spurious signals generated by vibration produced by the impeller motor. The amplifier (Analog Devices 40K) has an F.E.T. input resulting in a very low input bias current (20 pA) which may be regarded as negligible compared with the signal current. The feedback network provides a sensitivity adjustable by VR2 from 10 to 175 nA full scale, and an offset of ±10 nA can be introduced by the zero control VR1. Larger offsets were corrected by means of the optical shutters on the phototransistors. The amplifier output is displayed on a 5" scale moving coil meter. Resistor R1 protects the phototransistors from

Figure 10

Circuit Diagram for Colorimeter

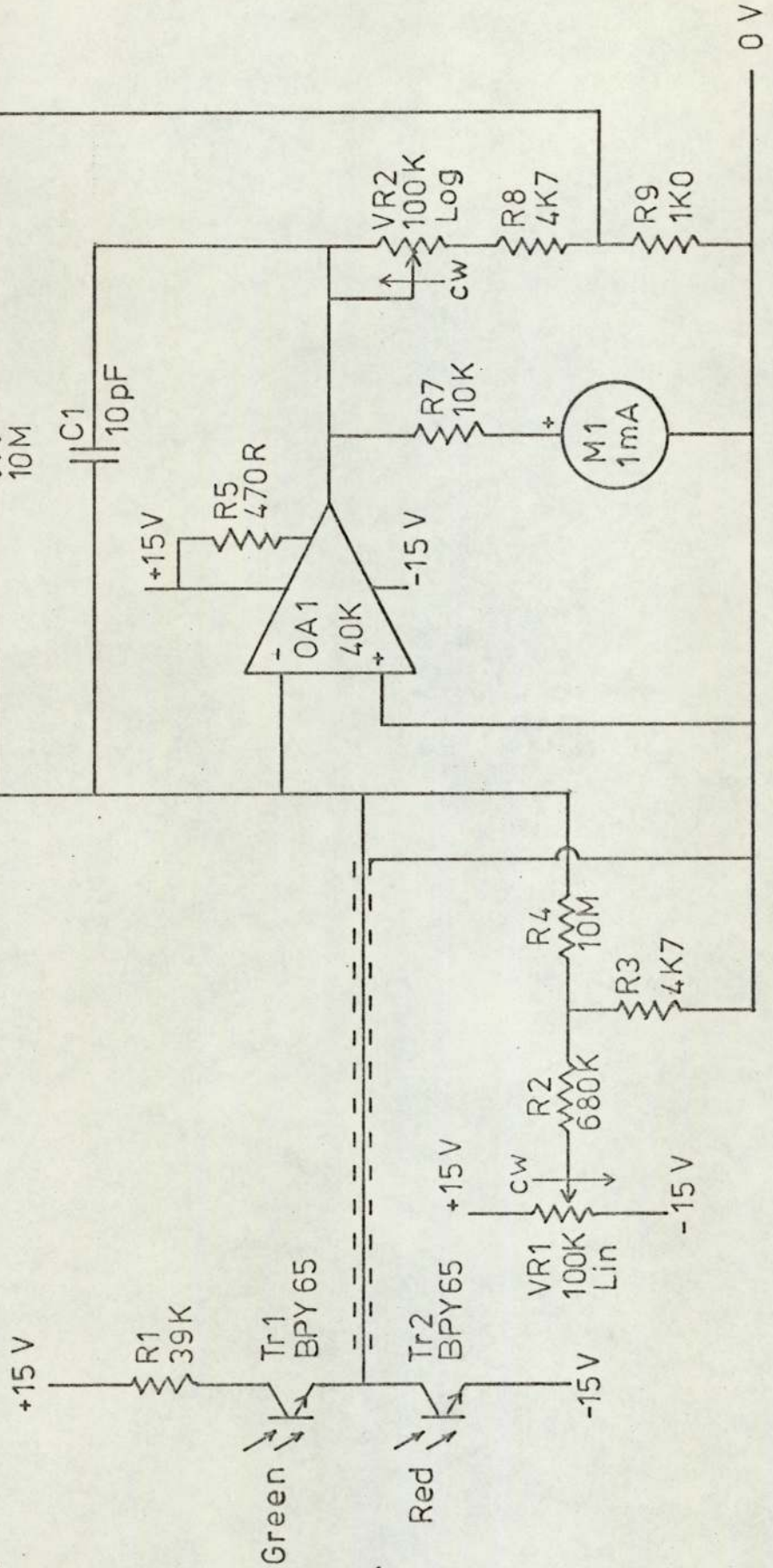

passing excessive current, as might occur if they were pointed directly at a light source, and C1 and R5 provide frequency compensation for the amplifier.

4.3.2. Method

The procedure used for the majority of measurements was as follows:

1. The tank was filled to the desired depth, the temperature being adjusted to 20°C by filling with hot and cold tapwater.
2. 50 ml of a solution containing 10 g.p.l. of methyl red in 0.2 N sodium hydroxide was added by measuring cylinder and mixed in.
3. The colorimeter and the fluorescent lights were allowed to warm up for at least half an hour, and the zero control was set to midrange. The impeller was set at a fairly high speed.
4. One of the phototransistor shutters was closed until a meter reading of nearly zero was obtained, fine adjustment then being carried out with the electronic zero control.
5. 20 ml of 2N hydrochloric acid solution was added and mixed in, and the gain control adjusted to give a reading of full scale.
6. 25 ml of 2N sodium hydroxide solution was added, and the

zero adjustment reset to correct for any shift occurring when the gain control was reset.

7. 25 ml of 2N hydrochloric acid were added from a burette, and a graph was plotted of the colorimeter reading against the volume of acid added (Fig 11). The acid was added about 0.5 ml at a time, allowing sufficient time for the colorimeter reading to settle down to a steady value between additions.
8. The 'neutral point' was taken as the point obtained by projecting the linear portion of the calibration curve towards the abscissa. This gave a well-defined point at which the colorimeter reading had nearly reached zero. About 18 ml of sodium hydroxide solution were added and the colorimeter reading was noted. Sufficient sodium hydroxide was then added to bring the level to 5 ml less than the neutral point, as calculated from the calibration curve. In this way the starting pH could be set accurately. This step was repeated every three or four readings.
9. 25 ml of 2N hydrochloric acid was pipetted into a 50 ml beaker, and added to the tank. As the beaker was used repeatedly without rinsing, any small variations in the amount of liquid wetting the walls of the beaker were not cumulative.

Figure 11

Calibration Curve for Colorimeter

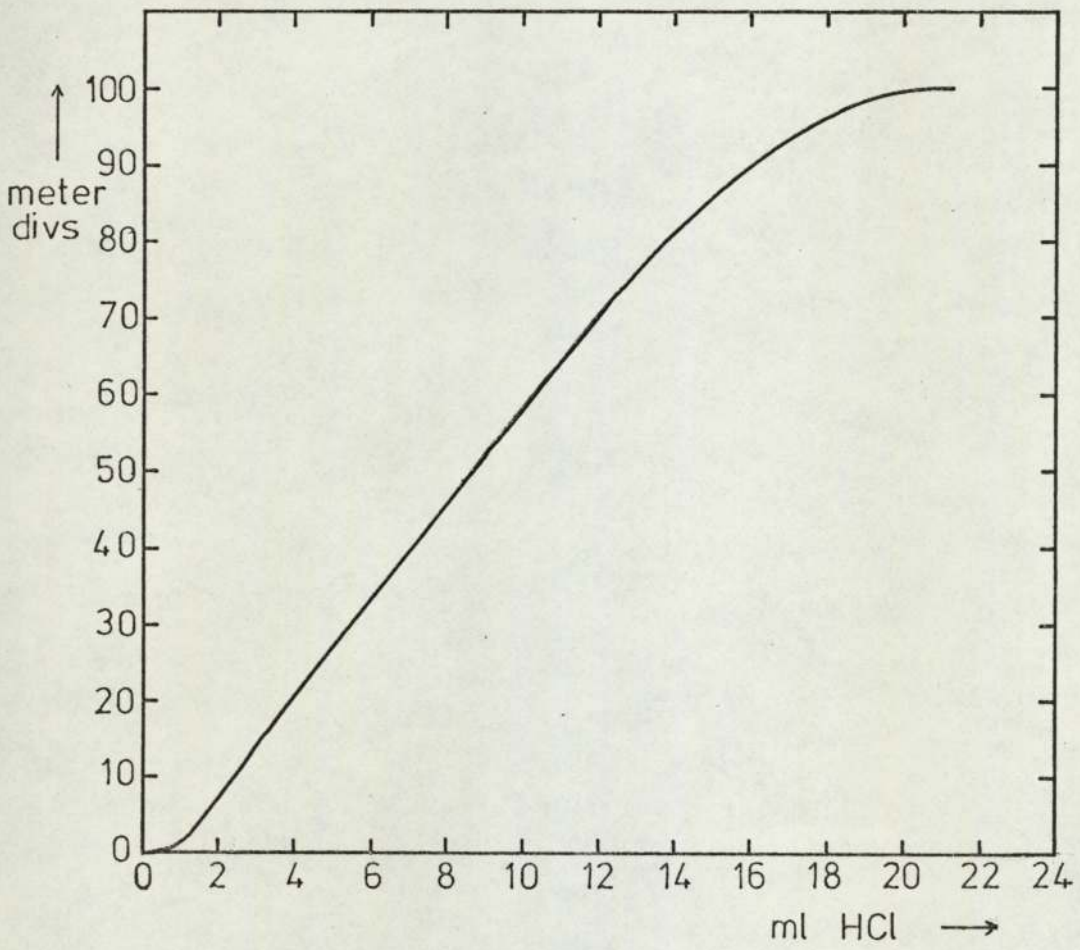

10. After allowing the acid to mix into the tank for at least twice the expected terminal mixing time, a 25 ml portion of sodium hydroxide was added from a 50 ml beaker, and a stopwatch was started simultaneously. The stopwatch was stopped when the colorimeter reading had dropped to 5% of full scale.

11. The stopwatch reading was noted, and steps 9 & 10 were repeated at least ten times under each set of conditions. For measurements at liquid depths other than 200 mm and 300 mm the quantities of acid and base were varied at the rate of 12.5 ml / 100 mm of water.

4.4. Measurement of Mixing Times by the Conductivity Method

4.4.1. Meter and Probes

In order to measure mixing times by the conductivity method, an electrical conductivity meter and a set of geometrically similar probes were used. The design of the probes, shown in Fig. 12, was based on that of Biggs (52). They consisted of a helix of platinum wire forming one electrode, with a straight wire along the axis as the second electrode. This arrangement provides good sensitivity and ease of construction and allows a free flow of liquid through the probe. The wires were sealed with

Figure 12

Conductivity Probe (Scale 5:1)

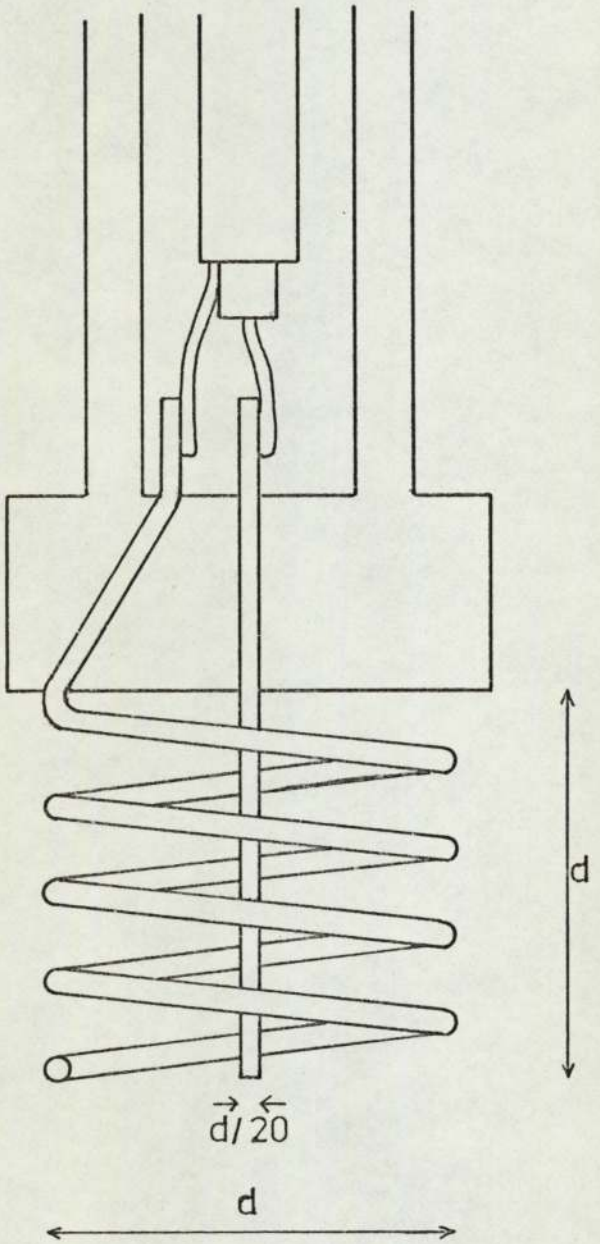

epoxy resin into an acrylic disc mounted on the end of a tube of the same material. An electrical plug on the other end of the tube allowed the probes to be interchanged. The wires used were 5, 9, 15, 25, and 40 thousandths of an inch in diameter, and the dimensions of the probe were twenty times greater in each case.

The conductivity meter, which was specially constructed for the purpose, was of a novel design. It is necessary to measure the conductivity using alternating current to prevent polarization of the electrodes. Previous workers have used either bridge circuits (Biggs (52), Landau & Prochazka (13)) or an amplifier measuring the voltage drop across a small series resistor (Lamb et al. (54)), as shown in Fig. 13. In the first case, the sensitivity depends on the bridge setting, and consequently on the background conductivity, and since neither electrode is at earth potential, the presence of earthed fittings in the tank is liable to lead to stray currents, so that the circuit can be influenced by variations in conductivity outside the probe. The second method overcomes these objections, but it requires an amplifier having exceptional common mode rejection combined with good stability, as well as a powerful and stable signal generator to supply current to the probe. In order to

Figure 13

Principles of Conductivity Measurement

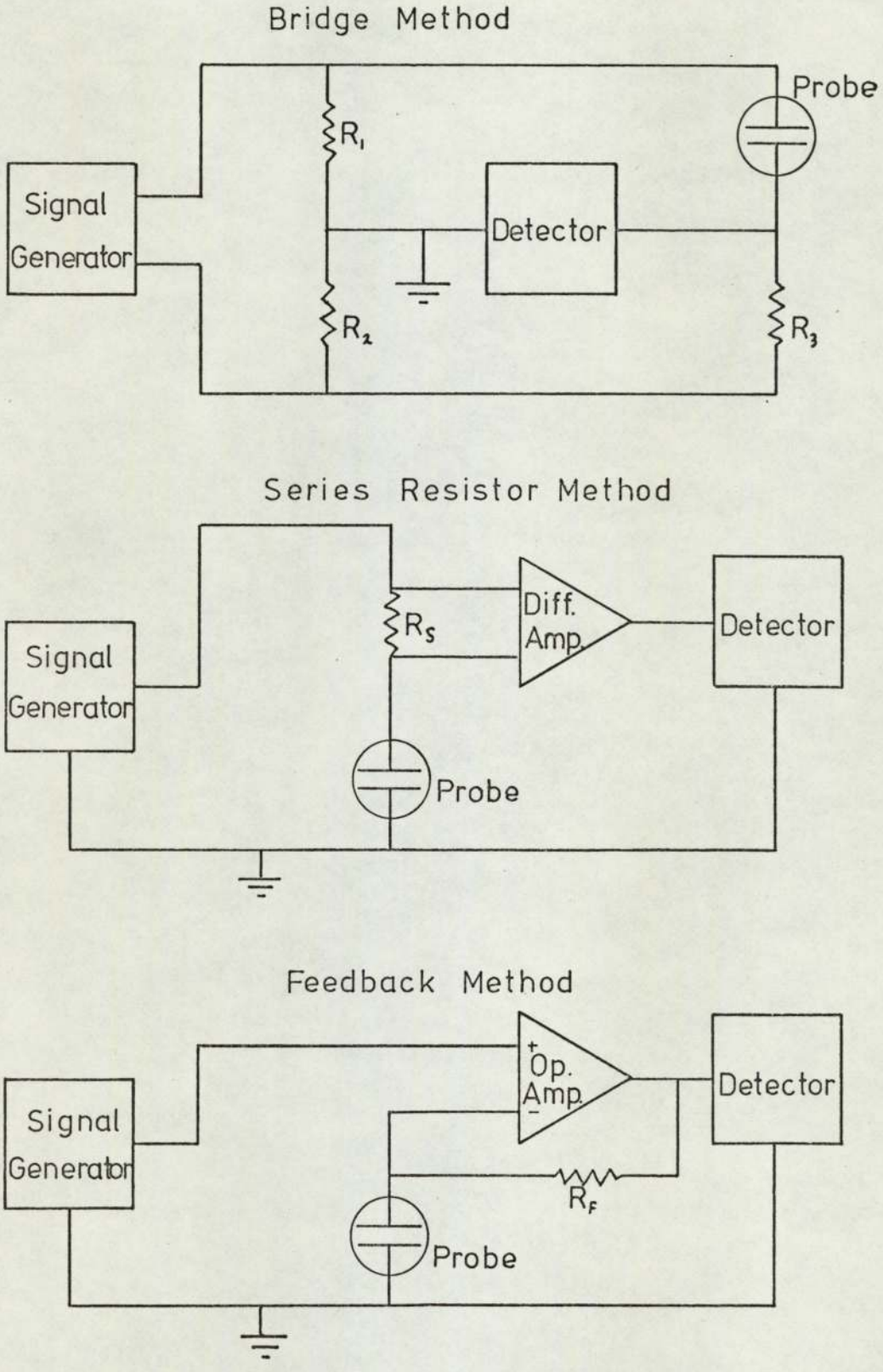

avoid non-linearity the series resistance must be made negligible compared with that of the probe, so that the differential voltage across it is small compared with the common-mode voltage from the signal generator.

In the circuit used in the present work, the probe is placed in the feedback loop of an operational amplifier. This arrangement provides better linearity than the series resistor method, and since the output signal is virtually independent of the amplifier gain, a cheap monolithic operational amplifier can be used. Since no power is drawn from the signal generator, it can readily be made to provide a stable output voltage, and the probe can still be used with one electrode (the outer helix) grounded. Details of the electronic circuitry are given in Appendix 3. The electrolyte used was hydrochloric acid, as this has a very high specific conductivity.

4.4.2. Method

The procedure used was as follows:

1. The conductivity probe was connected to the meter and the zero control adjusted for zero reading.
2. The calibration switch was set to the calibrate position, and the probe was immersed in a solution containing 0.73 g/l of sodium chloride in distilled water. The gain control was

set for a reading of full scale.

3. The calibration switch was set to the normal position and the probe was placed in the tank. The zero control was adjusted for zero reading.
4. The U.V. chart recorder was started, and 10 ml of 2N hydrochloric acid , measured into a 50 ml beaker with an automatic pipette, were tipped into the tank. At the same time the marker button on the recorder was pressed.
5. When the meter reading reached its final value of about 80% of full scale, the chart recorder was stopped, and the zero control was used to reset the meter to zero. Steps 4&5 were repeated at least ten times under each set of conditions. When the zero control reached the end of its travel, the tank was emptied and refilled.

The recorder trace was analysed by measuring the distance between the marker indicating the time at which the tracer was added, and the last point at which the reading differed by 20% from the final reading as shown in Fig. 14. The figure of 20% was chosen as this corresponded to the point at which the colour change is complete in the indicator method.

Figure 14

Typical Chart Record from Conductivity Meter

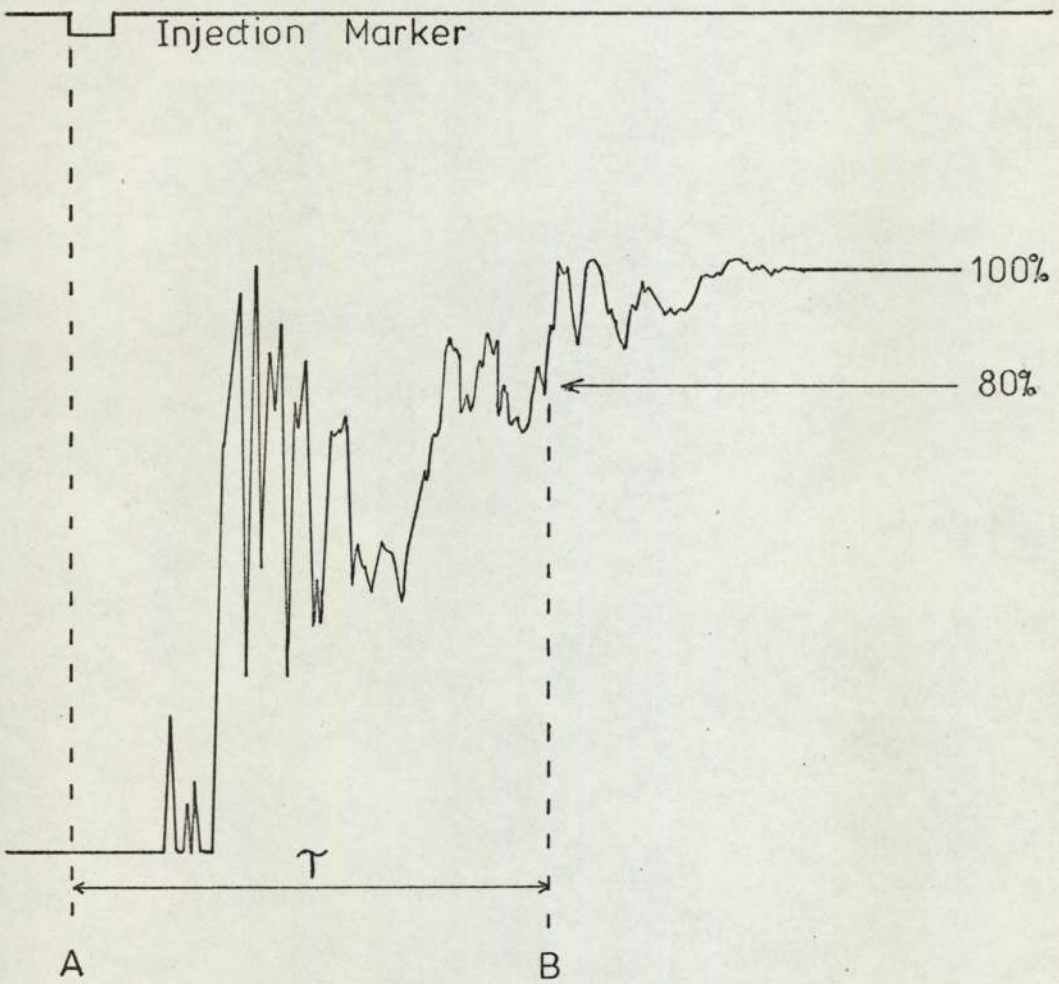

4.5.1. 70 mm Tank

In order to enable a large number of measurements to be carried out using the indicator method with different chemical systems, a second rig was constructed containing a 70 mm diameter tank, shown in Figs. 15 & 16. The tank was made from a section of glass tube 70 mm in diameter by 70 mm long, cemented to a glass plate with epoxy resin. It was mounted horizontally with the rim sealed against a $\frac{1}{8}$" sheet of P.T.F.E. using Silastic sealant. The tank was clamped between $\frac{1}{4}$" brass plates, the larger one of which was mounted in a framework of slotted angle. This plate carried a mechanical shaft seal, through which the impeller shaft protruded into the tank, and also a set of four lines for filling, emptying, venting and tracer addition. The other plate carried a 50 mm diameter copper cylinder brazed into a circular hole, so that a photocell placed at the end received light diffused by the P.T.F.E. sheet. The inside of the cylinder was painted matt black to ensure that stray light did not reach the photocell without passing through the whole depth of the tank.

Since terminal mixing times for this tank were of the order of one second, it was necessary to record the signal from the photocell on a U.V. chart recorder and measure the

Figure 15

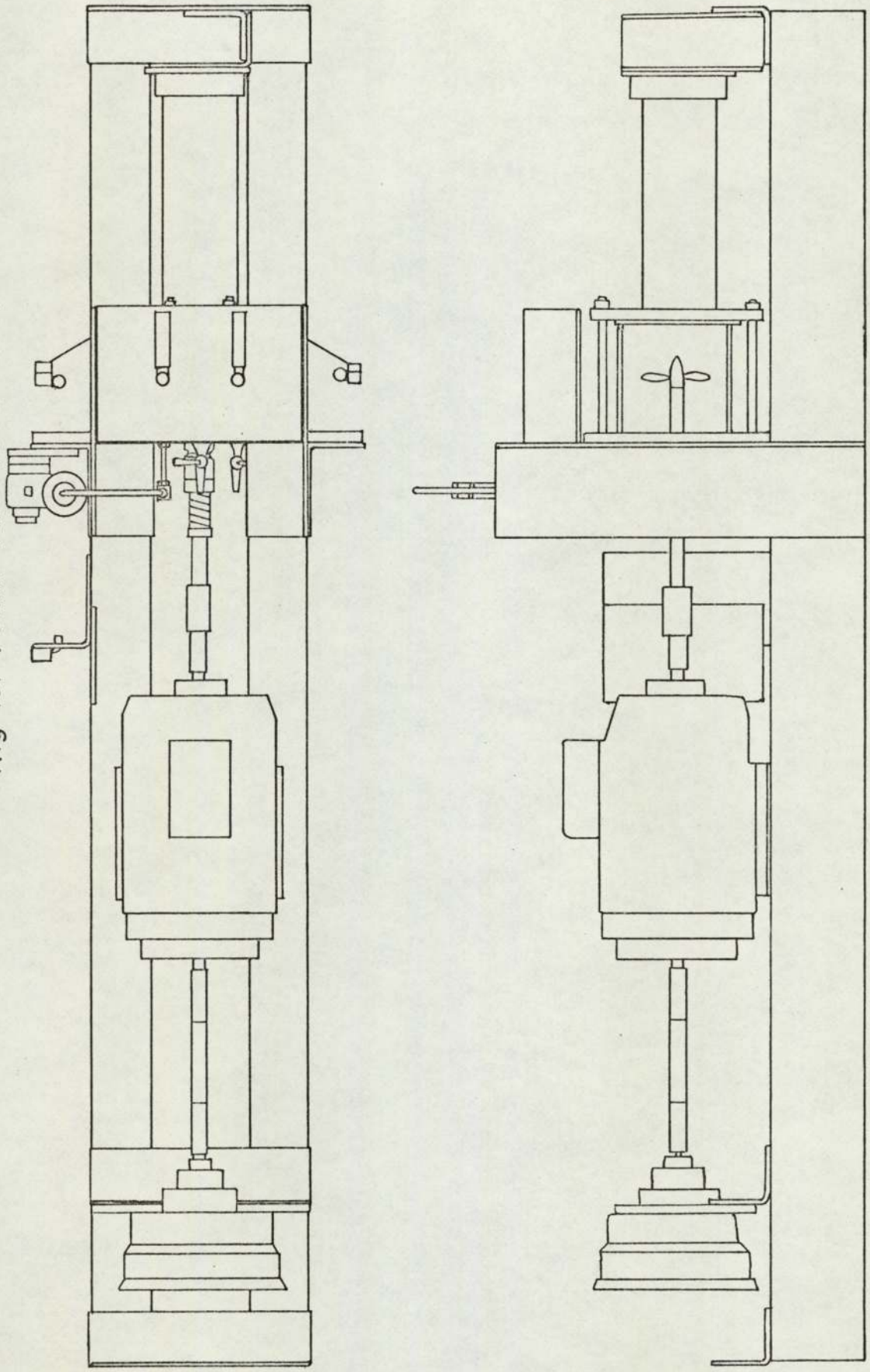

Rig for 70mm Tank (Scale 1:4)

Figure 16

70mm Diameter Tank

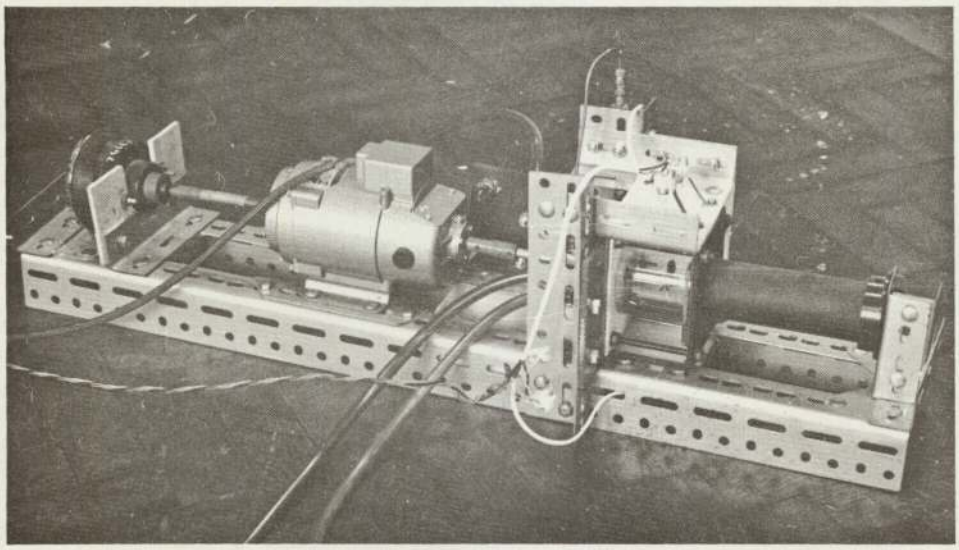

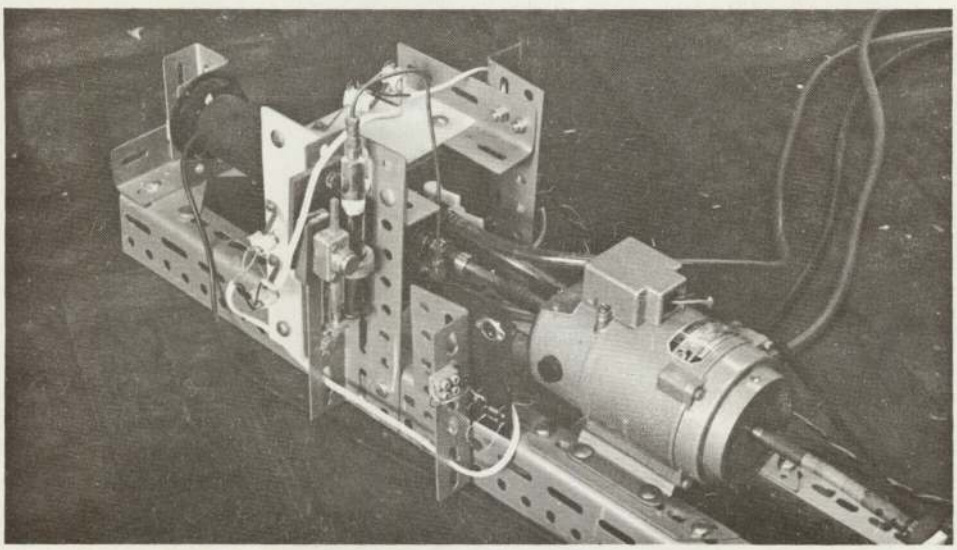

trace produced, rather than measure times directly with a stopwatch. The bandwidth of the recording system was greater than 100 Hz, and consequently it was necessary to use a D.C.-powered light source to illuminate the tank without producing any flicker at this frequency. Eight 2 Watt flashlamp bulbs were used, mounted in pairs behind translucent polypropylene diffusing screens, and powered by the same stabilized power supply that was used for the photocell amplifier. It was found that these bulbs produced so much infra-red radiation that the silicon phototransistors could not be balanced, the one with the red filter giving a greater current under all conditions. They were therefore replaced by a selenium photocell having good response in the green, falling off sharply towards the red end of the spectrum. The response curve, shown in Fig. 17, is such that this photocell could be used without any optical filter, the meter zero reading being set by an electrical offset rather than by the signal from a second photocell. The photocell amplifier circuit was suitably modified as shown in Fig. 18, and since it was now necessary to exclude mains hum from the output signal, it was placed in a metal screening box, and connected to the photocell with low-noise screened lead.

Figure 17

Spectral Response Curves

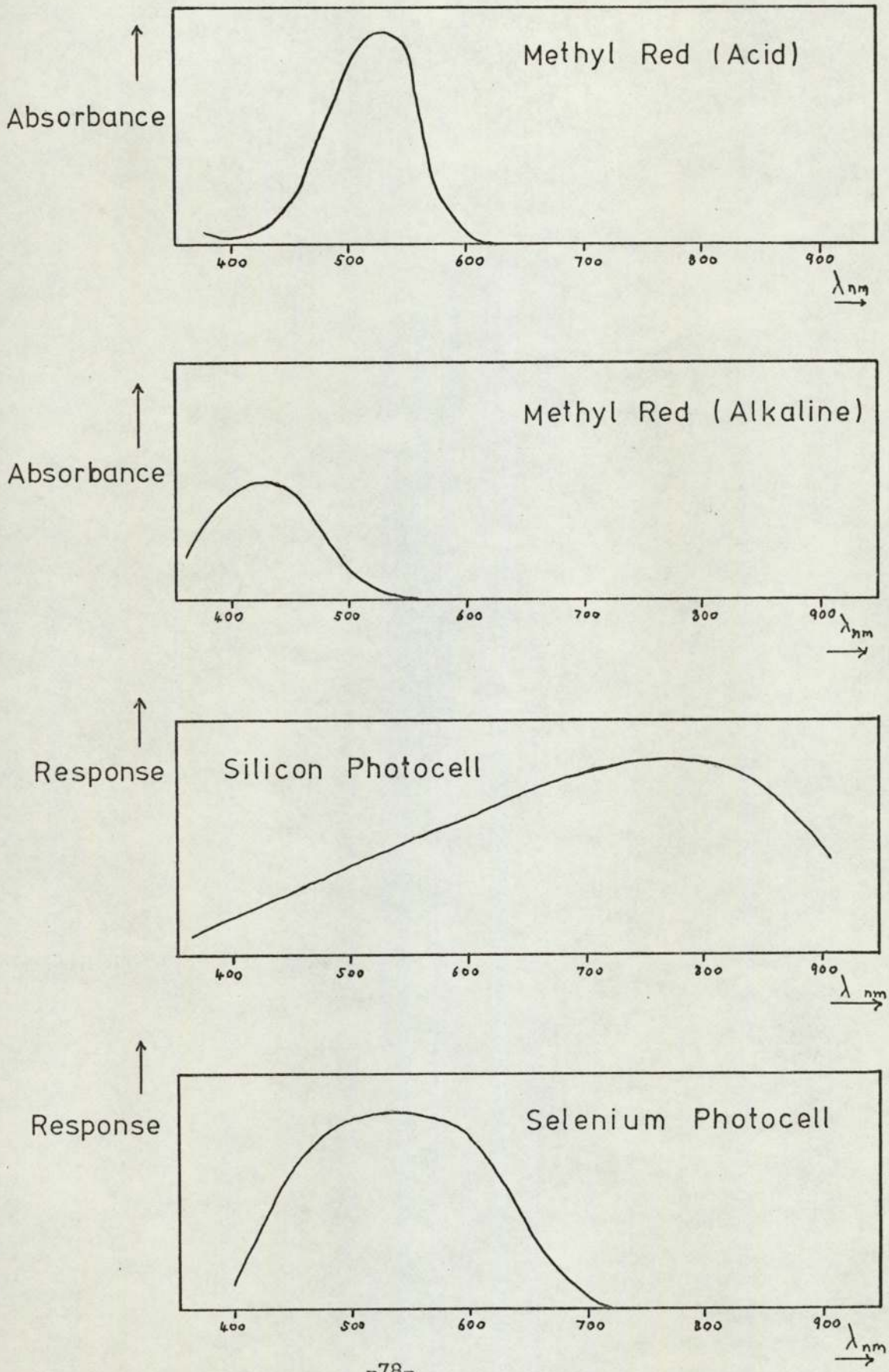

Figure 18

Circuit For Selenium Photocell

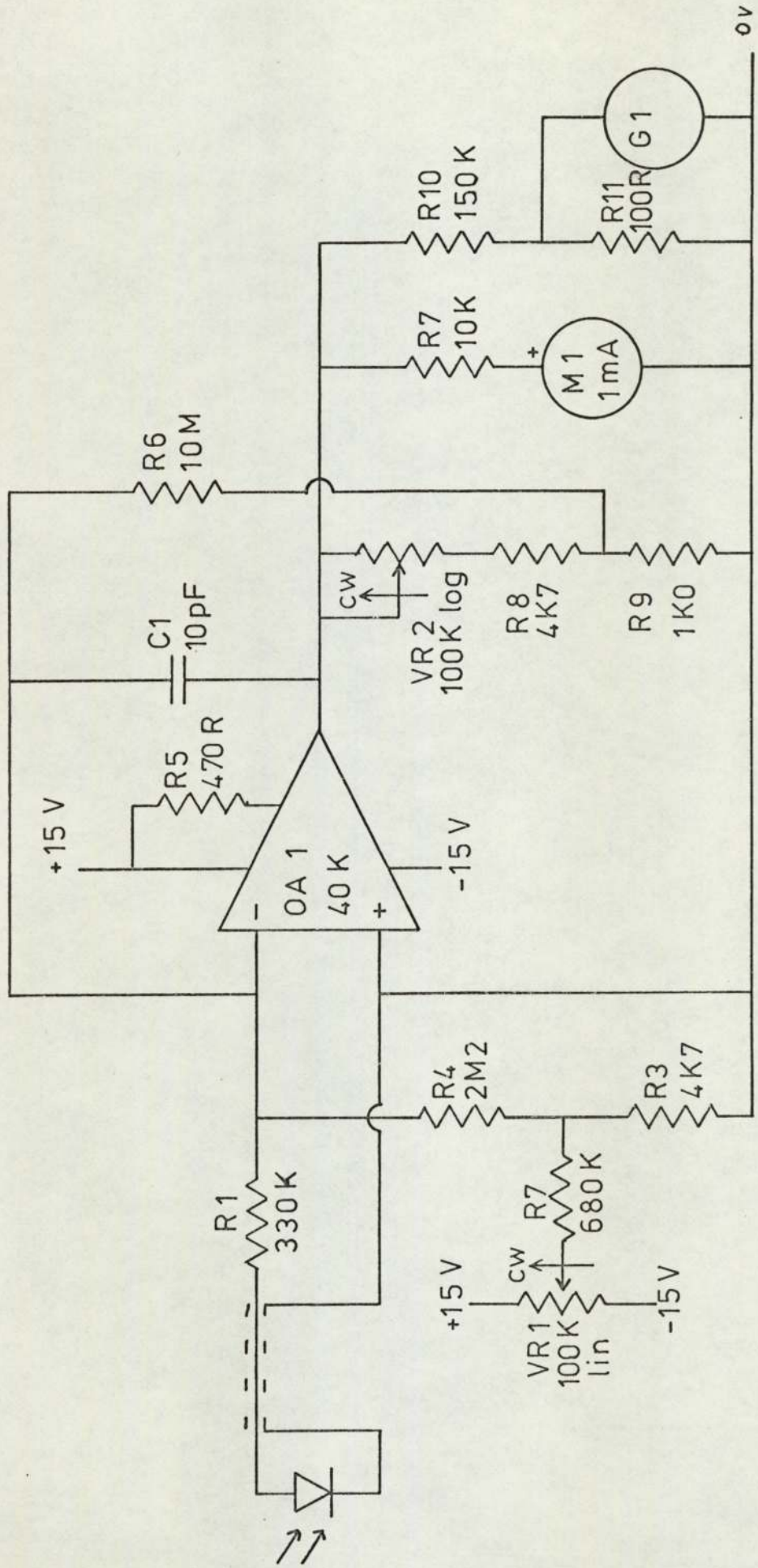

The impeller shaft was threaded 4 B.A. to fit the impeller placed centrally in the tank, and was coupled to the shaft of a $\frac{1}{8}$ H.P. D.C. motor whose bearings were used to take up the thrust from the mechanical shaft seal and the impeller. The P.T.F.E. sheet acted as a steady bush to prevent the shaft from fouling the seat of the seal. The other end of the motor shaft was connected by a short flexible drive to a mechanical tachometer scaled 0-3000 r.p.m.

The tank was filled from a 20 litre aspirator bottle on a platform about 1 m above the rig, through a brass $\frac{1}{8}$" draincock tapped into the brass plate. A second draincock at the bottom of the tank was used to dump the contents after each measurement, and a ventline at the top connected to a vertical length of plastic tubing was used to prevent air from being trapped in the tank. The holes for these three lines were drilled through the P.T.F.E. sheet at an angle to avoid trapping air bubbles in them, and in use the tank was overfilled so that there were several inches of liquid in the vent line to avoid any possibility of air being entrained.

The tracer was injected through a miniature non-return valve constructed from a piece of $\frac{1}{8}$" O/D copper tubing as shown in Fig. 19. The end was ground onto a conical mandrel to provide a belled opening, and then onto a $\frac{1}{8}$"

Figure 19

Miniature Non-Return Valve (Scale 10:1)

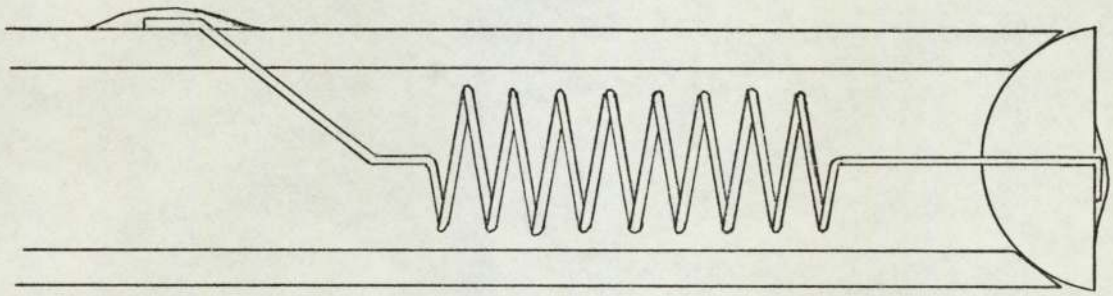

diameter polystyrene sphere. Another polystyrene sphere was cut in half and a fine hole drilled through one of the halves. A spring made from 38 s.w.g. beryllium-copper wire was fastened through this hole with epoxy resin, and the other end was threaded through a hole in the side of the tube and soldered in place, so as to locate the hemispherical bead firmly in the end of the tube. This valve was mounted through a drilled-out coupling tapped into the brass plate so as to extend 25 mm into the tank.

The valve was connected with $\frac{1}{8}$" O/D copper tubing and suitable fittings to a 10 ml glass syringe fitted with a P.T.F.E. plunger, and mounted in a PB-100 dispenser. This enabled 200 µl portions of tracer to be injected into the tank within 20 mS by pressing a button on the dispenser which was bolted to the brass plate. A slot was machined in this plate adjacent to the plunger and covered with translucent polypropylene sheet so that the slot was illuminated by the same flashlight bulbs used to light the tank. A BPY 65 phototransistor was mounted so as to accept light from this slot, and the signal from this was amplified by a second transistor connected as an emitter-follower as shown in Fig. 20, and fed to one of the galvanometers in the U.V. recorder. When the button was pressed to inject

Figure 20

Injection Marker Circuit

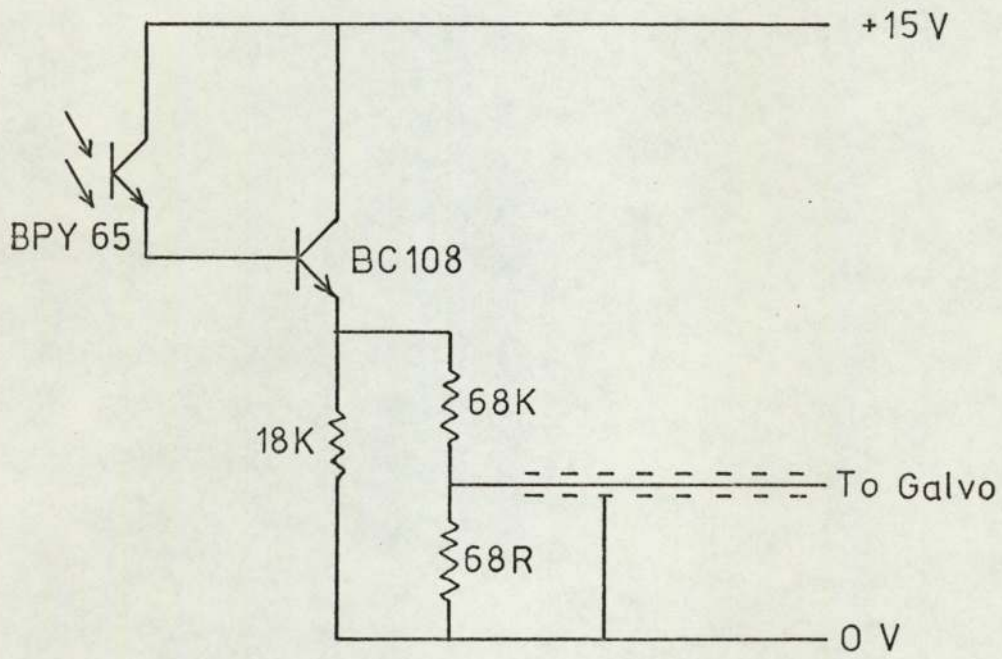

the tracer, the plunger moved forward exposing a greater length of the slot, and consequently a step was produced on the recorder trace. This was used to provide an indication of the moment of injection when the trace was analysed.

4.5.2. Method

The operating procedure was as follows:

1. A solution was made up in the 20 litre aspirator bottle containing the indicator, the acid, and any salt that was required. The syringe was filled with base from a wash-bottle with the tip removed, and the button was pressed several times to eliminate any air from the piping. The tank was washed through once or twice with the material in the aspirator.
2. The tank was filled, using the aspirator stopcock to regulate the flow rate to avoid generating bubbles, and the end of the rig was raised to ensure that all the air was expelled from the tank.
3. The motor was started and the speed adjusted to the desired value.
4. The 'shot' button on the U.V. chart recorder was pressed, and immediately afterwards the injector button. The chart speed was chosen so as to produce a trace about 100 mm long. The recorder shut off the chart feed automatically when about 200 mm of paper had been used.

5. The motor was shut off and the tank contents were discarded by opening the drain valve. The vent line was kept open throughout.

4.6. Hot Film Anemometry

4.6.1. Probe Arrangement

To measure liquid velocities, a hot film anemometer (DISA 55M10) was used, fitted with a right-angle probe type 55A83. This probe was mounted on a 24" long support fixed to a micrometer slide as shown in Fig. 21. The stationary part of the micrometer assembly was fixed to a framework extending over the tank and suitably braced so as to prevent the probe from vibrating. With this arrangement the probe could be traversed through the boundary layer on the floor of the tank with very good accuracy. The micrometer slide incorporated a magnetic device capable of exerting a small downwards force on the probe, so that the point at which the probe touched the tank floor could be readily felt as a stiffening of the movement of the micrometer barrel, but it was impossible to exert enough force through the micrometer to damage the probe. This point was used as a datum when measuring boundary layers.

Figure 21

Micrometer Probe Mount (Scale 1:4)

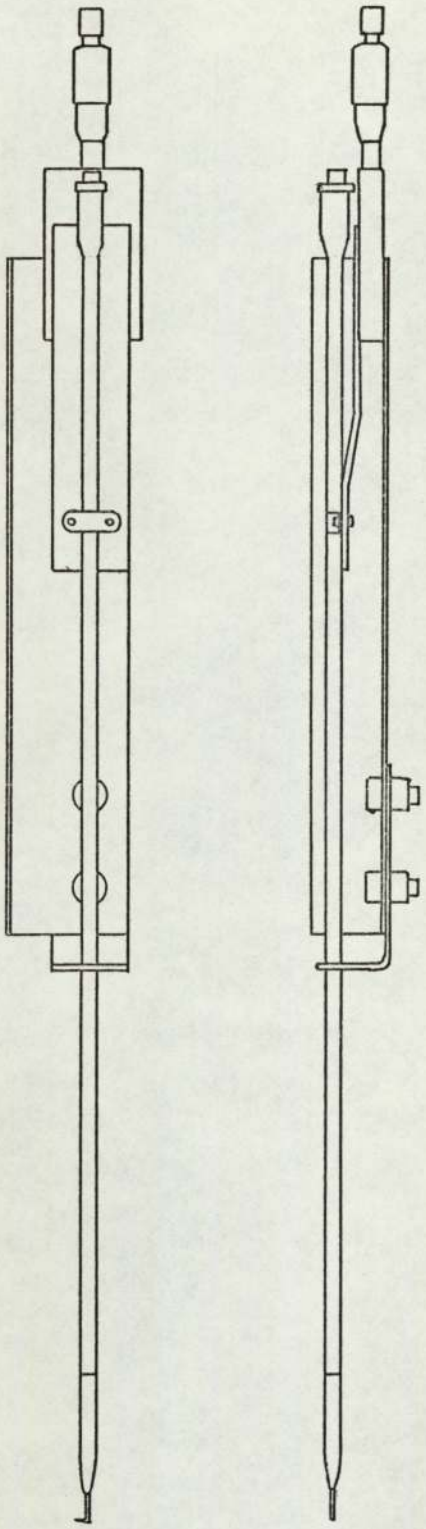

4.6.2. Degasser

It was found that the results obtained from the hot film anemometer were erratic unless the water used was filtered to remove dust and partially degassed by agitating under vacuum, as the hot tip of the probe tended to nucleate air bubbles. A rig was built for this purpose as shown in Figs. 22 & 23, capable of providing 70 litres an hour of filtered, degassed water. The degassing chamber consisted of a 24" section of 18" QVF glass pipe, an 18" to 12" reducing section and a 12" to 1" cone section. A 3-way drain stopcock at the bottom allowed the outlet to be shut off or directed either to waste or to the filter. The top of the 18" pipe was covered with a $\frac{1}{2}$" aluminium plate sealed with a rubber gasket, and this carried filling and overflow lines, a vacuum take-off point, a vacuum gauge and an agitator. The agitator was driven by a $\frac{1}{8}$ H.P. motor through a mechanical shaft seal mounted in a well formed by a short section of 3" diameter acrylic tube glued to the aluminium plate. This well was filled with water to cool and lubricate the seal as it was out of contact with the liquid in the degasser. The motor was mounted on slotted angle and drove a 72 mm diameter impeller through a $\frac{3}{8}$" stainless steel shaft. Since it was desired to achieve

Figure 22

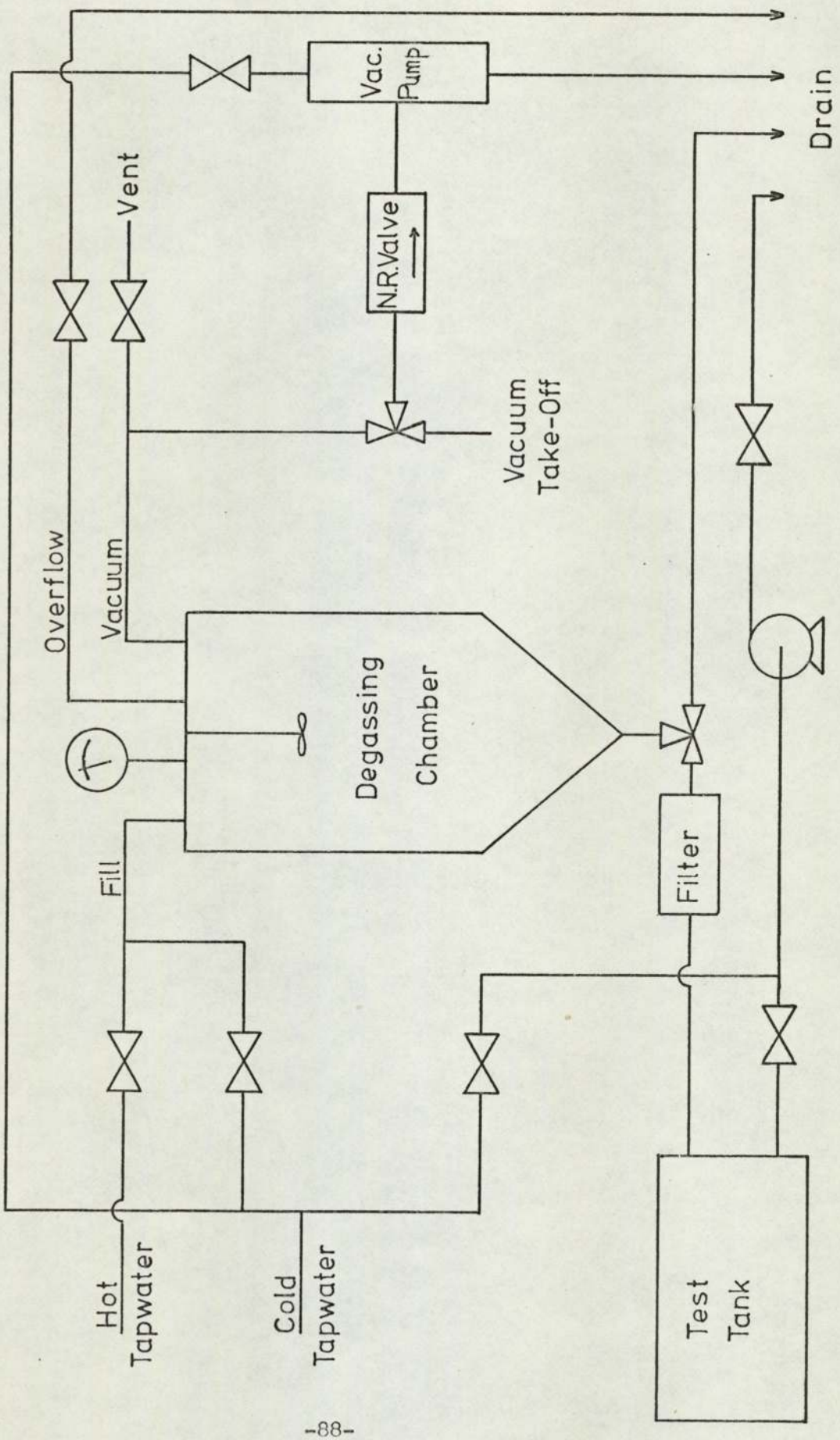
Vac. Pump
Drain
Vent
N.R.Valve
Vacuum Take-Off
Overflow
Vacuum
Degassing Chamber
Fill
Filter
Hot Tapwater
Cold Tapwater
Test Tank

Figure 23

Degasser

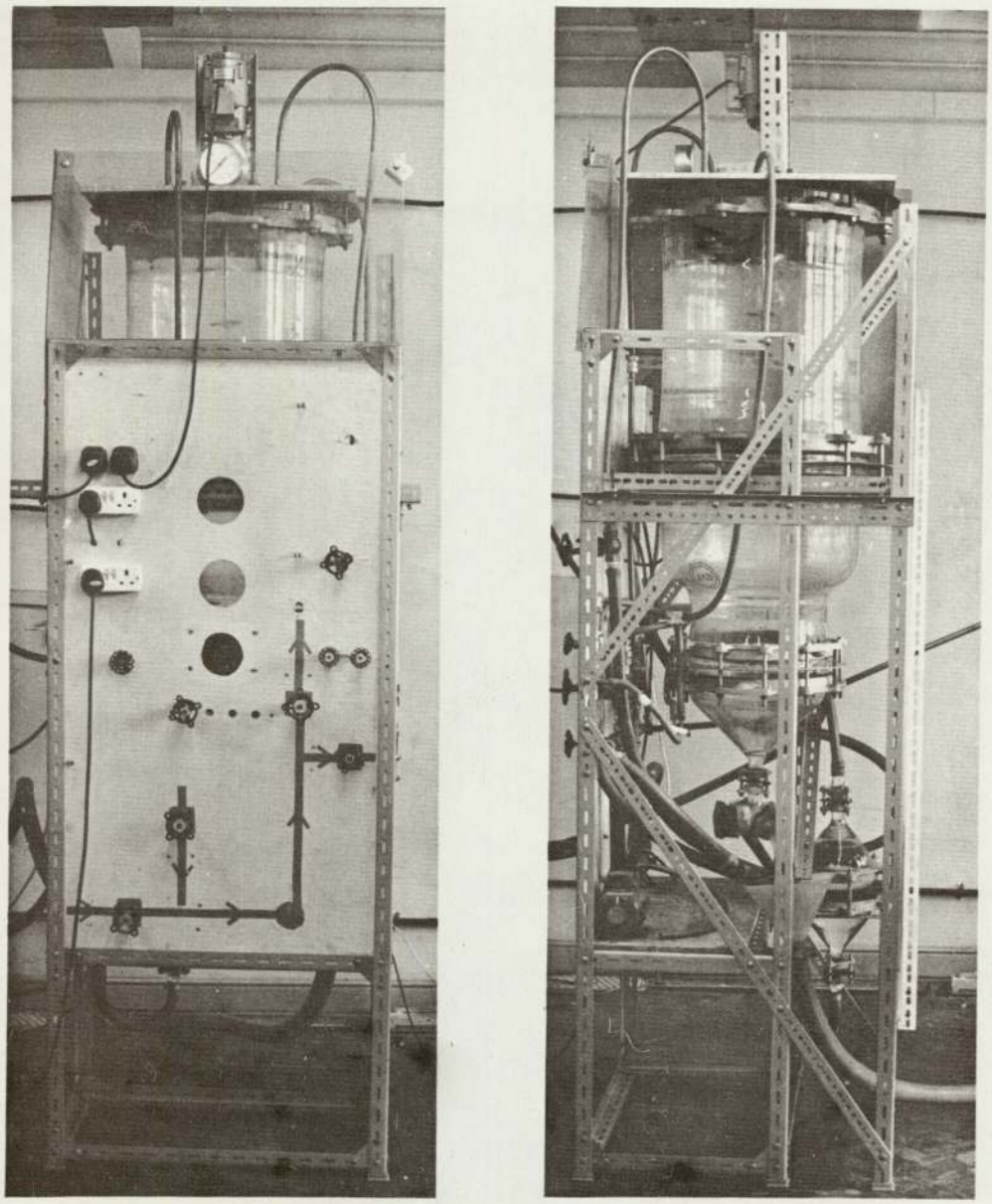

good contact between the air and the liquid, the agitator was placed centrally and the degassing chamber left unbaffled to promote vortexing.

The filling line was connected via $\frac{1}{2}$" ball valves to hot and cold tapwater supplies, so that the temperature could be adjusted to the calibration temperature of the anemometer. The overflow line went via another ball valve to waste. The vacuum take-off was connected with rubber pressure tubing to a T-piece, one side of which went to a $\frac{1}{4}$" needle valve acting as a vent, and the other to an ejector-type vacuum pump through a non-return valve, the water supply for this pump being taken from the mains via a $\frac{1}{4}$" gate valve. A two-way stopcock enabled the pump to be connected to a vacuum take-off line which was used to remove bubbles trapped under the floating roof of the test tank. The degassing chamber was mounted in a well-braced framework of slotted angle carrying the various valves, and was surrounded by an implosion guard of hardboard and wired PVC sheet.

The filter consisted of a 175 mm diameter plate of porosity No. 1 sintered glass which was sealed into a stack of four 6" neoprene rubber gaskets held together with contact adhesive, the inner two being cut away to fit the plate.

This assembly was cautiously clamped between two 6" to 1" QVF cone pieces fitted with hose adaptors, and the filter was connected between the degasser and the tank using $\frac{3}{4}$" rubber hose. It was found necessary to clean the filter with chromic acid after about 1000 litres of water had been filtered as the flow rate was reduced due to blockage of the filter.

The mode of operation of the degasser was as follows:

1. The drain stopcock was shut off, the overflow line was opened, and the degassing chamber was filled with tapwater from the hot and cold supplies to give a mean temperature of 20°C.
2. When the chamber was full, the filling lines, overflow line and vent line were shut off, and the water feed to the ejector pump was turned on. The agitator motor speed was set at around 1000 r.p.m.
3. During degassing, the vacuum gauge reading increased from around 15" of mercury initially to 27" after about 15 min. The agitator motor was then switched off and the chamber left under vacuum for a further 5 mins. to allow bubbles produced by the agitator to settle out.
4. The water feed to the ejector pump was turned off and the vent line opened. The drain stopcock was then turned so as to feed the degassed water through the filter to the tank.

4.6.3. Calibration

The hot film anemometer was calibrated using laminar pipe flow to provide a known steady velocity. In order to keep the flow laminar up to high velocities, a pipe of small diameter is needed, so a $\frac{1}{4}$" bore glass tube was used. The calibration rig is shown in Fig. 24. The flow of water from a 20 litre aspirator bottle was controlled by a small needle valve, a sintered glass filter removed any dust, and the water was fed to a 1 metre long section of $\frac{1}{4}$" bore glass tubing with the probe inserted in the end. A further short length of tubing was added to ensure that the liquid flowed steadily round the probe, without distorting the flow pattern upstream. The outside of the tubes was coated with silicone grease to ensure that the liquid continued to flow through the second tube. All the tubing was lagged with glass wool to avoid temperature fluctuations due to air currents in the room.

Flow inside a smooth circular pipe is known to produce a parabolic velocity profile provided that the Reynolds number is less than 2100, and the entry length greater than 74 pipe diameters (Bird, Stewart & Lightfoot (55)). The centre-line velocity is then twice the mean velocity. For the pipe used, this allows a centre-line velocity of up to 660 mm s^{-1}, and the second condition is adequately satisfied

Figure 24

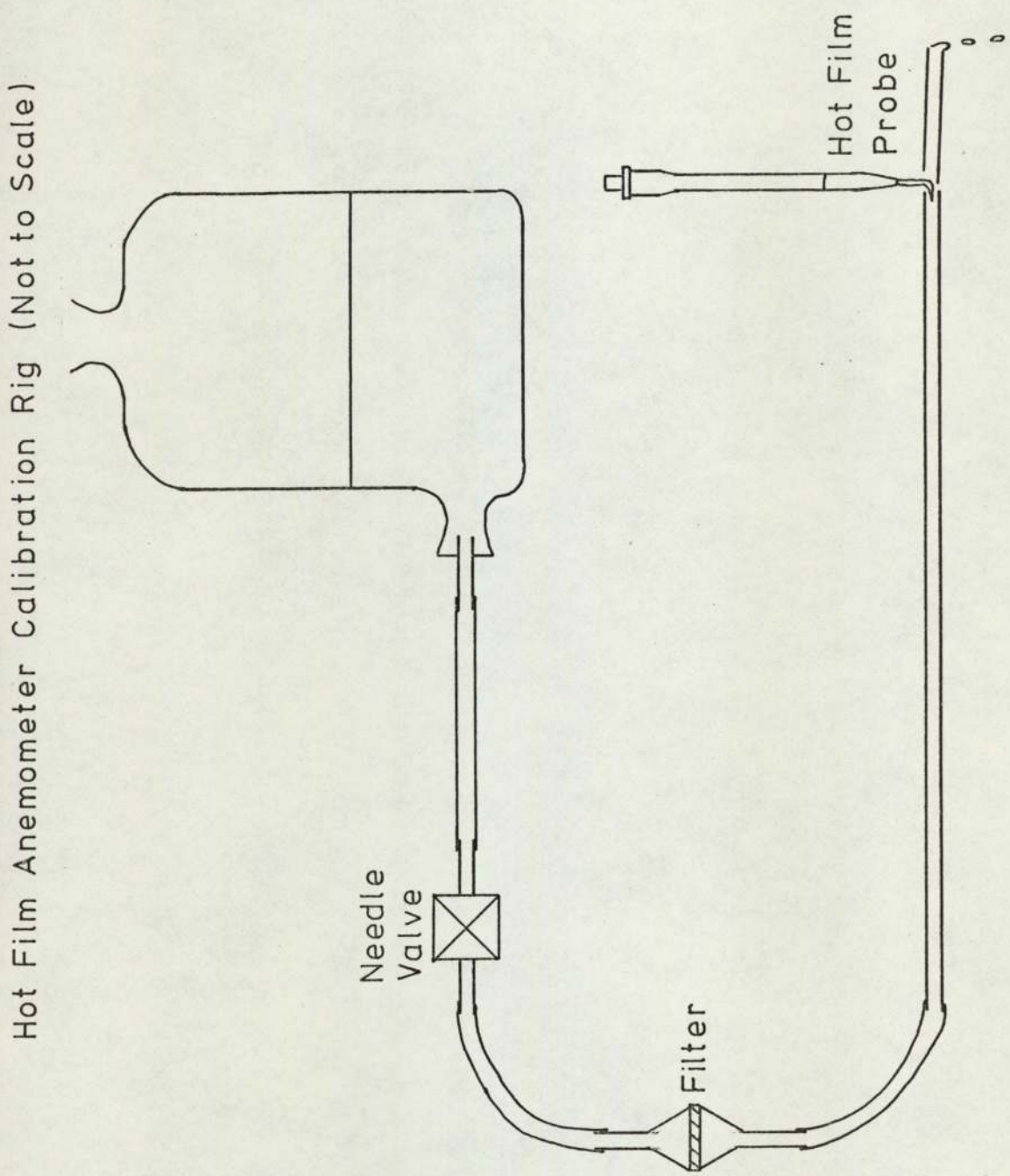
Hot Film Anemometer Calibration Rig (Not to Scale)
Hot Film Probe
Needle Valve
Filter

as the pipe length is equal to 150 diameters. It can be shown (Appendix 4) that the velocity averaged over the width of the probe is equal to the centre-line velocity within 1%.

The anemometer output was fed through suitable attenuators and filters to a chart recorder, a digital voltmeter and an electronic integrator as shown in Fig. 25. The digital voltmeter was used to provide a quick indication of the voltage during calibration and the integrator to average readings obtained from turbulent flows in the tank.

The calibration procedure was as follows:

1. The aspirator was filled with degassed water at 20°C, and the needle valve opened to give a low flow rate.
2. The anemometer, having been allowed to warm up for at least half an hour, was set to the 'resistance measure' position, and the decade resistors adjusted to obtain a balance on the meter.
3. The indicated resistance was increased by 15%, and the anemometer was set to the 'operate' position.
4. The probe position was adjusted to give a maximum reading on the chart recorder, indicating that the film was positioned on the centre-line of the pipe.
5. The flow-rate was adjusted over a wide range by means of the needle valve, and was measured by catching the water in a beaker and weighing the amount collected in a measured time.

Figure 25

Hot Film Anemometer Interconnection Diagram

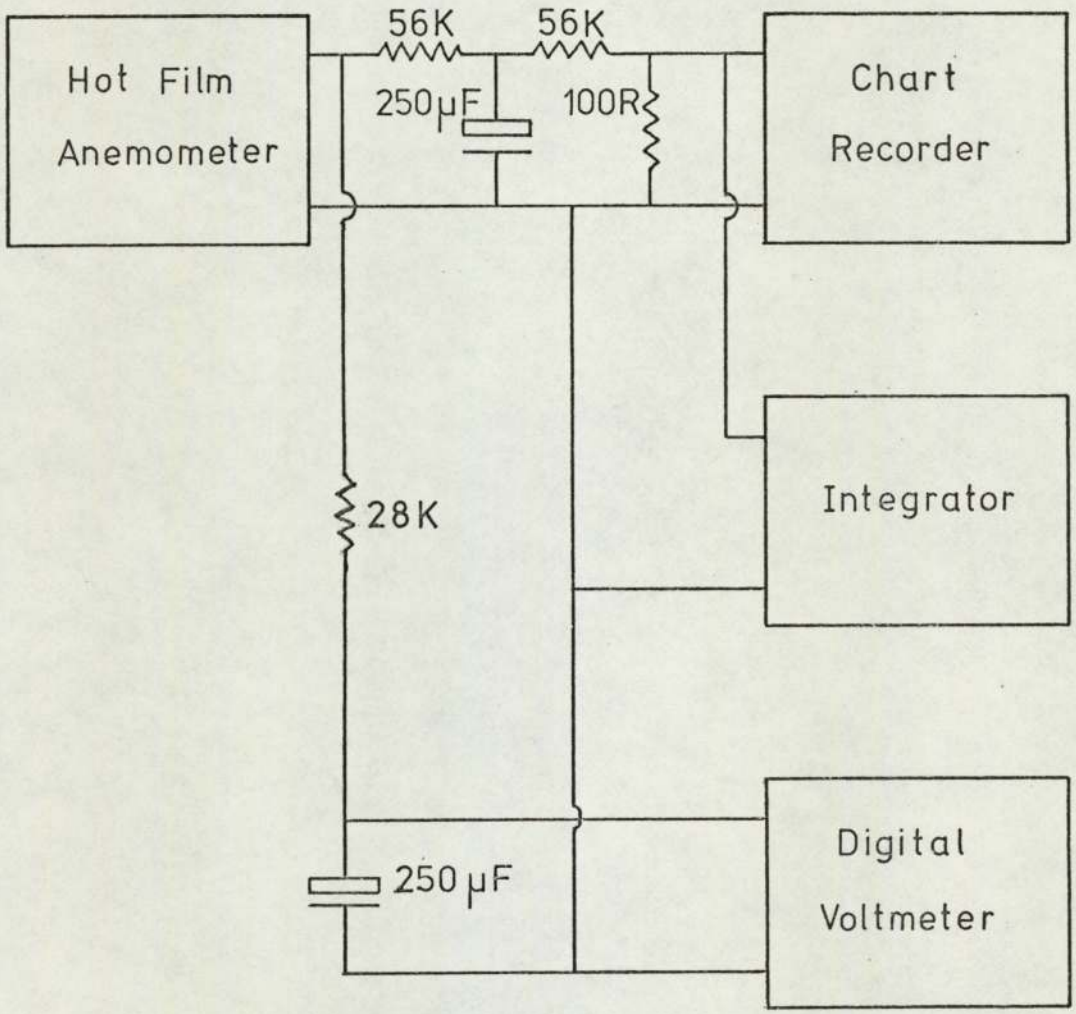

A calibration curve was plotted of the digital voltmeter reading against the flow-rate, points being obtained at intervals of about 0.25 V.

The procedure used to measure flow velocities in the tank was similar, the probe being rotated about a vertical axis to obtain a maximum reading. For precise results it was found necessary to average the signal over about five minutes. This was done by switching the integrator to the 'integrate' mode for this length of time and comparing the reading printed out after this time with that obtained with a steady voltage input from the calibration rig.

4.7. 31 Metre Tank

Some measurements of mixing times were also carried out on a 31 metre diameter tank using the conductivity method. The tank contained aviation turbine kerosine, and the tracer used was ASA-3 anti-static additive. This is capable of acting as an electrolyte when dissolved in a hydrocarbon, and a concentration of 0.5 ppm is capable of increasing the electrical conductivity by 200 psiemens/m. The conductivity probe was a 'Maihak' conductivity meter reading 500 psiemens/m full scale. The tank was fitted with a 0.61 m diameter side-entry mixer angled 10° left of centre as shown in Fig. 26.

Fig. 26

31m. Diameter Tank

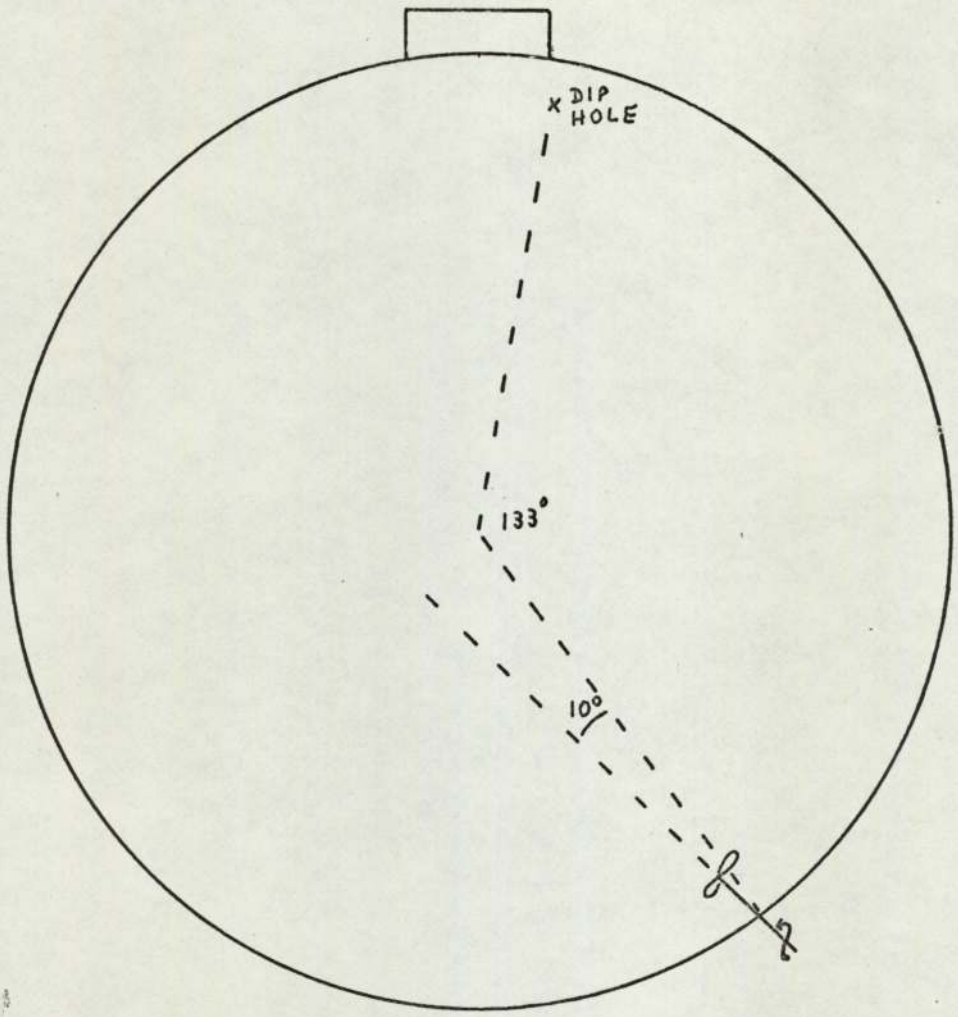

The tracer was added as a solution in 4 litres of kerosine through a 25 mm bore nitrile rubber hose weighted with a section of steel pipe at the end, passed through a sampling hole in the tank roof, discharging at a point 2 metres above the base of the tank. The tracer solution was poured into a funnel in the top of the hose, and flushed through with kerosine within one minute. The conductivity meter probe was dropped through the same sampling hole to a depth equal to half the liquid depth, and the conductivity was measured at intervals of 30 seconds to 1 minute. The terminal mixing time was determined in the same way as for the model tank.

5. Results and Discussion

5.1. Distribution of Mixing Times

Most of the measurements of terminal mixing times were carried out by the indicator method, and each measurement was repeated ten times. Although it seems reasonable to take the arithmetic mean of these measurements as the best estimate of the 'typical' value, this is correct only if the measured values follow a Gaussian distribution. Although only a small number of values are available for any one set of conditions, a reasonable estimate of the distribution function can be obtained by using measurements obtained under different conditions, normalised by dividing by the mean value for that set of conditions. This distribution function can be used not only to determine the correct way of combining several values, but also to provide a means of estimating the correct safety margin to use when applying the results. The standard deviation and skewness were calculated separately for the 70 mm and 1.2 m tanks, but since they were found to be nearly equal for the two systems, all the results were combined to provide an estimate of the distribution function obtained from as many experimental values as possible. The results are plotted as a histogram in Fig. 27 obtained from a total of 800 data points.

The distribution shows considerable skewness to the

Figure 27

Distribution of Values of $\tau/\bar{\tau}$

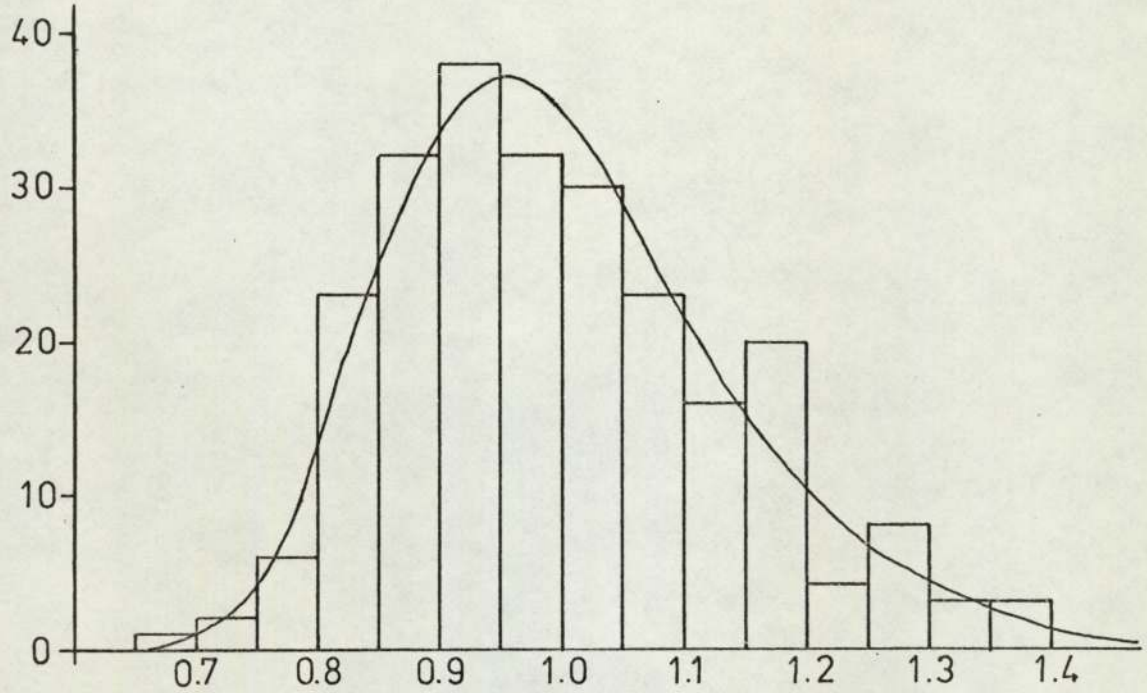

Distribution of Values of $\bar{\tau}'/\tau$

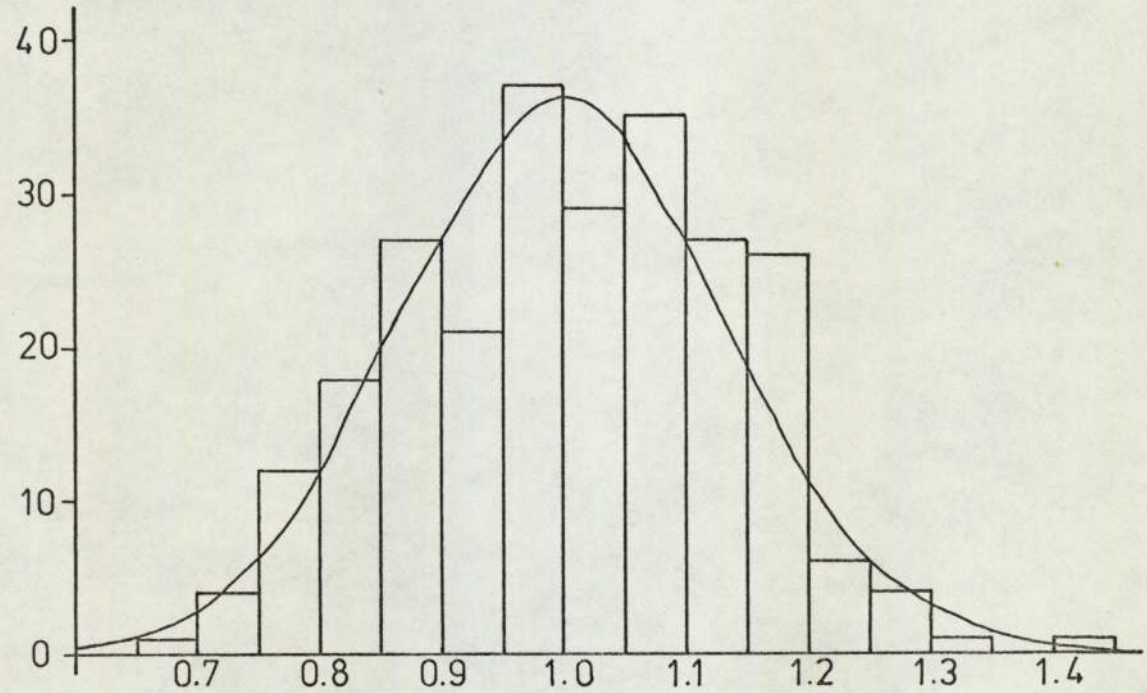

right (skewness = 0.35), and a χ^2 test rejected the hypothesis that the mixing times are normally distributed at the 95% confidence level. An alternative possibility is that the mixing rates (rather than mixing times) are normally distributed so that $\bar{\tau}'/\tau$ should be normally distributed, where $\bar{\tau}'$ is the harmonic mean given by

$$\frac{1}{\bar{\tau}'} = \frac{1}{n}\sum_{i=1}^{n}\frac{1}{\tau_i}$$

The data were recomputed on this basis, and the resultant distribution had a skewness of only 0.12. A χ^2 test failed to reject the hypothesis that this distribution was normal at the 95% confidence level, and this was therefore assumed to be the case. The corresponding distribution function for τ is superimposed on the histogram of Fig. 27. The best estimate of the centre of the distribution is given by $\bar{\tau}'$, and this quantity has therefore been used in all measurements of mixing times. The deviation from $\bar{\tau}$ is less than 5% in all cases.

The standard deviation from the mean was 0.109. Since the values of $\bar{\tau}'$ were obtained as the harmonic mean of ten values, the best estimate of the standard error in a single value is $0.109\ \frac{10}{9} = 0.115$. The 99.9% level of the cumulative normal probability function occurs at 3.1 standard deviations, so in order to be certain of mixing for a time

greater than τ_1 with 99.9% confidence, $\bar{\tau}'/\tau_1$ must be allowed to be low by 3.1 S.D.s, i.e. by 0.36. This gives $\bar{\tau}'/\tau_1 = 0.64$, $\tau_1 = 1.6\,\bar{\tau}'$. A safety factor of 60% should therefore be allowed to take account of random fluctuations in the mixing time.

The harmonic mean of the terminal mixing times will hereafter be referred to simply as the mixing time τ.

5.2. Mixing Times

5.2.1. Indicator Method

Using the indicator method in the 1.2 m tank, the mixing time was measured as a function of the impeller speed, impeller diameter, liquid depth and impeller angle. The results are tabulated in Tables 1-6 and plotted in Figs. 28-33.

It was found that the graph of mixing time against impeller speed was different for different liquid depths. Fig. 28 shows the graph for a depth of 200 mm, and Fig. 29 for 300 mm on logarithmic axes in each case. Comparison with the results of Fox & Gex (12) and Norwood & Metzner (18) shows that the graph of Fig. 28 corresponds to the turbulent regime, and that of Fig. 29 to the incipient laminar regime. In the works cited the different regimes were obtained

Figure 28

Mixing Time as a Function of Impeller Speed in the Turbulent Regime by the Indicator Method

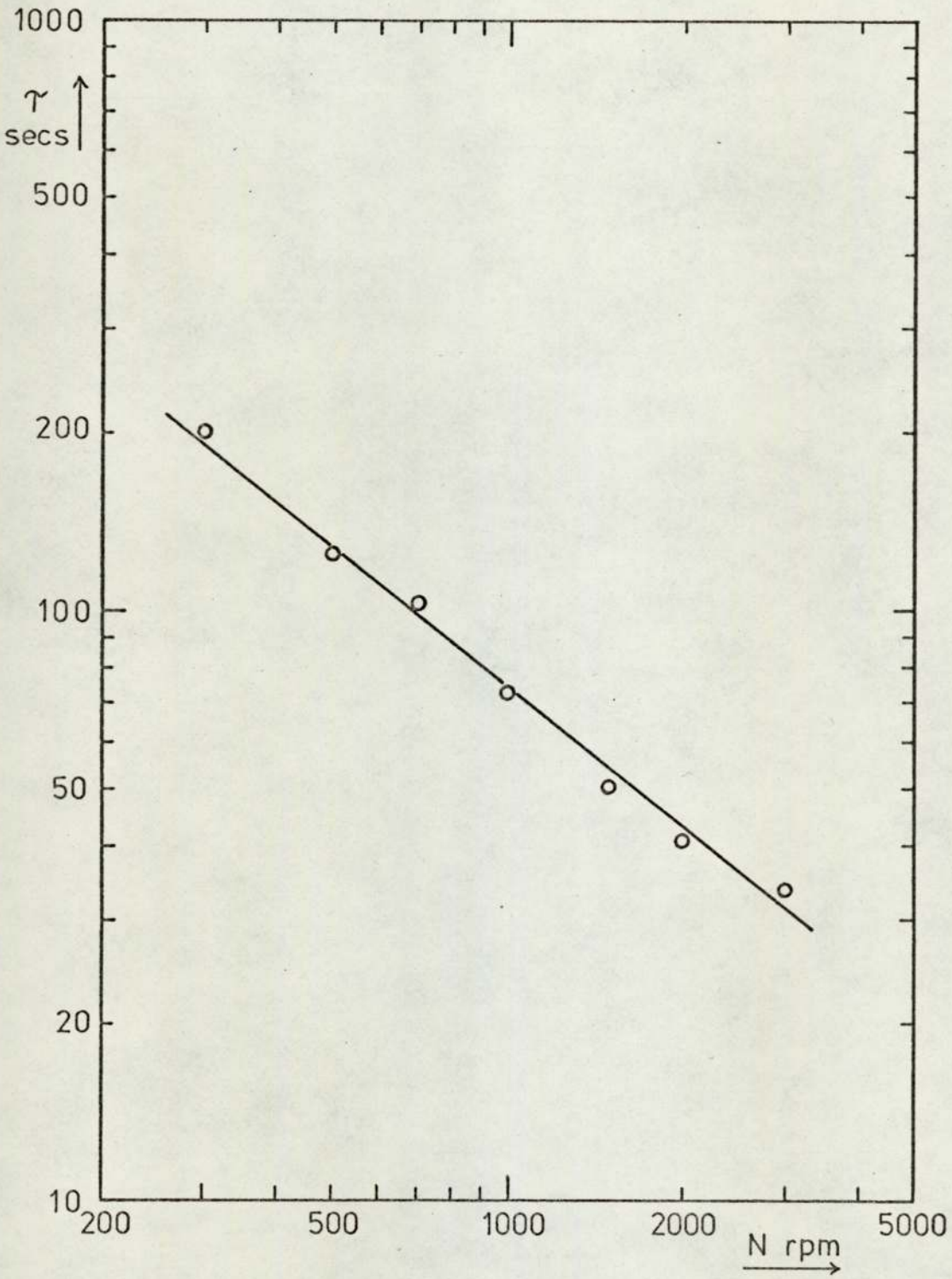

Figure 29

Mixing Time as a Function of Impeller Speed in the Laminar Regime by the Indicator Method

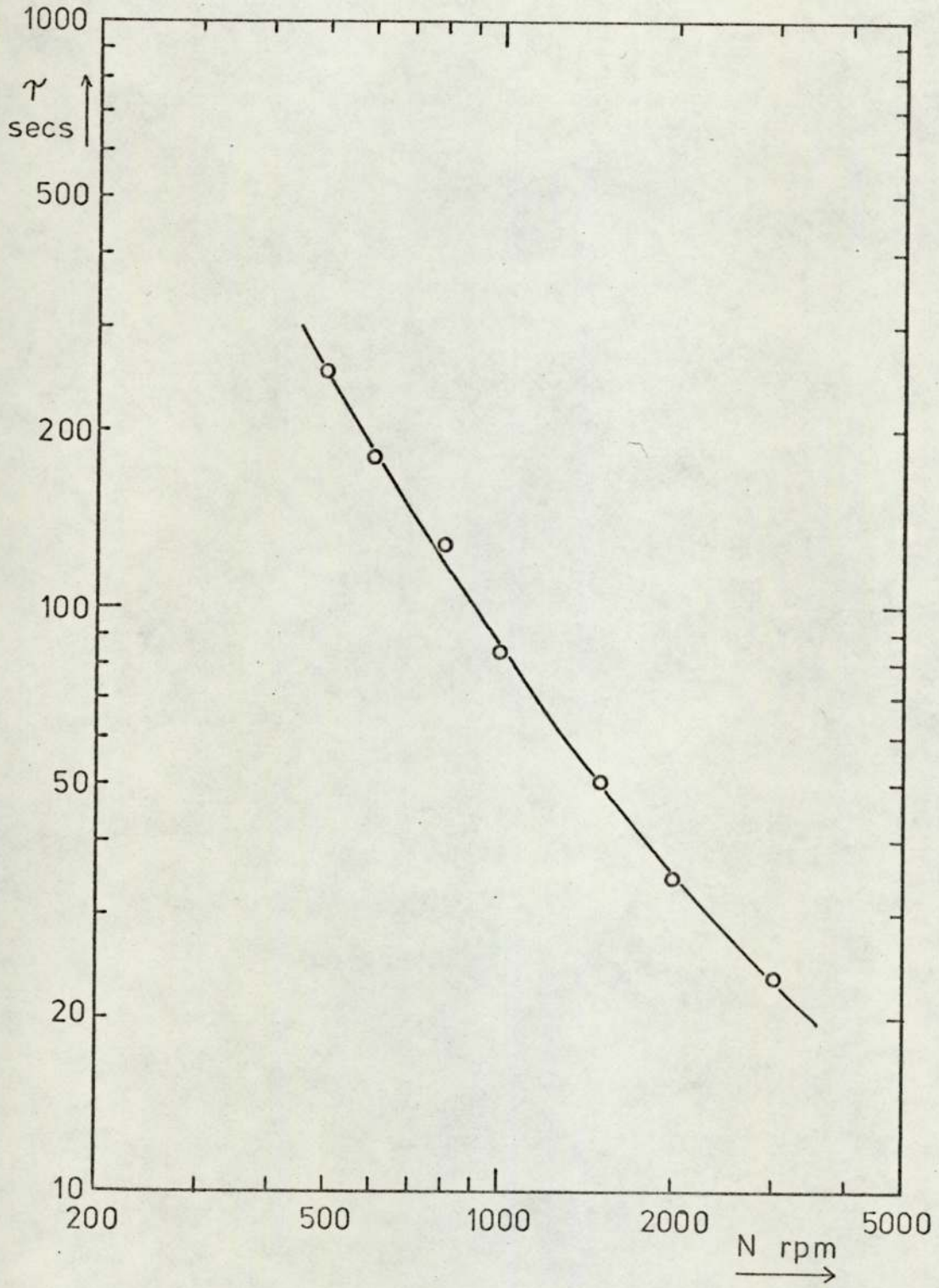

Figure 30

Mixing Time against Impeller Diameter in the Turbulent Regime

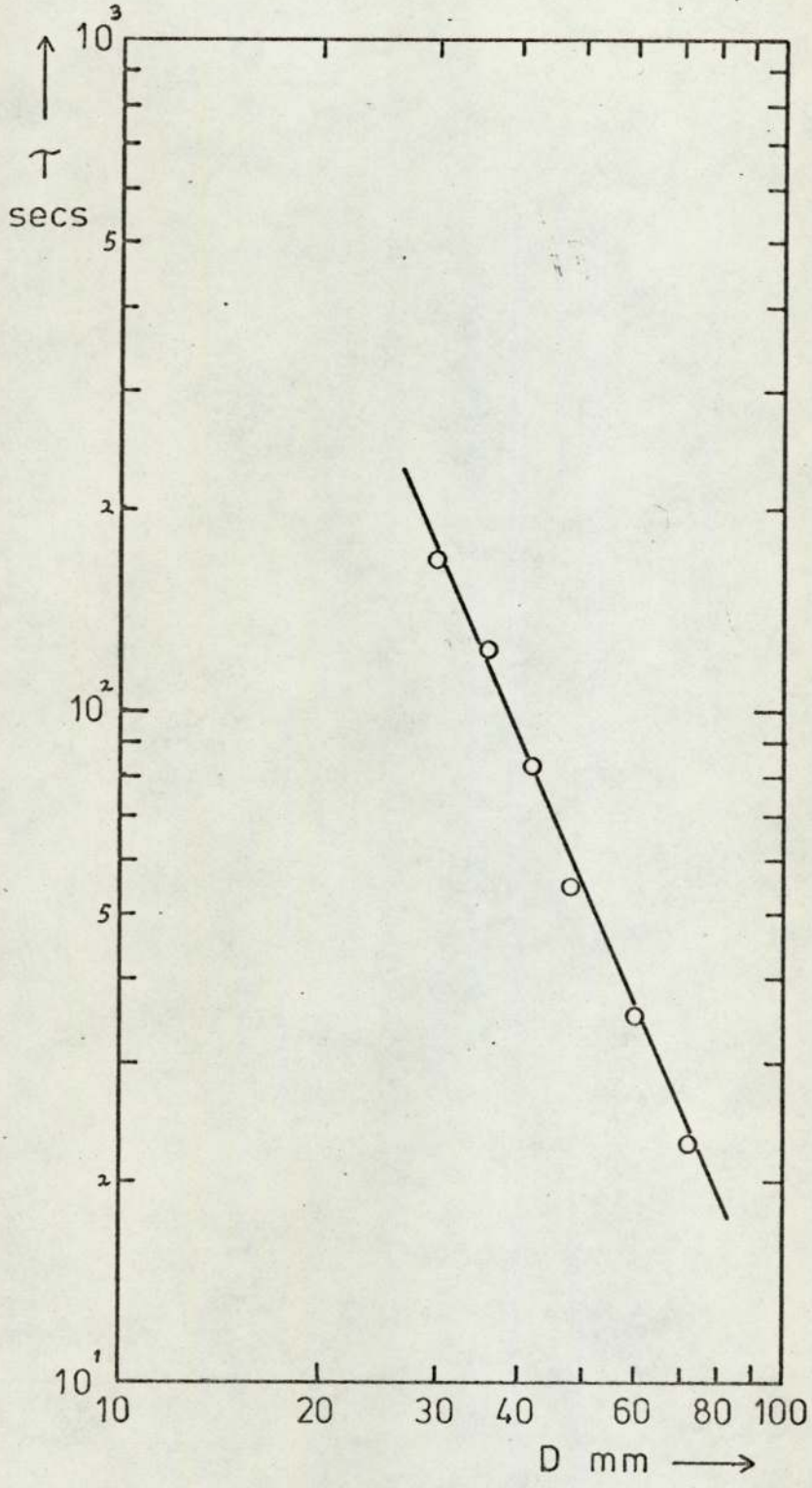

Figure 31

Mixing Time against Impeller Diameter in the Incipient Laminar Regime.

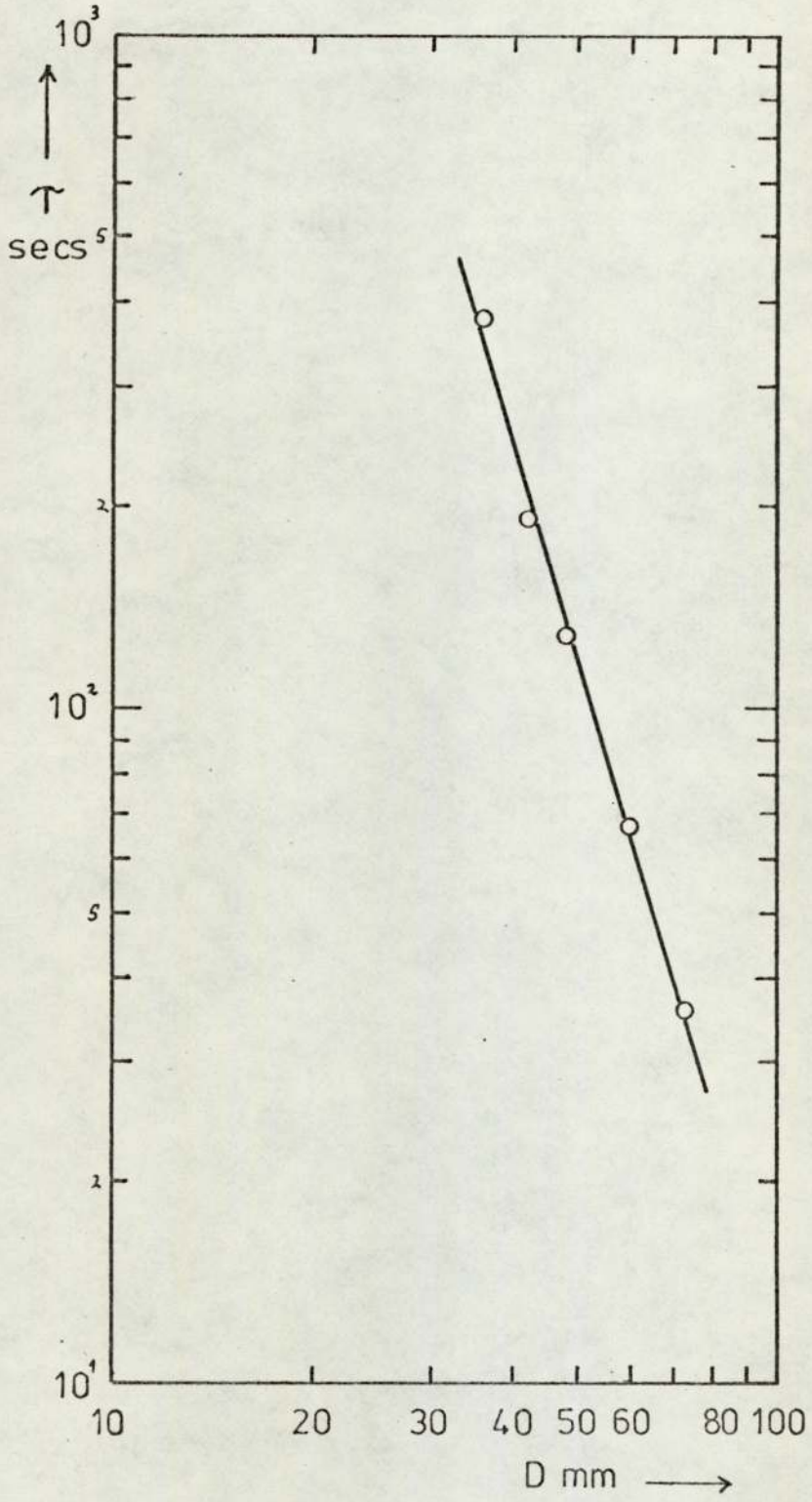

Figure 32

Mixing Time against Liquid Depth

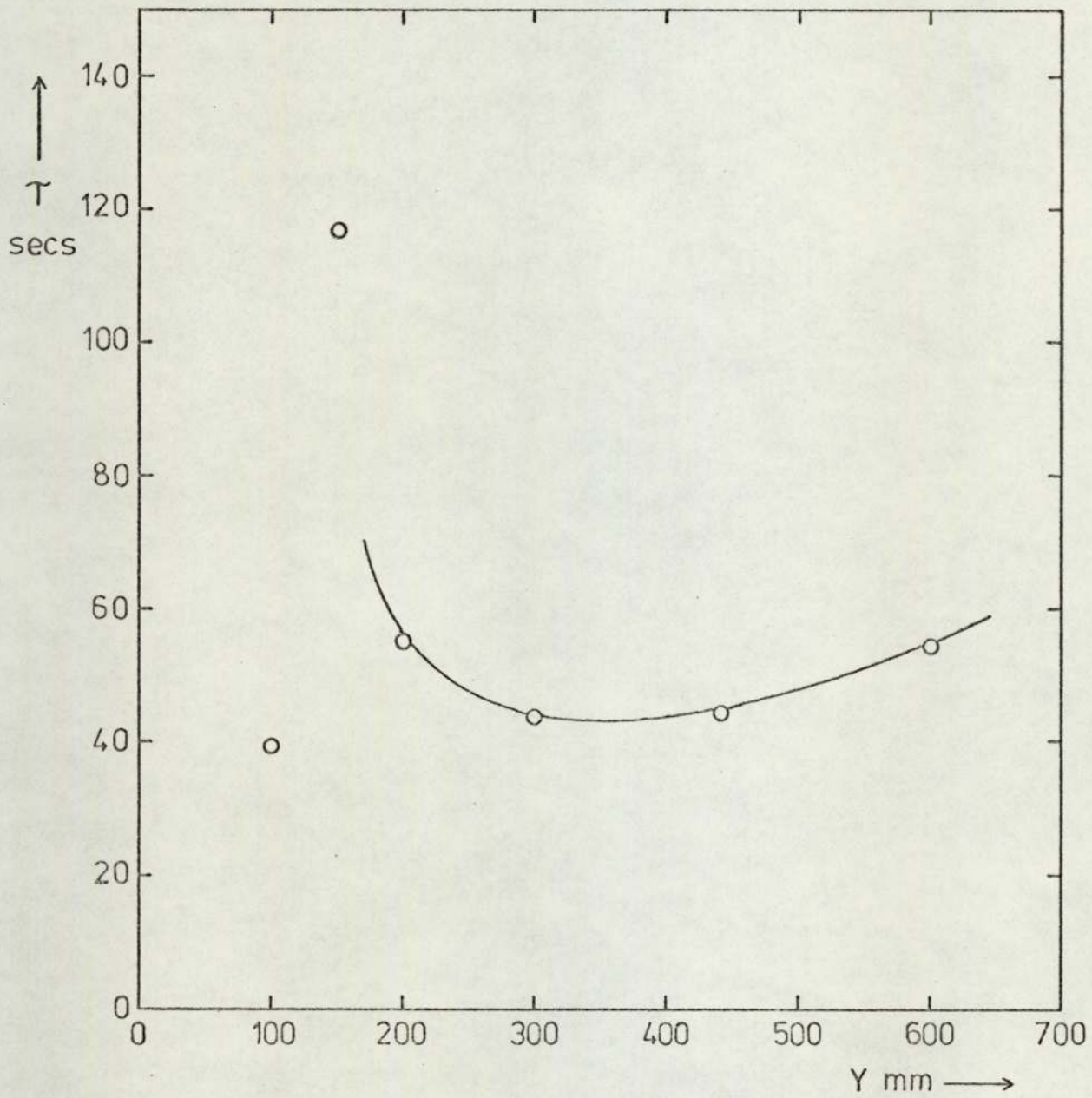

Figure 33

Mixing Time against Impeller Angle

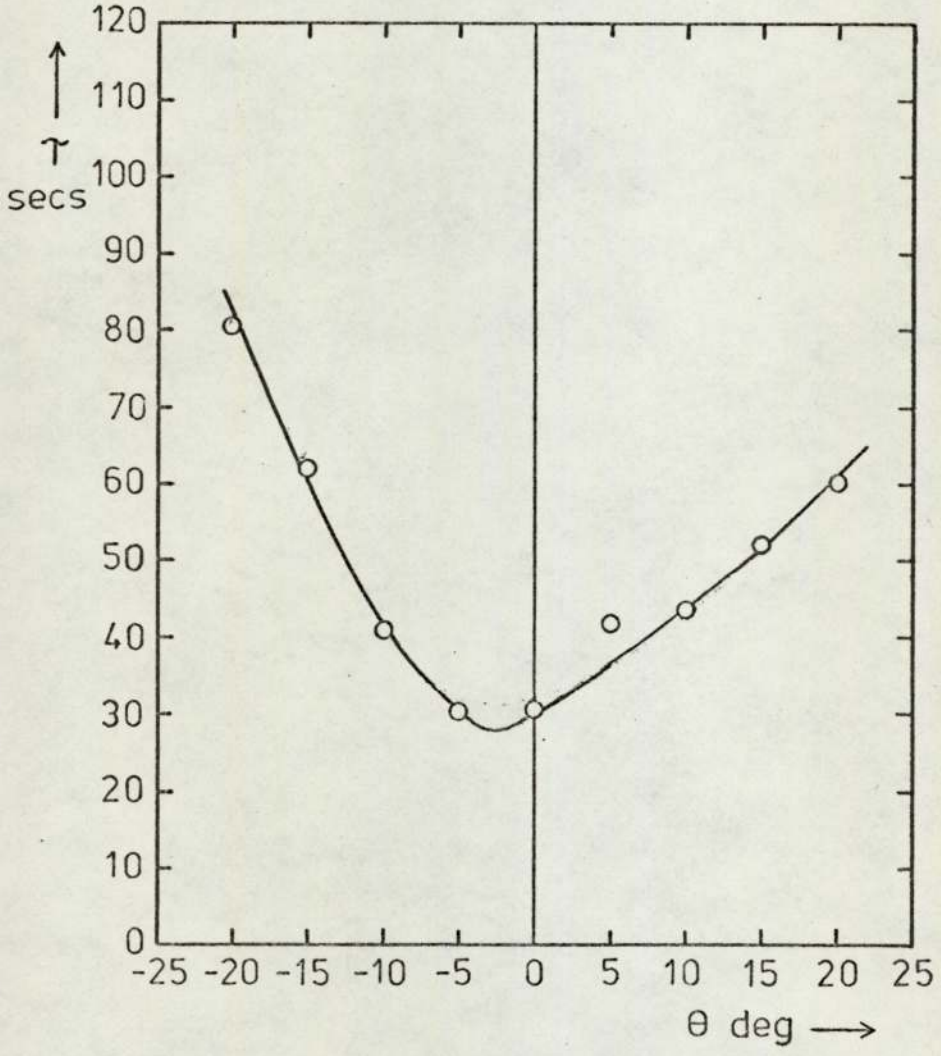

simply by varying the impeller Reynolds number. This indicates that the transition from incipient laminar to turbulent flow depends on the system geometry as well as the impeller Reynolds number. With a liquid depth of 300 mm the slope of the graph varies from -1.7 to -1.0, indicating that the flow is tending towards the turbulent regime at high Reynolds number, so that the conditions here should more correctly be termed transitional. For a liquid depth of 200 mm, the flow is fully turbulent throughout, giving a straight line of slope -0.79 ± 0.03, as determined by linear regression on logarithmic axes using the computer program described in Appendix 5. This value is in quite good agreement with the value of $-\frac{5}{6}$ found by Fox & Gex (12) using the same method. In carrying out their dimensional analysis they assumed that, for geometrically similar situations, the important parameters were impeller speed, impeller diameter, liquid viscosity, and gravitational acceleration, giving rise to the correlation

$$N\tau \propto \left(\frac{ND^2}{\nu}\right)^{-\frac{1}{6}} \left(\frac{N^2D}{g}\right)^{+\frac{1}{6}}$$

which written in dimensional form gives

$$\tau \propto N^{-\frac{5}{6}} D^{-\frac{1}{6}} \nu^{+\frac{1}{6}} g^{-\frac{1}{6}}$$

In the present case, a side-entry mixer was used so that no vortex was formed, and the liquid surface was almost

undistorted. Consequently g cannot be one of the parameters affecting the mixing time, and some other parameter must be introduced to enable a satisfactory dimensional analysis to be carried out. It is not sufficient merely to use N, D & ν as this would imply $N\tau \propto \left(\frac{ND^2}{\nu}\right)^{+1/6}$ suggesting that the mixing time would decrease with increasing viscosity, which is at variance with the data of Fox & Gex (12).

The only other non-geometrical parameter which appears to be capable of influencing the mixing time is the molecular diffusivity, $\mathcal{D}$, of the tracer material. If this is used, the correlation can then be written, in dimensionless form, as

$$N\tau \propto \left(\frac{ND^2}{\mathcal{D}}\right)^{+0.21}$$

which in dimensional form is

$$\tau \propto N^{-0.79} D^{0.42} \mathcal{D}^{-0.21}$$

Furthermore, the diffusivity of ions in solution is itself a function of the viscosity. Thus for H^+ ions, $\mathcal{D} \propto \nu^{-0.63}$, and for OH^- ions $\mathcal{D} \propto \nu^{-0.73}$ (56,57). Taking a mean value $\mathcal{D} \propto \nu^{-0.68}$ this gives

$$\tau \propto N^{-0.79} D^{0.42} \nu^{+0.14}$$

The index for viscosity is then in excellent agreement with that obtained by Fox & Gex of $+1/6$.

This correlation may thus be used for both the present data and that of Fox & Gex (12) and does not involve the

gravitational acceleration. The index of Reynolds number is zero, as would be expected for fully turbulent conditions, although the viscosity still influences the mixing time through its effect on the molecular diffusivity.

Measurements of the mixing time as a function of impeller diameter were carried out using geometrically similar brass impellers, and it was attempted to cover both the incipient laminar and the fully turbulent regimes. For the incipient laminar regime, the liquid depth was 300 mm, and the impeller speed was kept low (800 r.p.m.). The graph of mixing time against impeller diameter on logarithmic scales (Fig. 31) was linear with slope -3.29±0.15 in accordance with the theoretical result that it should have a slope twice that of the N-τ curve in this region i.e. 2 x -1.7. For the turbulent regime, the liquid depth was 200 mm and the speed was kept high (2000 r.p.m.). The graph, shown in Fig. 30, had a slope of -2.34±0.07. This is considerably higher than the expected value of -1.6. Probably this is because fully turbulent conditions were not reached with the smaller impellers, so that the results tended towards those obtained in the incipient laminar regime.

The curve of mixing time against liquid depth shows a rather complicated behaviour, as shown in Fig. 32. At large depths the mixing time increases slowly with the

depth. Around 150 mm depth, a large stagnant region is formed at the centre of the tank, leading to very long mixing times. This suggests that the optimum impeller angle is probably a function of the liquid depth. For 300 mm depth, the curve of mixing time against impeller angle shown in Fig. 33 shows that the conventional angle of 10° left of centre gives a slightly longer mixing time than can be obtained with the optimum angle of 5°. The irregular shapes of these curves suggest that the flow pattern changes considerably as the geometry is altered, and it seems unlikely that any general expression can be obtained for the effect of the various geometrical parameters. It is therefore necessary to model any particular mixing situation separately.

5.2.2. Conductivity Method

If the additional quantity in the dimensional analysis is the molecular diffusivity, this should apply only to measurements made by the indicator method, and not to measurements made by the conductivity method, in which homogeneity is required down to the scale of the probe rather than down to a molecular scale. This was tested by measuring the mixing time as a function of impeller speed by the conductivity method at high Reynolds number.

The results are listed in Table 7 and plotted in Fig. 34. Comparison with results obtained by the indicator method shows that the data points at the lower values of N were taken in the transitional regime, and these points lie below the best fit straight line. If these points are eliminated, the line has a slope of -1.03 ± 0.03, in good agreement with the expected value of -1. Although it seems curious that the points in the transitional regime have a smaller value of $N\tau$, implying that increasing the viscosity can decrease the mixing time, this result is not unreasonable, since the viscosity affects the flow pattern, which could lead to a decrease in mixing time in the vicinity of the probe, although the overall mixing time is increased, as observed by the indicator method. A similar result was found by Landau et al. (23) who found that for a top-entry propeller mixer in a baffled tank, the dimensionless mixing time at low Reynolds number was lower near the impeller, but higher elsewhere, compared with values obtained in the turbulent regime.

In order to determine the effect of probe size on the measured mixing time, a series of measurements were carried out using a set of geometrically similar conductivity probes. The results are listed in Table 8 and plotted in Fig. 35. The slope of the regression line was -0.03 ± 0.02, indicating

Figure 34

Mixing Time as a Function of Impeller Speed in the Turbulent Regime by the Conductivity Method

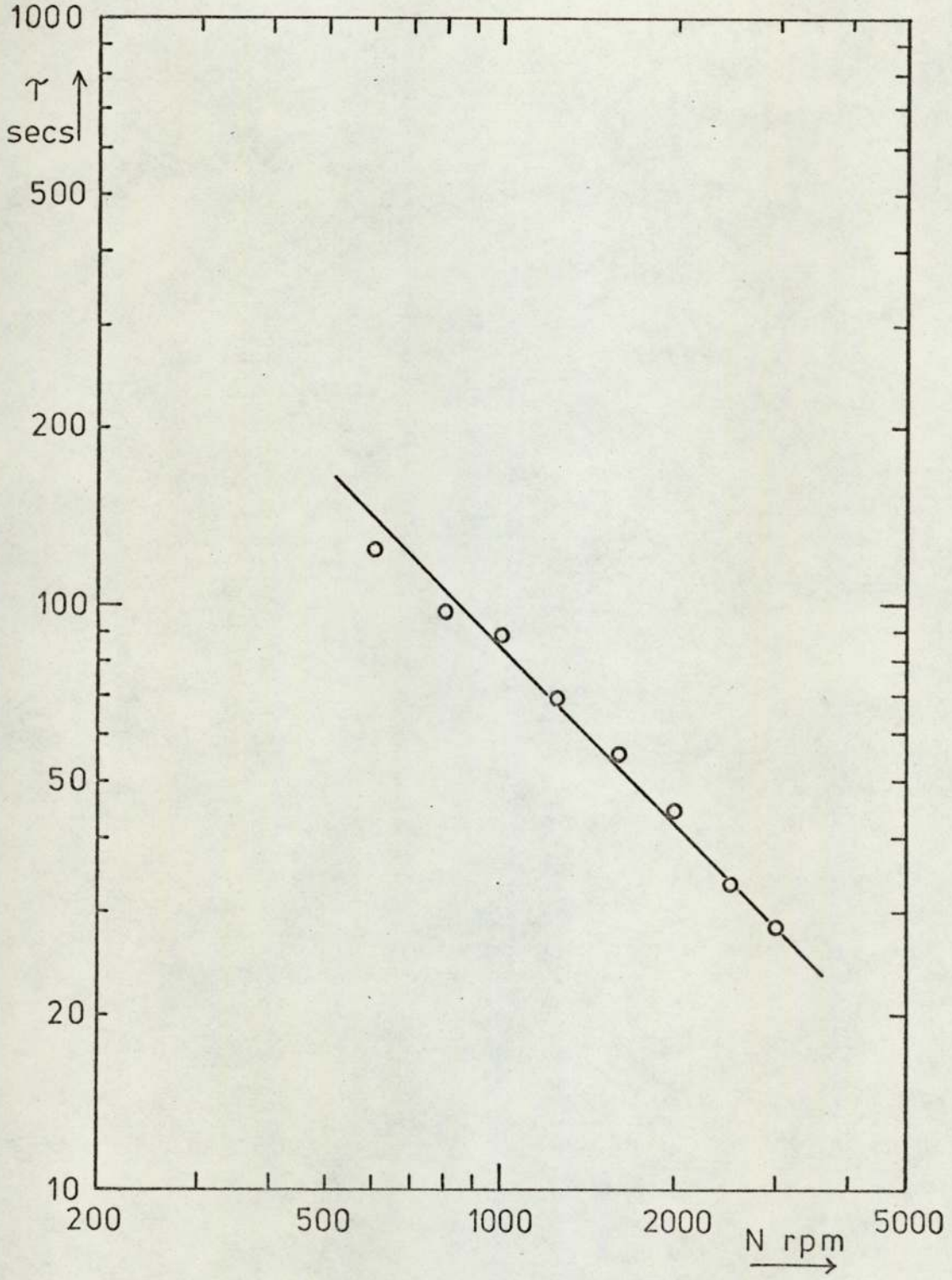

Figure 35

Mixing Time as a Function of Probe Diameter for the Conductivity Method

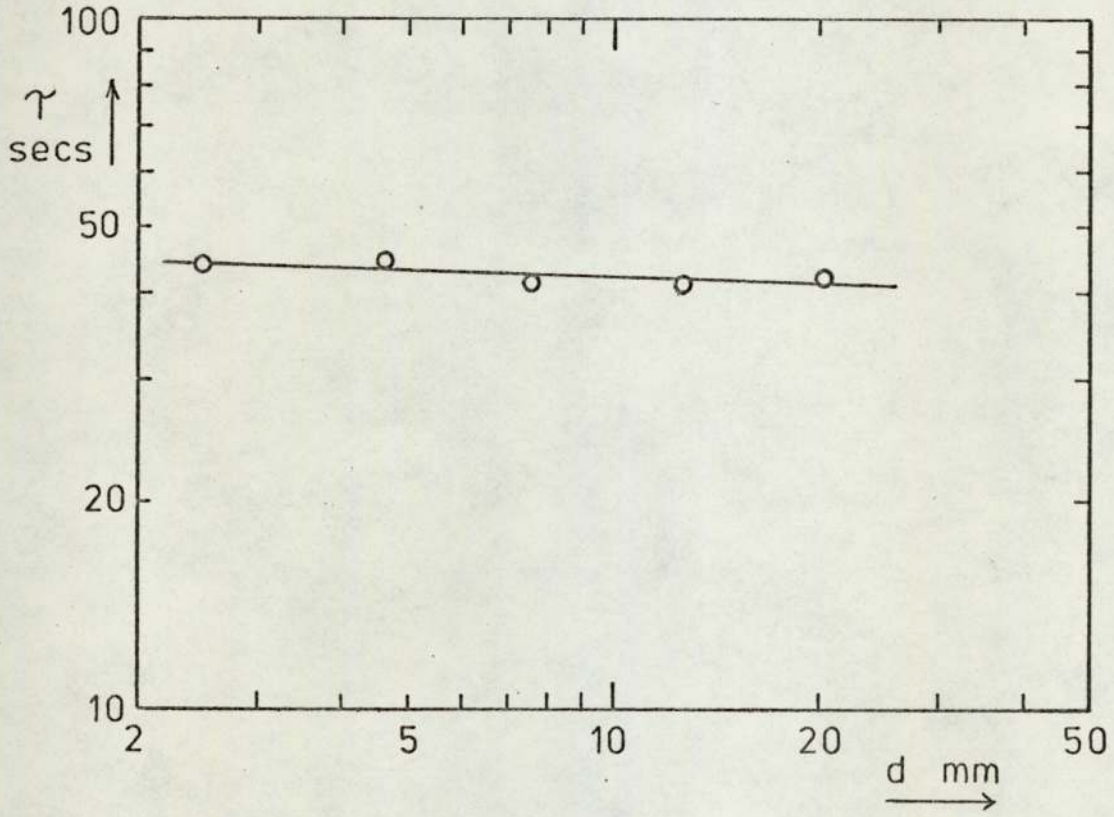

that probe size has very little effect on the mixing time. The scaling rule for measurements by the conductivity method in the turbulent regime can therefore be written simply as

$$N\tau D^2/T^2 = \text{const.}$$

5.2.3. Full Scale Measurements

In order to test the scaling rule over as wide a range as possible, measurements were made of the mixing time for a 31 m diameter tank using the method described in Section 4.5. The tracer concentration was measured as a function of time with the liquid depth at 3.59 m and 7.24 m, and the results are listed in Table 9 and plotted in Fig. 36. The terminal mixing times were 670 s and 720 s respectively. These runs were simulated on the 1.2 m diameter tank using the floating roof and injector with a 4.6 mm conductivity probe. The propeller was a plastic one of similar design to that in the full-scale tank. The full-scale Reynolds number of 9×10^5 could not be reached with this impeller, but since this value corresponds to the turbulent regime, in which mixing time becomes independent of Reynolds number, any sufficiently high Reynolds number may be used, and the model tank was operated at Re = 10^5. The results are listed in Table 10, and are compared with the full-scale values in the table below:

Figure 36

Conductivity Fluctuations in 31m. Tank.

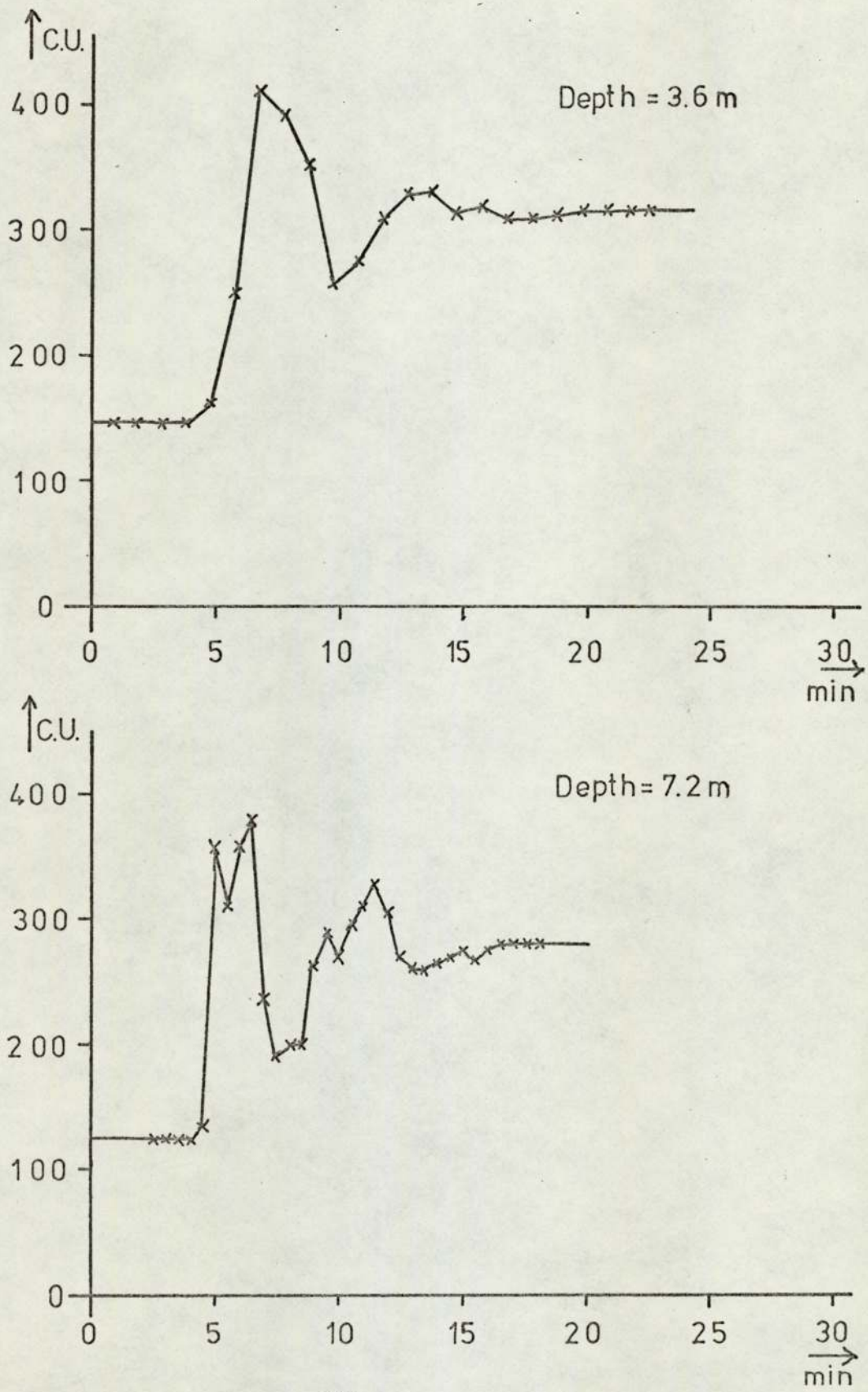

Tank Diameter	31 m	1.2 m
Impeller Speed	7 s^{-1}	50 s^{-1}
Impeller Diameter	610 mm	44.8 mm
Terminal Mixing Time at Y/T=0.116	670 s	24.8 s
Terminal Mixing Time at Y/T=0.234	720 s	20.6 s
$N\tau D^2/T^2$ at Y/T=0.116	1.82±0.20	1.73
$N\tau D^2/T^2$ at Y/T=0.234	1.95±0.22	1.44

The results with the lower liquid level agree within experimental error, but at the higher liquid level, the value obtained in the full-scale tank was high by 2.3 standard deviations. This may have been due to the fact that the tracer, which was slightly denser than the bulk material in the tank, was injected at a point which was lower than the conductivity probe, so that negative buoyancy effects would tend to lengthen the mixing time. As shown in section 3.1, this effect would be much smaller in the model tank than in the full-scale one.

5.2.4. 70 mm Tank

In order to test the results of the dimensional analysis, a series of measurements were carried out on the 70 mm tank using various chemical systems. This tank could be filled completely, eliminating the possibility of the

mixing time being affected by the gravitational acceleration, and with a similar system to that used in the 1.2 m tank (potassium hydroxide and hydrochloric acid), a slope of -0.85 was obtained for the graph of mixing time against impeller speed shown in Fig. 37 obtained from the data in Table 11. The same system was used, with sucrose added to vary the viscosity, and the graph of mixing time against viscosity shown in Fig. 38, from the data in Table 12, had a slope of 0.045 ± 0.03, in reasonable agreement with the expected value of 0.10 ± 0.02. Several attempts were made to verify the conclusion that the mixing time was a function of the molecular diffusivity by varying the diffusivity directly. The first system tried used lithium hydroxide and trichloroacetic acid. Trichloroacetic acid is a very strong acid, so that at the concentration used it is almost completely dissociated

$$K_A = \frac{[H^+]\,[CCl_3COO^-]}{[CCl_3COOH]} = 0.2 \text{ mole } l^{-1} \qquad (58)$$

$$[H^+] \simeq [CCl_3COO^-] \simeq 1.2 \times 10^{-3} \text{ mole } l^{-1}$$

$$\frac{[CCl_3COOH]}{[H^+]} = \frac{1.2 \times 10^{-3}}{0.2} = 6 \times 10^{-3}$$

The acid is therefore initially 99.4% dissociated, and this figure will increase as mixing proceeds. Any change in mixing time would therefore be due to the change in diffusivity

Figure 37

Mixing Time as a Function of Impeller Speed for 70mm Tank

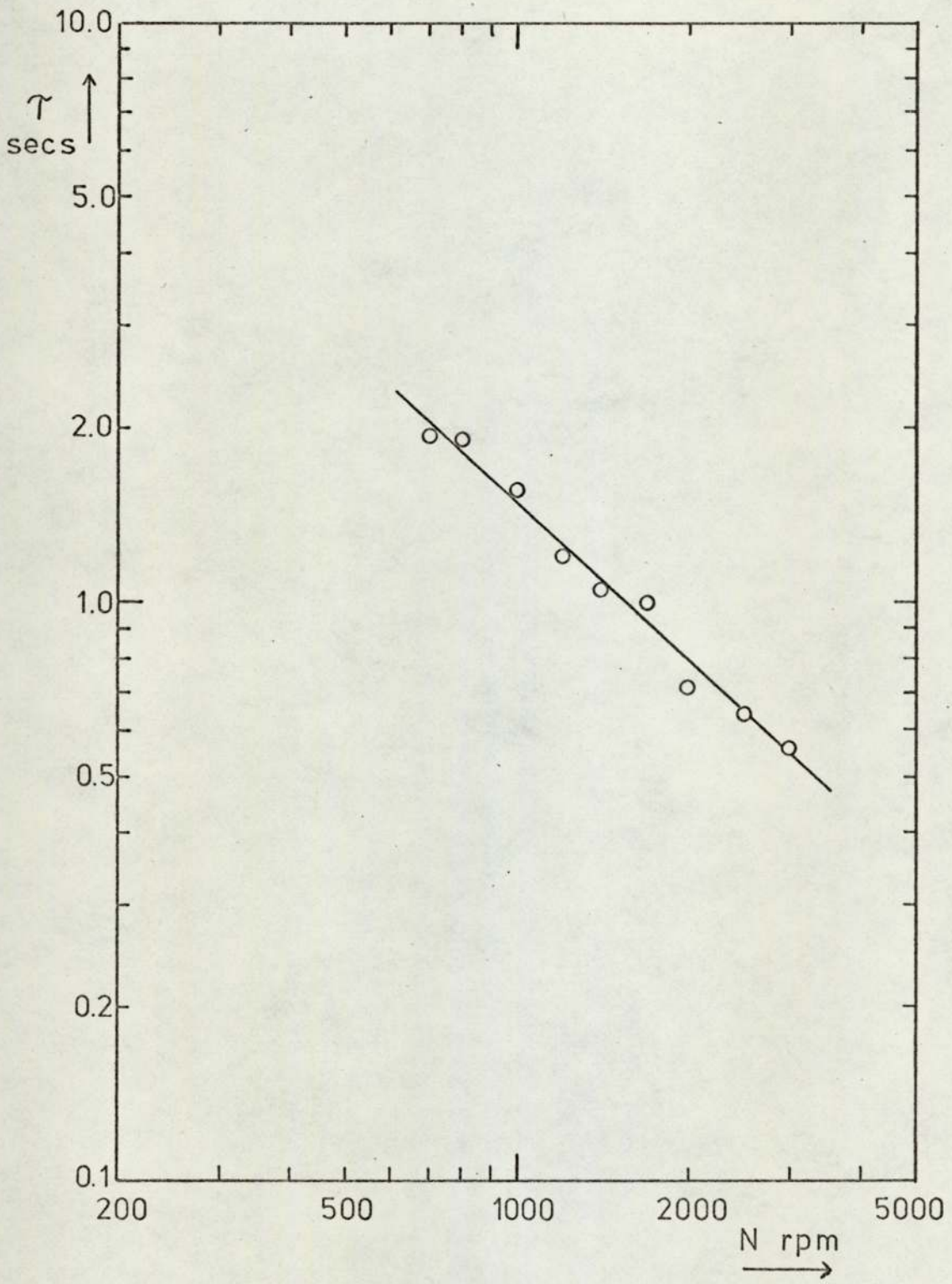

Figure 38

Mixing Time as a Function of Kinematic Viscosity for 70 mm Tank

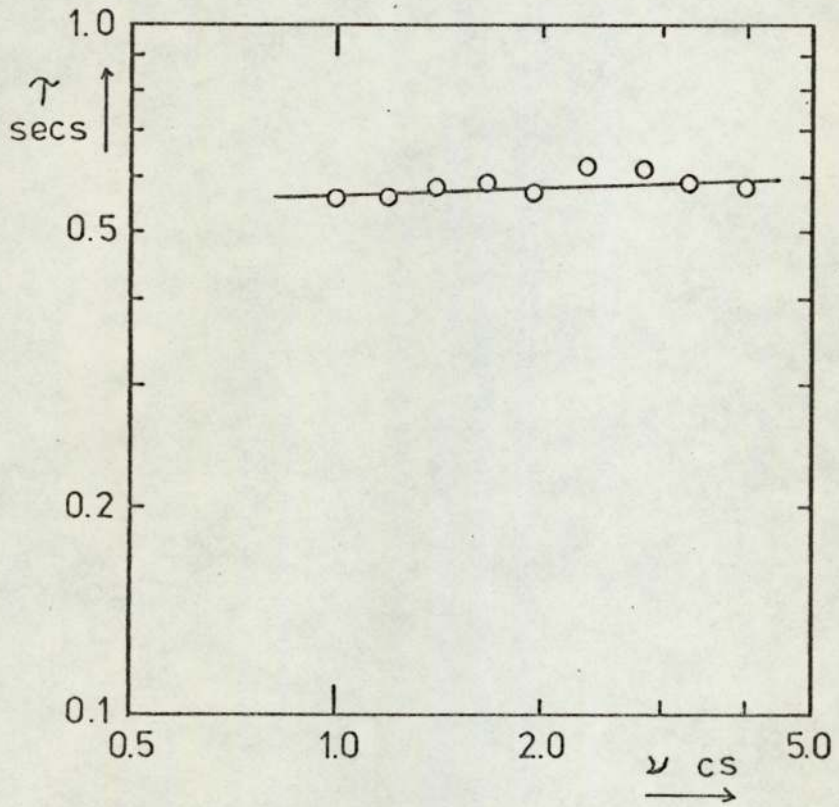

rather than to incomplete dissociation.

When an ionic substance diffuses in pure water, the flow must be such as to keep the solution electrically neutral everywhere. Thus the flow of anions must be balanced by an equal flow of cations, and so the two ionic species diffuse at the same rate, which depends on both their ionic mobilities, in accordance with the Nernst law (56)

$$\mathcal{D} = \frac{RT_o}{F^2} \frac{|z_1|+|z_2|}{|z_1 z_2|} \left(\frac{\lambda_1^\circ \lambda_2^\circ}{\lambda_1^\circ + \lambda_2^\circ} \right)$$

Using this expression with the published data for the individual ionic mobilities gives

$$\mathcal{D}_{KOH} = 2.86 \times 10^{-9} m^2 s^{-1} \quad \mathcal{D}_{LiOH} = 1.72 \times 10^{-9} m^2 s^{-1} \quad \frac{\mathcal{D}_{KOH}}{\mathcal{D}_{LiOH}} = 1.66$$

$$\mathcal{D}_{HCl} = 3.34 \times 10^{-9} m^2 s^{-1} \quad \mathcal{D}_{CCl_3COOH} = 1.85 \times 10^{-9} m^2 s^{-1} \quad \frac{\mathcal{D}_{HCl}}{\mathcal{D}_{CCl_3COOH}} = 1.81$$

The diffusivity of the materials comprising the first system is thus greater by a factor of about 1.7, so one might expect the mixing time to be greater by a factor of $(1.7)^{1/6} = 1.10$ for the second system. In fact the measured difference is not significantly different from unity. This null result can be accounted for when it is realised that the Nernst law applies only to diffusion into pure water. Under the conditions obtained in the stirred tank, several ions are present, and the situation approximates more closely to self-diffusion in which each ionic species diffuses independently. The OH^- and H^+ ions are thus free to diffuse

without their mobilities being appreciably affected by the mobilities of the other ions in the system, which accounts for the failure of this experiment.

The problem of changing the molecular diffusivity without altering the other parameters of the system can be overcome by using a system in which the diffusing species are molecules rather than ions. This can be achieved by the use of weak acids and bases under conditions such that they are only slightly ionised. The ionisation of a weak acid such as acetic is governed by

$$\frac{[H^+]\,[CH_3COO^-]}{[CH_3COOH]} = K_A$$

$$\frac{[CH_3COOH]}{[H^+]} = \frac{[CH_3COO^-]}{K_A}$$

This quantity can be made large by keeping $[CH_3COO^-]$ high and by choosing an acid for which K_A is sufficiently small. A weak base will behave similarly. Thus if ammonium hydroxide and acetic acid are used in the presence of ammonium acetate, it is possible to ensure that $[CH_3COOH] \gg [H^+]$ and $[NH_4OH] \gg [OH^-]$. The upper limit on this ratio is set by the requirement that the initial pH should be low enough to ensure that the indicator is fully converted to the red state. This pH can be found from

$$[H^+] = K_A \frac{[CH_3COOH]}{[CH_3COO^-]}$$

The value of K_A for acetic acid is 1.76×10^{-5} mole l^{-1} (58). The initial concentration of ammonium acetate was 8.2×10^{-4} mole l^{-1} and of acetic acid 1.18×10^{-3} mole l^{-1}.

$$[CH_3COO^-] + [CH_3COOH] = 8.2 \times 10^{-4} + 1.18 \times 10^{-3}$$
$$= 2.00 \times 10^{-3} \text{ mole } l^{-1}$$

$$[CH_3COOH] + [H^+] = 1.18 \times 10^{-3} \text{ mole } l^{-1}$$

Since $[CH_3COOH] \gg [H^+]$, $[CH_3COOH] \simeq 1.18 \times 10^{-3}$ mole l^{-1}

So $[CH_3COO^-] \simeq 8.2 \times 10^{-4}$ mole l^{-1}

$$[H^+] = \frac{1.76 \times 10^{-5} \times 1.18 \times 10^{-3}}{8.2 \times 10^{-4}} = 2.5 \times 10^{-5} \text{ mole } l^{-1}$$

$$pH = -\log_{10}(2.5 \times 10^{-5}) = 4.6$$

This is the point at which the colour change commences in methyl red. Since $[CH_3COO^-] > 8.2 \times 10^{-4}$ at all times,

$$\frac{[CH_3COOH]}{[H^+]} > \frac{8.2 \times 10^{-4}}{1.76 \times 10^{-5}} = 47$$

Similarly for ammonium hydroxide, $K_B = 1.79 \times 10^{-5}$ mole l^{-1}

$$\therefore \quad \frac{[NH_4OH]}{[OH^-]} > \frac{8.2 \times 10^{-4}}{1.79 \times 10^{-5}} = 46$$

Data is not available for the diffusivity of these molecules but it will be approximately equal to that of the corresponding ion. Since diffusivity is proportional to the limiting equivalent conductivity λ°,

$$\frac{D_{CH_3COOH}}{D_{H^+}} \simeq \frac{D_{CH_3COO^-}}{D_{H^+}} = \frac{\lambda^\circ_{CH_3COO^-}}{\lambda^\circ_{H^+}} = \frac{40.8}{350} = 0.117$$

The relative contributions of these two species to the diffusive flux will therefore be of the order:

$$\frac{[CH_3COOH]}{[H^+]}\frac{\mathcal{D}_{CH_3COOH}}{\mathcal{D}_{H^+}} \simeq 47 \times 0.117 = 5.5$$

Similarly $\frac{[NH_4OH]}{[OH^-]}\frac{\mathcal{D}_{NH_4OH}}{\mathcal{D}_{OH^-}} \simeq 46 \times \frac{74.5}{192} = 18$

Under these conditions, therefore, the diffusive flux will be influenced more by the diffusivity of the molecules than of the ions in the system. This diffusivity can be changed by using an acid and base having larger molecules of lower mobility. Provided that they have the same dissociation constants as acetic acid and ammonia, any change in mixing time must be due solely to the different diffusivity.

In practice, it is impossible to find an acid and base with dissociation constants identical to those of acetic acid and ammonium hydroxide. However γ-phenylbutyric acid has a dissociation constant of 1.74×10^{-5} mole l^{-1}, slightly lower than that of acetic acid, while benzylamine has a constant of 2.14×10^{-5} mole l^{-1}, a little higher than that of ammonium hydroxide. The use of a weaker acid and a stronger base should tend to decrease the mixing time, so that any increase in mixing time using these materials is evidence for an effect due to the decrease in diffusivity.

The mixing time was measured at various impeller speeds, and the results are listed in Table 13 for acetic acid and ammonia, and in Table 14 for γ-phenylbutyric acid and

benzylamine, and plotted together in Fig. 39. Mixing times for the latter system were, on average, greater by a factor of 1.039 ± 0.017. A one-tailed test indicated that this was significantly greater than unity at the 95% confidence level. The expected value can be roughly estimated although the molecular diffusivities are not known, from published values of the equivalent conductivity of the corresponding ions. Where data was not available for the precise ions, the value of λ° was estimated by comparison with similar ions.

Molecule	Ion	λ°
NH_4OH	NH_4^+	74
$C_6H_5NH_2$	$C_6H_5NH_4^+$	39 (est)
	$C_6H_5(CH_3)_4N^+$	35
CH_3COOH	CH_3COO^-	41
$C_6H_5(CH_2)_3COOH$	$C_6H_5(CH_2)_3COO^-$	28 (est)
	$C_6H_5COO^-$	32
	$C_4H_7COO^-$	32

The effective ratios of the diffusivities in the two systems are

$$\frac{[NH_4OH]\mathcal{D}_{NH_4OH} + [OH^-]\mathcal{D}_{OH^-}}{[C_6H_5NH_2]\mathcal{D}_{C_6H_5NH_2} + [OH^-]\mathcal{D}_{OH^-}} = \frac{74 + \frac{192}{46}}{39 + \frac{192}{46}} = 1.81$$

and

$$\frac{[CH_3COOH]\mathcal{D}_{CH_3COOH} + [H^+]\mathcal{D}_{H^+}}{[C_6H_5(CH_2)_3COOH]\mathcal{D}_{C_6H_5(CH_2)_3COOH} + [H^+]\mathcal{D}_{H^+}} = \frac{41 + \frac{350}{47}}{28 + \frac{350}{47}} = 1.37$$

Figure 39

Mixing Time as a Function of Impeller Speed for Buffered Systems.

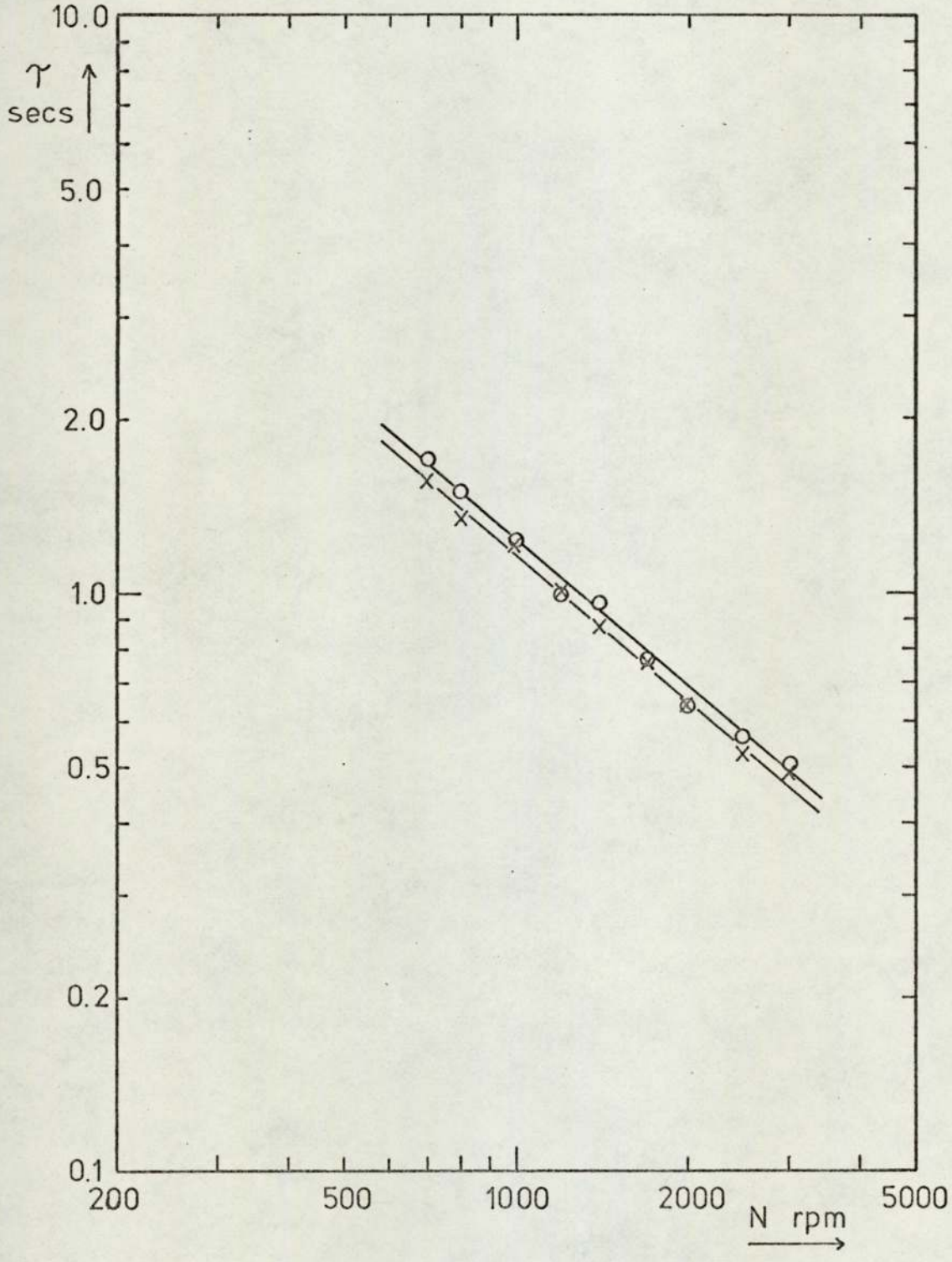

x Acetic Acid & Ammonia

o γ-Phenylbutyric Acid & Benzylamine

Taking a mean value of 1.59

$$\frac{\tau_1}{\tau_2} = 1.59^{0.17} = 1.08$$

In view of the considerable uncertainties involved in this calculation, this result should be regarded merely as a guide to the magnitude of the difference to be expected. The effect of imperfectly matching the dissociation constants in the two systems will be to reduce the observed effect, so the measured value of 1.039 ± 0.017 is not at variance with this result.

The theoretical model presented in Section 3.1 implies that mixing is a two-stage process, such that material is first transported across the streamlines by the turbulent fluctuations, and is then blended in through shear-assisted diffusion. The quantity of material which has reacted, as indicated by the colorimeter, depends only upon the second process. If the colorimeter reading used as a criterion for terminal mixing is taken as a further variable, only the term describing the shear-assisted diffusion should be affected by this value, X. The expression for mixing time can therefore be written

$$N\tau = A + C(X)N^n$$

The index n indicates the dependence of the second stage of the process on the impeller speed. The theory given in

Section 3.1 indicates that $n = \frac{1}{3}$, but this will not be assumed here.

The data obtained from the 70 mm tank with the KOH/HCl system were analysed by measuring the mixing time over a range of values of N for several values of X. The results are listed in Table 15 and plotted in Fig. 40. The best fit values of A and n were found by fitting straight lines to the data using the program for linear regression on logarithmic axes described in Appendix 5. This gives a slope m.

$$m = \frac{d(\ln N\tau)}{d(\ln N)} = \frac{1}{\tau}\frac{d(N\tau)}{dN}$$

Values of m, and the corresponding value of $N\tau$ at the geometric mean value of N are listed in Table 16. Differentiating the assumed form for $N\tau$

$$N\tau = A + C(X)N^n$$

$$\frac{d(N\tau)}{dN} = nC(X)N^{n-1} = m\tau$$

$$\therefore \quad mN\tau = nC(X)N^n = n(N\tau - A)$$

Thus a plot of $mN\tau$ against $N\tau$ should be linear of slope n and X-intercept A, providing a means of determining these quantities without any knowledge of C(X) which depends on the exact characteristics of the colorimeter. The graph is shown in Fig. 41. The weighted regression line had a slope of 0.36 ± 0.04 and X-intercept of 12.6. This result

Figure 40

Dimensionless Mixing Time as a Function of Impeller Speed with Various Criteria for Terminal Mixing

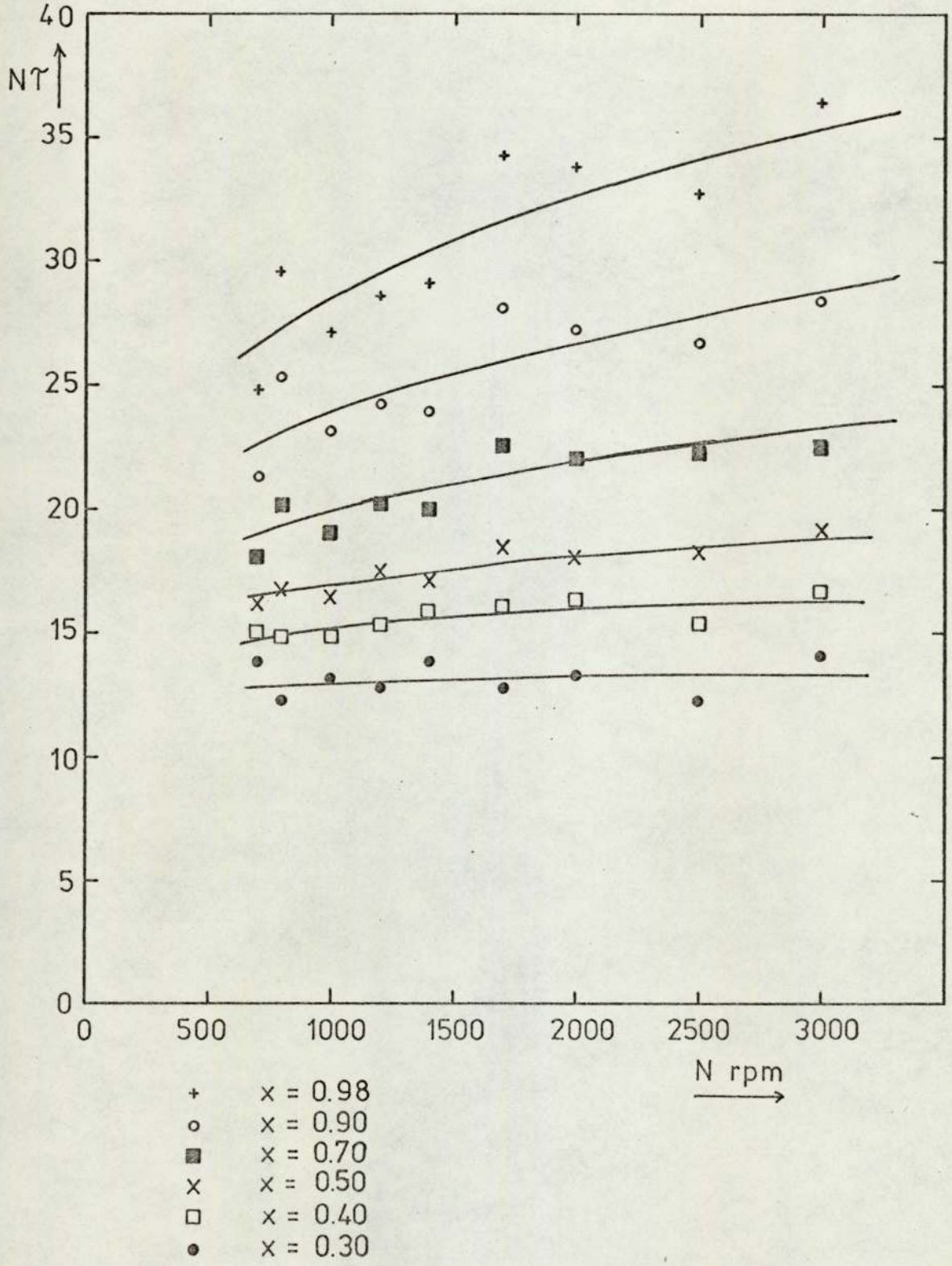

Figure 41

Variation in Dependence of Dimensionless Mixing Time on Impeller Speed with Various Criteria for Terminal Mixing

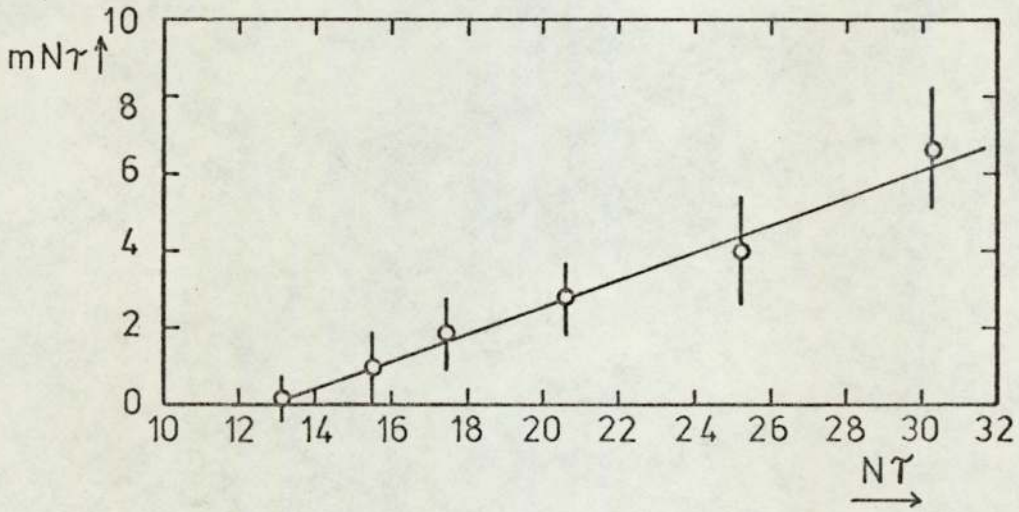

is in excellent agreement with the theoretical value for n of $\frac{1}{3}$, which provides strong confirmation for the theoretical form. Taking A = 12.6, n = $\frac{1}{3}$, the best fit values of C(X) were found, and the corresponding curves are superimposed on Fig. 40. The fit is seen to be satisfactory.

5.3. Hot Film Anemometry

A calibration curve was prepared for the hot film anemometer as described in Section 4.6.3 and the results are given in Table 17 and Fig. 42. The curve is highly non-linear, and in order to enable interpolation and smoothing to be carried out accurately, it was decided to fit a suitable analytical curve to the data. The first form tried was King's Law (59)

$$v = A + BU^n$$

It was not found possible to obtain a satisfactory fit over the whole of the curve for any values of A, B and n. This was therefore rejected, and polynomial curve fitting was used instead, assuming the form

$$U = A + Bv + Cv^2 + Dv^3 + Ev^4$$

A computer program was written to determine the best values for the coefficients A-E using weighted regression analysis (Appendix 6). The corresponding curve is shown in Fig. 42, and it can be seen that a very good fit is obtained.

Figure 42

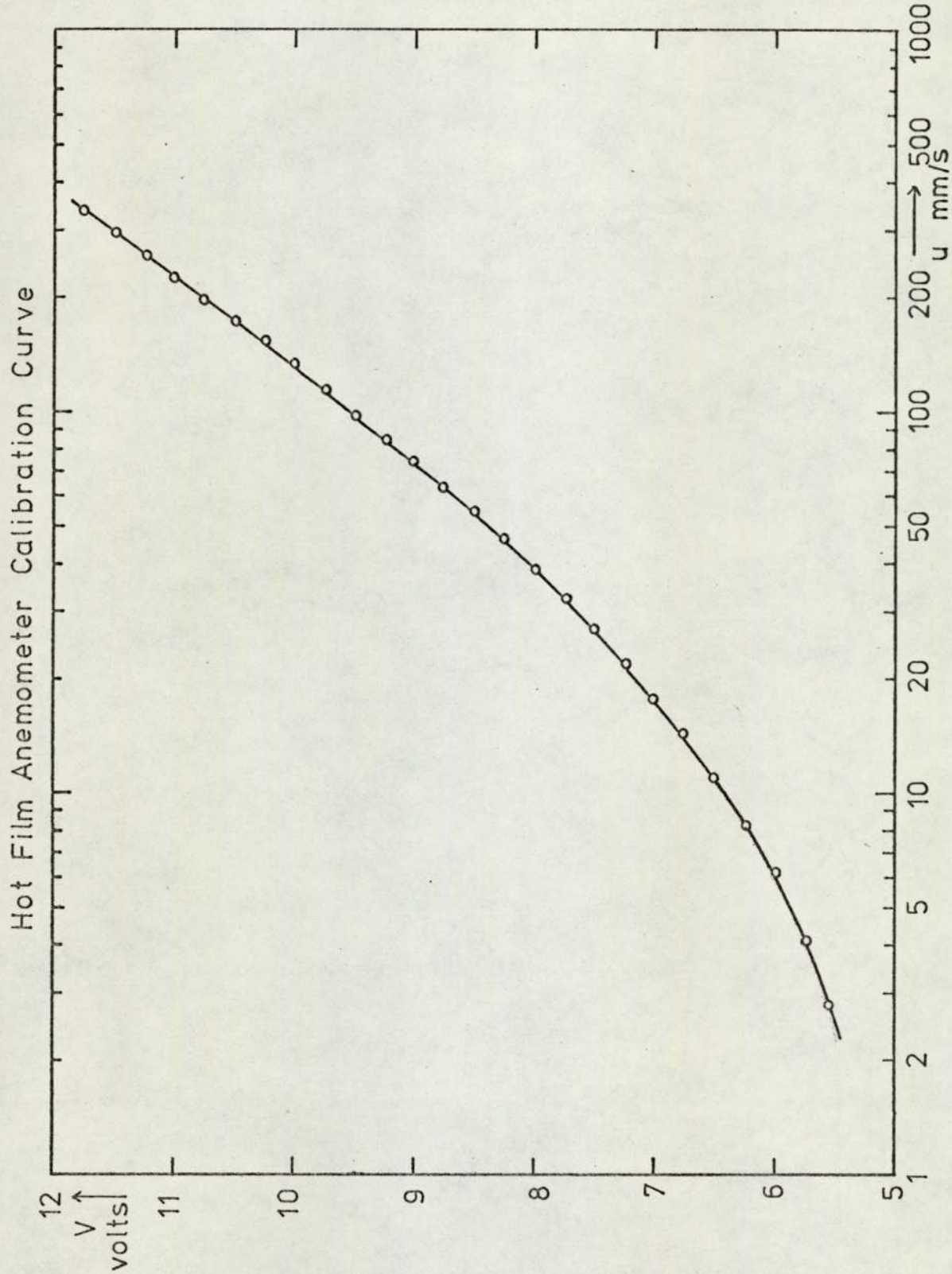
Hot Film Anemometer Calibration Curve
V ↑ volts
12
11
10
9
8
7
6
5
1
2
5
10
20
50
100
200
500
1000
u mm/s ⟶

Figure 43

Velocities in Boundary Layer

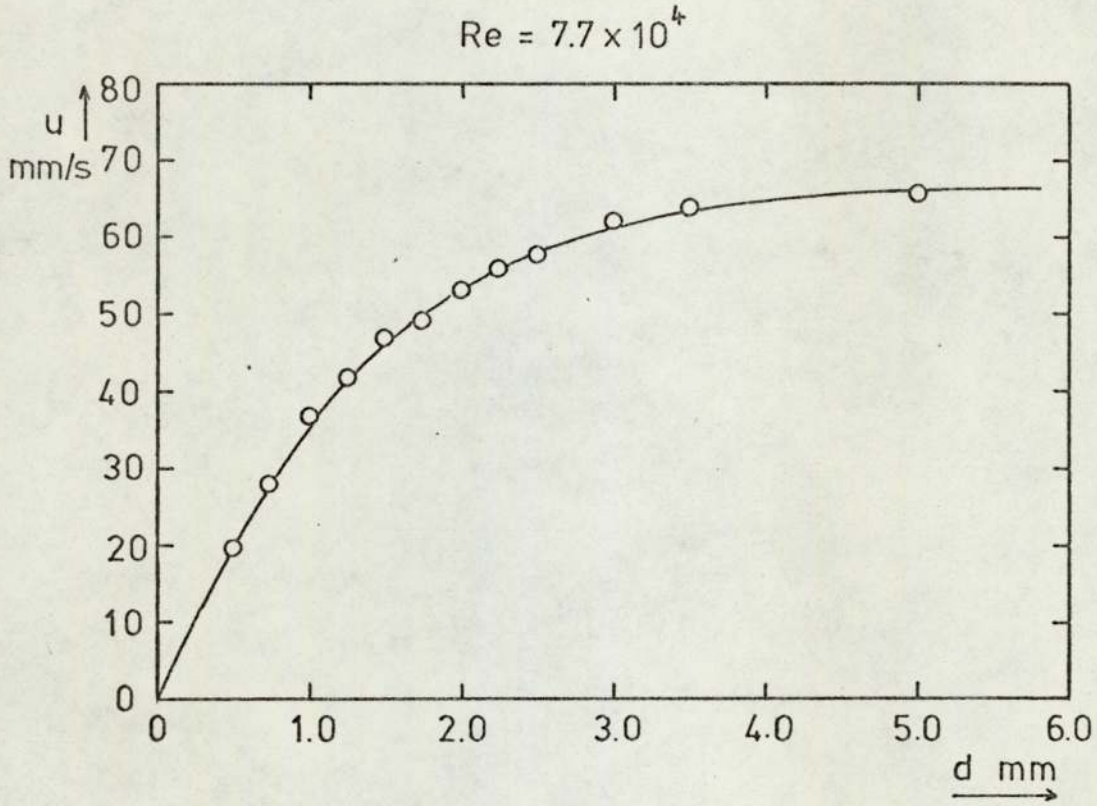

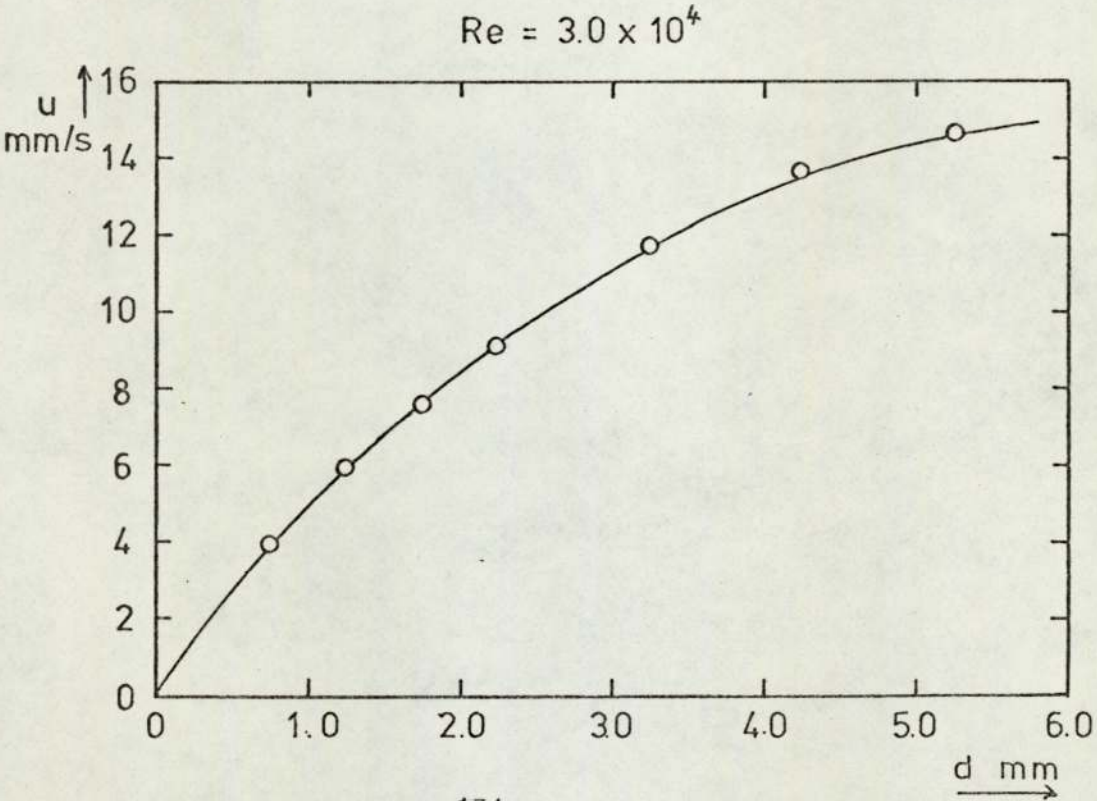

The greatest deviation between the fitted curve and the measured velocity amounts to 2% in the velocity. The standard deviation is 0.7%. All voltage measurements were converted to velocities using another program to evaluate this expression (Appendix 7).

A convenient position was selected in the tank well away from the impeller stream, as shown in Fig. 2, and the probe was traversed through the boundary layer on the floor of the tank for two different values of the impeller Reynolds number. The results are listed in Table 18 and plotted in Fig. 43. It can be seen that the boundary layer profiles have the linear region near the wall characteristic of a laminar boundary layer. The position of the probe relative to the wall was determined by cautiously lowering the probe until resistance to the movement of the micrometer head could be felt. The boundary layer displacement thickness could then be found by numerical integration by Simpson's rule using

$$\delta = \int_0^\infty (1 - \frac{u}{u_1})\, dy$$

where u_1 is the velocity outside the boundary layer, and y is the height of the probe tip above the floor. This gave $\delta = 1.18 \pm 0.05$ mm for $Re = 7.7 \times 10^4$, and $\delta = 2.16 \pm 0.05$mm for $Re = 3.0 \times 10^4$. The theory of Section 3.3 indicates that

for a boundary layer which is everywhere laminar, $\delta \propto Re^{-\frac{2}{3}}$. This can be tested by comparing these values of δ.

$$\frac{\delta_1}{\delta_2} = \frac{1.18}{2.16} = 0.55 \pm 0.03$$

$$\left(\frac{Re_1}{Re_2}\right)^{-\frac{2}{3}} = \left(\frac{7.9x10^4}{3.6x10^4}\right)^{-\frac{2}{3}} = 0.53$$

These results are in good agreement, supporting the assumption of a laminar boundary layer over most of the tank surface. Further evidence is supplied by the variation in the velocity outside the boundary layer with Reynolds number. This was measured at a height equal to half the liquid depth, and the results are listed in Table 19 and plotted in Fig 44. The slope of the curve of $\frac{uT}{ND^2}$ against Re on logarithmic axes changes from $\frac{1}{3}$ at low Reynolds number to zero at high Reynolds number. This result is in agreement with the theory of Section 3.3, the transition from a laminar to a turbulent boundary layer occurring at Reynolds numbers between $5x10^4$ and $1.6x10^5$. These values are similar to the range over which the slope of the mixing time curve for the incipient laminar regime changes in slope, suggesting that it is the formation of a laminar boundary layer that is responsible for the increase in dimensionless mixing time at low Reynolds number.

Figure 44

Dimensionless Circulation Time as a Function of Impeller Reynolds Number

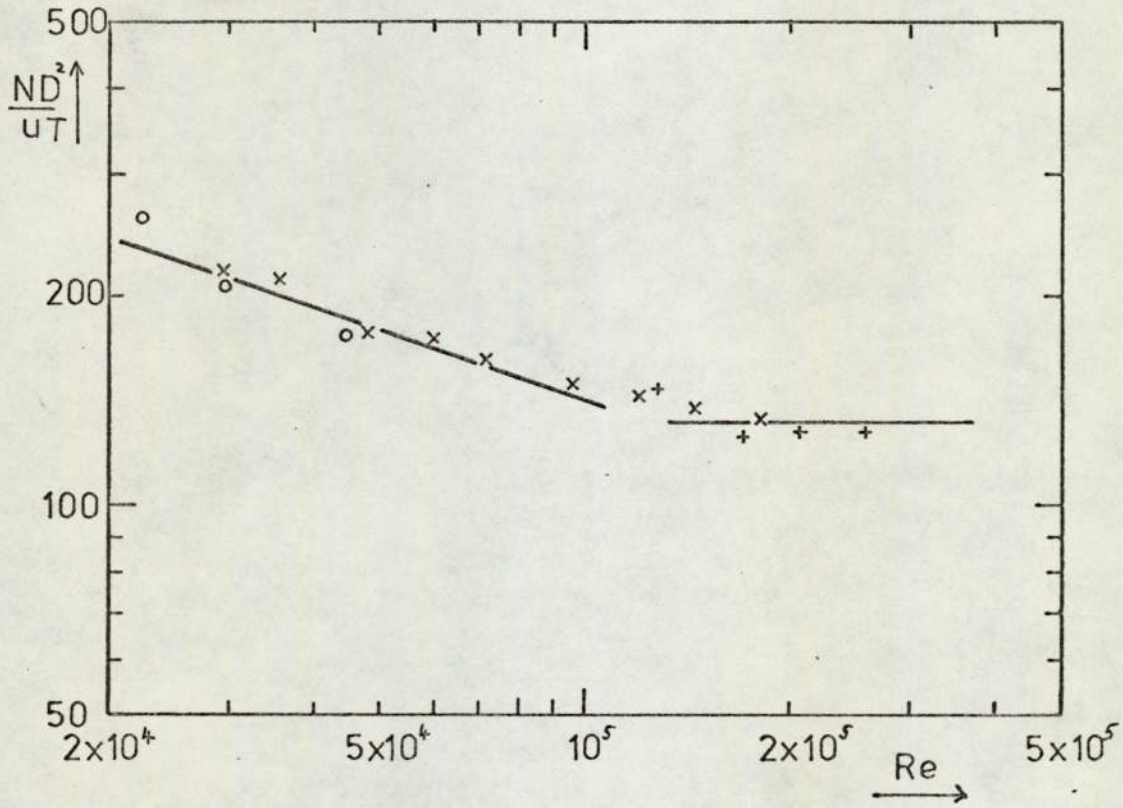

o D = 30 mm
× D = 60 mm
+ D = 72 mm

6. Conclusions

1. Mixing time measured by the indicator method is a function of the molecular diffusivity of the materials employed, and therefore is not suitable for scale-up. The conductivity method does not suffer from this limitation.
2. Scale-up can be carried out using the result $N\tau D^2/T^2 = \text{const.}$ for geometrically similar tanks provided the impeller Reynolds number is greater than some critical number, $\sim 10^5$, depending on the geometry.
3. Below the critical Reynolds number, the flow is affected by the formation of a laminar boundary layer; the rate of mixing and flow velocities become functions of the liquid viscosity.
4. The variation of mixing time with geometry is complicated and must be determined by experiment.
5. The influence of diffusivity on mixing times measured by the indicator method can be explained by a suitable model in which it is assumed that the effects of large-scale shearing are more important than those of small-scale turbulence.
6. For repeated measurements on a single system, it is the

rate of mixing that follows a Gaussian distribution rather than the terminal mixing time.

Appendix 1 - Mathematical Model

Let $\underline{a}$ and $\underline{b}$ be any two vectors lying in a surface of constant concentration, and let $\underline{c}$ be any other vector whose tip lies in a different surface of constant concentration. The distance x between the two surfaces is $\underline{c}.\underline{d}$ where $\underline{d}$ is a unit vector normal to the surfaces.

$$\underline{d} = \frac{\underline{a}\times\underline{b}}{|\underline{a}\times\underline{b}|}$$

$$x = \underline{c}.\underline{d} = \frac{\underline{a}\times\underline{b}.\underline{c}}{\underline{a}\times\underline{b}}$$

But $\underline{a}\times\underline{b}.\underline{c}$ represents the volume of the parallelepiped contained by $\underline{a}$, $\underline{b}$ and $\underline{c}$, which is constant for an incompressible fluid.

$$x = \frac{k_1}{|\underline{a}\times\underline{b}|}$$

$$\frac{k_1^2}{x^2} = |\underline{a}\times\underline{b}|^2$$

Putting $\frac{k_1^2}{x^2} = y$ and switching to tensor notation with the use of the summation convention

$$\begin{aligned} y &= \varepsilon_{ijk}\, a_j b_k \varepsilon_{ilm}\, a_l b_m \\ &= (\delta_{jl}\delta_{km} - \delta_{jm}\delta_{kl}) a_j a_l b_k b_m \\ &= a_j a_j b_k b_k - a_j a_k b_j b_k \\ &= a_j b_k (a_j b_k - a_k b_j) \end{aligned}$$

For a uniform steady shear, writing $\frac{\partial u_i}{\partial x_j} = \sigma_{ij}$, $\frac{\partial a_i}{\partial t} = u_i = \sigma_{ij}\, a_j$ and differentiating with respect to time

$$\frac{dy}{dt} = a_j b_k (a_j \sigma_{kl} b_l + \sigma_{jl} a_l b_k - a_k \sigma_{jl} b_l - \sigma_{kl} a_l b_j)$$
$$+ (a_j \sigma_{kl} b_l + \sigma_{jl} a_l b_k)(a_j b_k - a_k b_j)$$

Interchanging j & k in terms containing σ_{jl} gives

$$\frac{dy}{dt} = \sigma_{kl}(a_j a_j b_k b_l + a_k a_l b_j b_j - a_j a_k b_j b_l - a_j a_l b_j b_k$$
$$+ a_j a_j b_k b_l + a_k a_l b_j b_j - a_j a_k b_j b_l - a_j a_l b_j b_k)$$
$$= 2\,\sigma_{kl}(a_j b_l - a_l b_j)(a_j b_k - a_k b_j)$$

For a simple shear, with appropriately chosen axes, σ_{kl} has only a single element σ_{12}, so $\sigma_{kl} = \delta_{k1}\delta_{l2}\sigma_{12}$

$$\frac{dy}{dt} = 2\,\sigma_{12}(a_j b_2 - a_2 b_j)(a_j b_1 - a_1 b_j)$$

The second factor is zero for $j=1$, and the first factor for $j=2$, so the only non-zero term on summing over j is given by $j=3$.

$$\frac{dy}{dt} = 2\,\sigma_{12}(a_3 b_2 - a_2 b_3)(a_3 b_1 - a_1 b_3)$$

Differentiating again, since $\frac{\partial a_2}{\partial t} = \frac{\partial a_3}{\partial t} = \frac{\partial b_2}{\partial t} = \frac{\partial b_3}{\partial t} = 0$,

$$\frac{d^2y}{dt^2} = 2\,\sigma_{12}(a_3 b_2 - a_2 b_3)(a_3 \sigma_{12} b_2 - \sigma_{12} a_2 b_3)$$
$$= 2\,\sigma_{12}^2(a_3 b_2 - a_2 b_3)^2$$

$$\frac{d^3y}{dt^3} = 0$$

y can then be written as a Maclaurin series which will terminate after the third term, as all subsequent terms will be zero.

$$y = y_0 + t\left(\frac{dy}{dt}\right)_{t=0} + \frac{t^2}{2}\left(\frac{d^2y}{dt^2}\right)_{t=0}$$

$$\frac{k_1^2}{x^2} = \frac{k_1^2}{x_0^2} + 2\,\sigma_{12}\,t(a_3^\circ b_2^\circ - a_2^\circ b_3^\circ)(a_3^\circ b_1^\circ - a_1^\circ b_3^\circ) + \sigma_{12}^2 t^2 (a_3^\circ b_2^\circ - a_2^\circ b_3^\circ)^2$$

Multiplying through by $\frac{x_0^2}{k_1^2}$ and putting

$$\alpha = \frac{x_0^2}{k_1^2}(a_3^\circ b_2^\circ - a_2^\circ b_3^\circ)(a_3^\circ b_1^\circ - a_1^\circ b_3^\circ)$$

$$\beta = \frac{x_0^2}{k_1^2}(a_3^\circ b_2^\circ - a_2^\circ b_3^\circ)^2$$

we now have

$$\frac{x_0^2}{x^2} = 1 + 2\alpha\,\sigma_{12}t + \beta\,\sigma_{12}^2 t^2$$

α and β are dimensionless, and depend only on the initial orientation.

Appendix 2 - Effect of Hub Size on the Efficiency of Impellers

It is shown in Section 3.2 that the quantity determining the mixing efficiency of an impeller is the momentum transfer which is the product of the pumping capacity and the velocity of the fluid leaving the impeller. Dividing the impeller stream into annular sections we have for each section

Velocity = Ns

Flow = $Ns.2\pi r\ dr$

Momentum Transfer $= \int_{r_H}^{r_I} 2\pi N^2 s^2 r\ dr$

For the impellers used, the pitch s = r

$$M.T. = 2\pi N^2 \int_{r_H}^{r_I} \frac{r^3}{r_I^2}\ dr = 2\pi N^2 \left[\frac{r^4}{4}\right]_{r_H}^{r_I}$$

$$= \frac{\pi}{2} N^2 r_I^4 \left(1-\left(\frac{r_H}{r_I}\right)^4\right)$$

For the smallest impeller used, r_I = 15 mm, r_H = 4.8 mm,

$$1 - \left(\frac{r_H}{r_I}\right)^4 = 0.990$$

The presence of the hub therefore reduces the momentum transfer by only 1%.

Appendix 3 - Description of Conductivity Meter

The circuit diagram of the conductivity meter is shown in Fig. 45. OA1 acts as a square wave oscillator of frequency $1/(2R_3C_1\ln 3) = 1.0$ KHz, the amplitude being limited by D1 and D2 to 13.6 V peak-to-peak. A three-section R-C low-pass filter ($R_5, C_2, R_6, C_3, R_7, C_4$) extracts the fundamental and this is fed to the non-inverting input of the main operational amplifier OA2. The attenuation factor in each section of the filter is $\sqrt{1 + \omega^2 R^2 C^2} = 2.1$ for the fundamental, 5.6 for the third harmonic, ignoring loading of each section by the rest of the filter. The fundamental is therefore attenuated by the filter from $\frac{4}{\pi} \times 13.6 = 17.3$ V p-p in the square wave to $17.3/(2.1)^3 = 1.8$ V p-p, and the third harmonic from $17.3/3 = 5.8$ V to $5.8/(5.6)^3 = 0.03$ V p-p. Since the second harmonic is absent from the initial square wave, and higher harmonics are attenuated to an even greater extent, the voltage at the non-inverting input of OA2, V_I, is a nearly pure sinewave of frequency 1 KHz and amplitude 1.8 V p-p. The output voltage of OA2, V_o, is given by

$$V_o = A\left(V_I - V_o \frac{R_P}{R_P + R_F}\right), \quad V_I = V_o\left(\frac{1}{A} + \frac{R_P}{R_P + R_F}\right)$$

The open-loop amplifier gain, A, is typically 10^5, whereas $R_F/R_P < 10$, so the first term inside the brackets can be ignored.

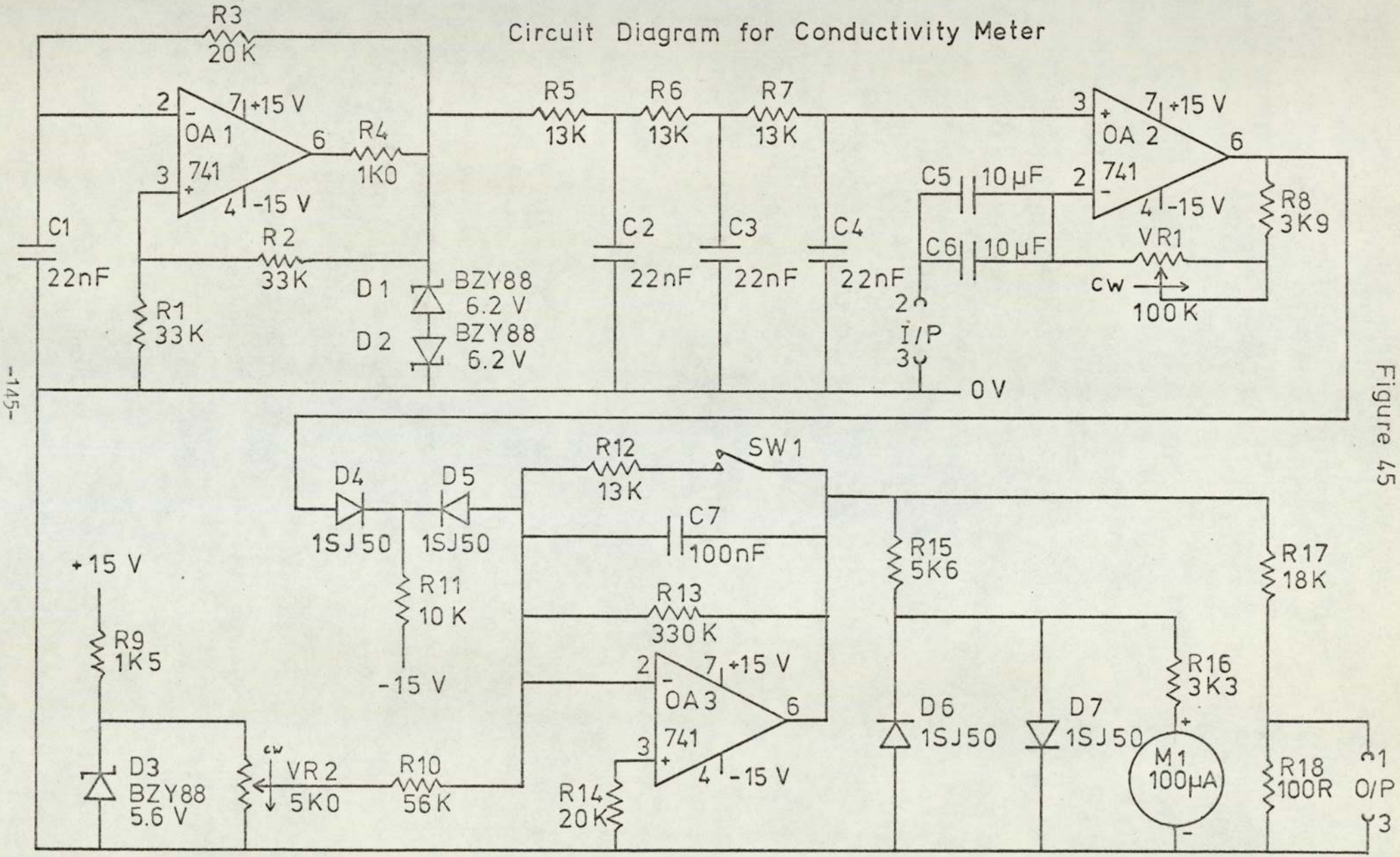
Circuit Diagram for Conductivity Meter
R3
20K
OA 1
741
+15 V
-15 V
R4
1K0
R5
13K
R6
13K
R7
13K
OA 2
741
+15 V
-15 V
C1
22nF
R2
33K
R1
33K
D1
BZY88
6.2 V
D2
BZY88
6.2 V
C2
22nF
C3
22nF
C4
22nF
C5
10µF
C6
10µF
VR1
CW
100K
R8
3K9
I/P
0 V
R12
13K
SW 1
D4
1SJ50
D5
1SJ50
C7
100nF
R11
10 K
-15 V
R13
330 K
OA 3
741
+15 V
-15 V
+15 V
R9
1K5
D3
BZY88
5.6 V
CW
VR2
5K0
R10
56K
R14
20K
R15
5K6
D6
1SJ50
D7
1SJ50
R16
3K3
M1
100µA
R17
18K
R18
100R
O/P

Figure 45

Figure 46

Power Supply for Conductivity Meter

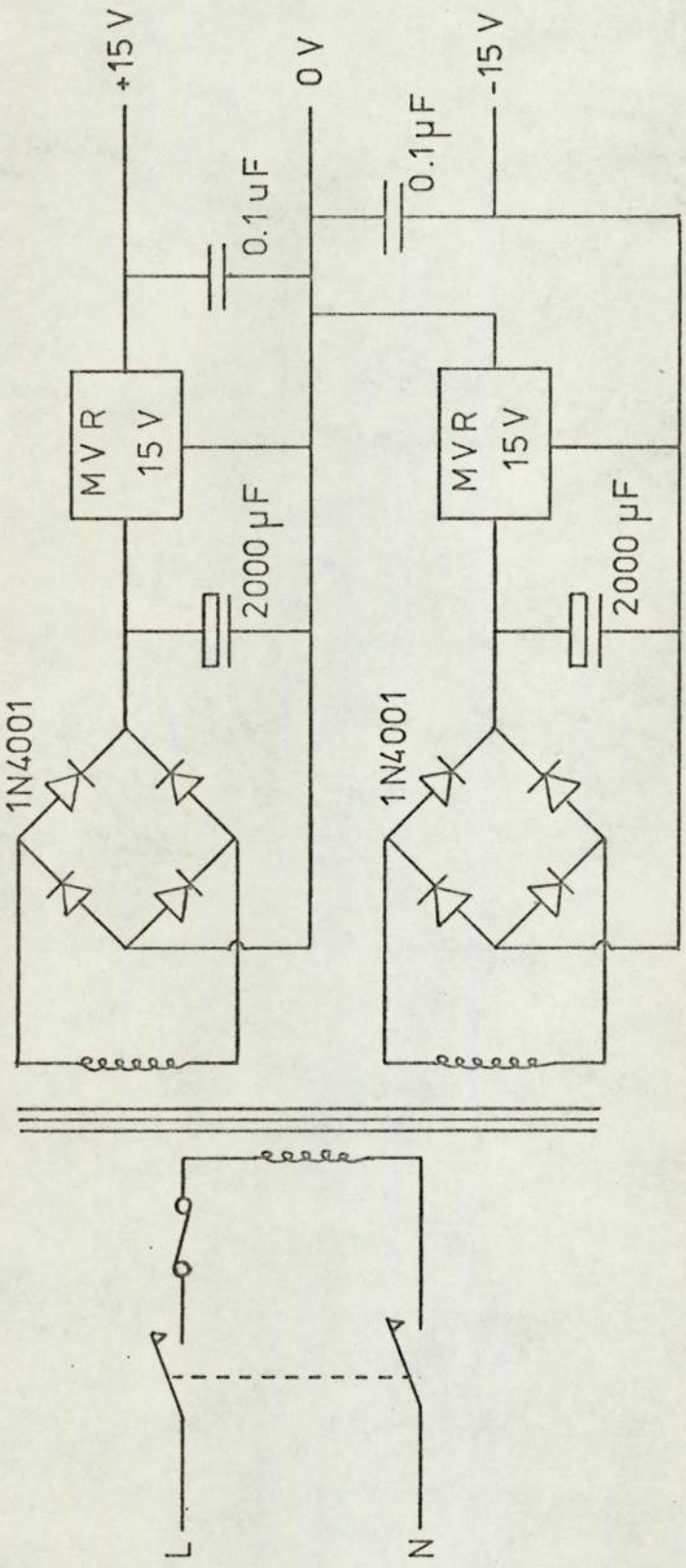

We then have

$$V_o = (1 + \frac{R_f}{R_p})V_I$$

The value of R_f can be varied by means of VR1. Polyester capacitors C5 and C6 provide D.C. blocking for the probe to prevent any small D.C. component in the voltage at the inverting input of OA2 from producing polarisation of the electrodes. They also limit the D.C. gain of the amplifier to unity, thereby minimising the effect of any voltage drift in this part of the circuit. The output voltage of OA2 is fed via R19 to the summing junction of a third operational amplifier OA3. D5 ensures that current only flows during negative half-cycles, so that the current flowing into the summing junction is proportional to the amplitude of V_o. D4 compensates for the forward voltage drop of D5, and R11 provides a bias current to hold D4 permanently in the conducting state.

The zero control VR2 provides a positive offset voltage which is fed via R10 to the summing junction. This is used to subtract both the constant voltage arising from the unity term in the expression for V_o, and also any signal caused by the background conductivity of the electrolyte. It is therefore possible to carry out up to thirty successive measurements, increasing the electrolyte concentration by a small amount each time, and backing this off by means of VR2.

In normal use, R13 acts as the feedback resistor, but a second resistor, R12, can be placed in parallel with it to reduce the sensivity by a factor of 26 for calibration purposes. C7 limits the frequency response to prevent the signal frequency from reaching the output. The output signal is displayed on a moving coil panel meter, M1, fitted with overload protection diodes D6 and D7, and is also fed to an output socket for connection to a U.V. chart recorder (S.E. 2000 Mk II).

Since the circuit is used to measure small increments in conductivity, it must be highly stable in operation, and this is achieved by extensive temperature compensation. The operational amplifiers used are monolithic devices having low thermal drift and good supply voltage rejection, enabling the use of a simple power supply using monolithic voltage regulators as shown in Fig. 46. The output of OA 1 is determined by D1 and D2, which have a reverse voltage temperature coefficient of +2 mV/°C, which compensates for their forward coefficient of -2 mV/°C. C1 is identical with C2, C3 & C4, so that a thermal increase in the values of these capacitors will lower the frequency by such an amount as to keep the attenuation of the filter constant. The forward voltage drop of D5 is compensated by a similar component D4, and therefore any

thermal variations will also be compensated. The zero voltage is derived from a zener-stabilized source using a zener diode of minimum temperature coefficient. R14 is used to compensate for the effect of the input bias current of OA3. These precautions ensure that the temperature stability is excellent, and the warm-up time minimal. It was found that temperature changes in the electrolyte were more significant than those in the instrument, despite the vastly smaller thermal inertia of the latter.

Appendix 4 - Effect of Finite Probe Size on Probe Calibration.

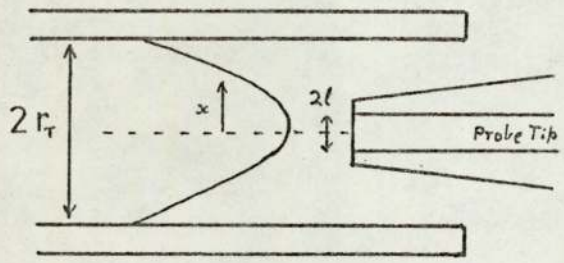

The velocity averaged over the probe tip is

$$\bar{u} = \frac{1}{\ell}\int_0^{\ell} u\, dx$$

where u is of parabolic form $u = u_c\left(1 - \frac{x^2}{r_T^2}\right)$

$$\bar{u} = \frac{1}{\ell}\int_0^{\ell} u_c\left(1 - \frac{x^2}{r_T^2}\right) dx = \frac{u_c}{\ell}\left[x - \frac{x^3}{3r_T^2}\right]_0^{\ell}$$

$$= u_c\left(1 - \frac{\ell^2}{3r_T^2}\right)$$

For the probe used $\ell = 0.5$ mm, and $r_T = 3.175$ mm

$$\therefore \quad \bar{u} = u_c\left(1 - \frac{0.5^2}{3 \times 3.175^2}\right) = 0.992\, u_c$$

Appendix 5 - Computer Program for the calculation of linear regression lines on logarithmic axes.

The program was written in BASIC for use on the Honeywell 316 computer, and is as follows:

```
50   X2=0
60   X3=0
70   X4=0
80   Y2=0
90   Y3=0
110  READ N
120  FOR J=1,N
130  READ A,B
140  X=LOG(A)
150  Y=LOG(B)
160  X2=X2+X/N
170  Y2=Y2+Y/N
180  X3=X3+X*X
190  X4=X4+X*Y
200  Y3=Y3+Y*Y
210  NEXT J
220  X5=X3-N*X2*X2
230  M=(X4-N*X2*Y2)/X5
240  S2=Y3-N*Y2*Y2-M*M*X5
250  V=S2/((N-2)*X5)
260  E=V↑.5
270  C=Y2-M*X2
280  RESTORE
```

Appendix 6 - Computer Program for Polynomial Curve Fitting

This program was used to process the calibration data for the hot film anemometer, and fit a polynomial curve to them by the method of least squares. The method used is based on that given by Hayes (61) using Chebyshev polynomials. Since the majority of the error in the measured values lies in the independent variable (the voltage) rather than the dependent variable (the liquid flow), the method was modified by applying weighting factors calculated from the slope of an approximately fitted curve, so that the quantity which was minimised was the sum of the squares of the deviations in the voltages. The weights were initially set to unity, and a curve was fitted. This curve was then used to calculate the weights, and the process repeated. This method converges rapidly since the slope of the curve is not a very sensitive function of the weights. The program was written in BASIC for use on the Honeywell 316 computer and is as follows:

```
10   REM  POLYNOMIAL CURVE FITTING
15   REM  CLEAR A,V,D
20   FOR I=1,10
30   V(I)=0
40   FOR J=1,10
50   A(I,J)=0
60   D(I,J)=0
```

```
70   NEXT J
73   NEXT I
77   FOR F=0,3
80   READ K,M,V1,V2
85   IF F=0 THEN GOSUB 500
87   IF F=3 THEN GOSUB 800
90   FOR G=1,M
100  READ V3,M2,T
110  Y=6.33*M2/T
120  X=2*(V3-V1)/(V2-V1)-1
125  REM GENERATE CHEBYSHEV POLYNOMIALS
130  P(1)=1
140  P(2)=X
150  FOR L=3,K+1
160  P(L)=2*X*P(L-1)-P(L-2)
170  NEXT L
180  IF F<3 GOTO 250
185  REM  COMPUTE POINTS ON FITTED CURVE
190  R2=0
200  FOR I=1,K+1
210  R2=R2+V(I)*P(I)
220  NEXT I
230  PRINT V3,Y,R2,100*(R2-Y)/Y
240  GOTO 310
245  REM  BUILD UP NORMAL EQUATIONS
250  GOSUB 700
255  FOR Q=1,K+1
260  FOR R=1,K+1
270  A(Q,R)=A(Q,R)+P(Q)*P(R)*W*W
280  NEXT R
```

```
290  V(Q)=V(Q)+Y*P(Q)*W*W
300  NEXT Q
310  NEXT G
320  IF F=3 THEN STOP
325  REM  SOLVE NORMAL EQUATIONS
330  FOR L=1,K+1
332  V(L)=V(L)/A(L,L)
333  H=A(L,L)
335  FOR J=1,K+1
337  A(L,J)=A(L,J)/H
338  NEXT J
340  FOR I=1,K+1
345  IF I=L GOTO 400
350  H=A(I,L)
360  FOR J=1,K+1
370  A(I,J)=A(I,J)-A(L,J)*H
380  NEXT J
390  V(I)=V(I)-V(L)*H
400  NEXT I
410  NEXT L
415  REM  STORE SOLUTION
420  FOR I=1,K+1
430  Z(I)=V(I)
440  NEXT I
450  RESTORE
460  NEXT F
490  REM  GENERATE MATRIX OF CHEBYSHEV COEFFICIENTS
500  FOR I=1,K+1
510  FOR J=1,K+1
520  IF I>1 GOTO 550
```

```
530  C(I,J)=0
540  IF J=1 THEN C(I,J)=1
545  GOTO 610
550  IF I>2 GOTO 580
560  C(I,J)=0
570  IF J=2 THEN C(I,J)=1
575  GOTO 610
580  IF J>1 THEN GOTO 600
590  C(I,J)=C(I-2,J)*(-1)
600  C(I,J)=2*C(I-1,J-1)-C(I-2,J)
610  NEXT J
620  NEXT I
630  RETURN
690  REM  COMPUTE WEIGHTING FACTORS
700  W=1
710  IF F=0 GOTO 780
720  W=0
730  FOR I=1,K+1
740  FOR J=2,K+1
750  W=W+C(I,J)*Z(I)*(J-1)*X↑(J-2)
760  NEXT J
770  NEXT I
775  W=1/W
780  RETURN
790  REM  COMPUTE POLYNOMIAL COEFFICIENTS
800  A2=2/(V2-V1)
804  B2=-(V2+V1)/(V2-V1)
806  B2=B2+5*A2
808  D(1,1)=1
812  FOR J=2,K+1
816  D(1,J)=B2*D(1,J-1)
```

```
820  FOR I=2,K+1
824  D(I,J)=B2*D(I,J-1)+A2*D(I-1,J-1)
828  NEXT I
832  NEXT J
834  REM  COMPUTE COEFFICIENTS OF X
836  FOR J=1,K+1
840  B(J)=0
844  FOR I=1,K+1
848  B(J)=B(J)+C(I,J)*V(I)
852  NEXT I
856  NEXT J
858  REM COMPUTE COEFFICIENTS OF U
860  FOR I=1,K+1
864  E(I)=0
868  FOR J=1,K+1
872  E(I)=E(I)+D(I,J)*B(J)
880  NEXT J
882  PRINT I-1,E(I)
884  NEXT I
888  PRINT
892  RETURN
900  DATA 4,23,5.5,11
```

After clearing the data stores, the main iterative loop is entered (line 77). The first four numbers read are: the order of the polynomial to be fitted, the number of data points, and the high and low values of the voltage to be used to normalise the data into the range ±1. The data for a single point are then read in as a set of three numbers: the voltage, the mass of

water collected, and the time taken during calibration. These are used to calculate X, the normalised voltage, and Y, the fluid velocity. The values of X are then used to evaluate the corresponding Chebyshev polynomials which are stored in the array P. These are then used to build up the set of normal equations, stored in a matrix A, and vector V, the contributions to these being determined by the weighting factor W. When all the data points have been read in, the set of normal equations are then solved by Gaussian elimination, leaving the result in V. This is transferred to array Z for storage, and the iterative loop is repeated. The result is in the form of a set of coefficients of the Chebyshev polynomials in the normalised variable, and these are used to calculate the coefficient of each power of X arising from all the polynomials B, and the results are then multiplied by a denormalising factor D, to give the appropriate coefficient E, which is printed out. For each data point the voltage, measured and calculated velocities, and percentage difference in these velocities is then printed out to provide a check on the accuracy of fit.

Appendix 7 - Computer Program for Calculation of Velocities from Anemometer Readings.

The program was written in BASIC for use on the Honeywell 316 computer, and is as follows:

```
10   FOR J=1,5
20   READ C(J)
30   NEXT J
35   V3=1.0019/.9982
36   V3=.1E-01*V3
38   PRINT "  RPM      VOLTAGE      VELOCITY      CIRC.TIME";
39   PRINT "      REYNOLDS NO."
40   PRINT
45   FOR K=1,18
50   U=0
60   READ D,N,V
63   V2=V
65   V=V*10.04/9.96
70   V=V-5
80   FOR J=1,5
90   U=U+C(J)*V↑(J-1)
100  NEXT J
105  Y=N*D*D/60
110  PRINT N,V2,U,Y/U,Y/V3
120  NEXT K
300  DATA .31034E-01,.340888,.241816,-.500019E-02,.99859E-02
```

Table 1 - Mixing time as a function of impeller speed in the turbulent regime by the indicator method.

Impeller diameter: 44.8 mm

Liquid depth: 200 mm

Impeller Angle: -10°

Run No.	24	20	21	25	28	26	22
N rpm	300	500	700	1000	1500	2000	3000
	210	126.5	89.6	83.6	55.9	44.8	33.7
	209	151.3	108.0	88.4	43.9	44.7	37.1
	223	119.5	102.2	67.4	53.4	37.4	38.2
	228	115.3	105.9	72.7	51.8	38.4	30.6
	203	104.6	112.0	80.7	53.7	52.2	29.4
	191	163.1	97.9	77.7	48.7	35.6	32.5
	190	104.2	93.9	90.7	61.4	42.8	34.7
	168	157.2	112.0	59.0	56.3	42.9	39.2
	196	116.1	-	65.9	39.7	36.2	31.8
	203	111.4	-	59.1	47.3	44.5	32.4
H.M.	200.7	123.8	102.1	72.9	50.4	41.4	33.7

Table 2 - Mixing Time as a Function of Impeller Speed in the Laminar Regime by the Indicator Method

Impeller diameter: 48 mm

Liquid depth: 300 mm

Impeller Angle: -10°

Run No.	61	68	66	60	67	59	65
N rpm	500	600	800	1000	1500	2000	3000
	212.2	161.5	111.5	89.6	47.1	35.0	23.6
	290.1	160.0	121.2	91.8	45.9	39.9	23.8
	229.4	162.6	134.6	86.4	54.5	36.6	22.3
	261.8	162.0	116.9	83.4	57.2	37.5	23.4
	235.7	227.6	134.0	89.9	47.4	31.2	22.4
	252.0	202.5	133.7	79.5	49.4	31.2	22.2
	263.8	180.9	128.6	75.9	49.8	37.2	23.2
	233.0	196.1	135.5	79.1	53.4	31.8	23.7
	259.4	195.4	131.5	92.5	48.1	37.8	24.6
	295.1	180.1	139.3	75.3	52.5	31.7	23.7
H.M.	250.8	180.5	128.1	83.9	50.3	34.7	23.3

Table 3 - Mixing Time as a Function of Impeller Diameter in the Turbulent Regime by the Indicator Method

Impeller Speed: 2000 rpm

Liquid depth: 200 mm

Impeller Angle: -10°

Run No.	48	51	47	52	49	50
D mm	30	36	42	48	60	72
	165.9	115.3	88.5	52.0	30.0	27.4
	176.7	175.3	78.5	64.6	34.5	21.5
	161.6	95.6	86.2	60.7	31.2	18.9
	183.0	132.8	89.0	53.8	30.6	20.0
	187.4	136.7	76.9	49.0	36.1	22.1
	170.5	139.7	84.3	73.8	44.7	25.9
	173.3	127.8	67.6	44.1	31.6	25.8
	170.6	93.3	88.0	45.6	35.3	18.3
	139.6	106.8	87.7	59.6	36.9	26.6
	151.5	108.8	78.9	48.2	41.2	22.1
H.M.	166.8	119.1	82.0	53.8	34.7	22.4

Table 4 - Mixing Time as a Function of Impeller Diameter in the Incipient Laminar Regime by the Indicator Method

Impeller Speed: 800 rpm

Liquid Depth: 300 mm

Impeller Angle: -10

Run No.	70	72	66	71	69
D mm	36	42	48	60	72
	320.1	182.4	111.5	70.8	39.1
	382.1	154.4	121.2	63.9	29.8
	360.6	172.8	134.6	67.3	35.1
	403.4	175.5	116.9	63.5	33.0
	403.8	174.2	134.0	66.9	34.7
	381.4	181.8	133.7	62.3	34.3
	391.9	217.7	128.6	69.6	42.8
	427.7	200.9	135.5	77.4	36.8
	361.7	217.6	131.5	66.3	38.2
	369.3	226.2	139.3	63.0	34.4
H.M.	378.0	187.7	128.1	66.8	35.5

Table 5 - Mixing Time as a Function of Liquid Depth by the Indicator Method

Impeller Diameter: 48 mm

Impeller Speed: 2000 rpm

Impeller Angle: -10°

Run No.	54	55	52	56	58	57
Y mm	100	150	200	300	440	600
	34.2	82.3	52.0	41.5	45.0	57.5
	45.1	137.8	64.6	41.9	44.2	59.7
	32.9	126.5	60.7	41.2	41.3	53.1
	53.0	101.4	53.8	42.8	49.1	60.3
	34.0	111.6	49.0	43.6	43.7	55.4
	34.7	81.0	73.8	45.4	41.0	54.4
	31.6	112.6	44.1	43.9	49.5	47.8
	37.8	138.6	45.6	46.9	45.3	47.8
	47.8	141.3	59.6	41.3	43.0	54.3
	44.6	134.7	48.2	44.2	41.1	50.9
H.M.	38.4	112.3	53.8	43.2	44.1	53.8

Table 6 - Mixing Time as a Function of Impeller Angle by the Indicator Method

Impeller Diameter: 48 mm

Impeller Speed: 2000 rpm

Liquid Depth: 300 mm

Run No.	81	75	77	79	74	80	78	76	82
θ deg	-20	-15	-10	-5	0	5	10	15	20
	76.8	52.1	43.9	28.9	27.8	35.4	52.2	57.5	70.9
	96.5	66.5	38.3	27.7	31.8	41.1	45.5	53.8	53.0
	73.3	72.3	46.3	33.6	33.5	35.7	43.5	50.1	53.1
	74.9	61.9	42.9	27.7	25.8	37.5	35.2	53.2	66.9
	85.9	63.4	37.6	31.0	34.5	41.7	39.1	56.7	64.0
	72.1	63.7	38.3	30.7	29.8	50.2	38.0	50.5	65.3
	102.2	46.4	47.0	30.4	33.6	44.6	49.9	52.8	59.3
	73.2	61.9	36.7	32.2	35.6	43.2	42.4	45.3	57.6
	71.5	68.1	40.5	27.9	27.1	44.5	46.1	55.9	52.1
	76.9	61.0	39.8	28.5	28.8	44.2	42.2	47.3	60.1
H.M.	79.2	60.8	40.8	29.7	30.4	41.3	42.8	52.0	59.6

Table 7 - Mixing Time as a Function of Impeller Speed in the Turbulent Regime by the Conductivity Method

Impeller Diameter: 72 mm

Liquid Depth: 300 mm

Impeller Angle: -10°

Run No.	95	92	91	94	93	90	96	89
N rpm	600	800	1000	1250	1600	2000	2500	3000
	98.1	113.9	81.5	68.8	57.7	45.9	35.6	22.9
	94.9	83.8	83.8	68.0	61.7	39.6	28.5	26.1
	133.7	108.4	94.9	68.0	33.2	51.4	32.4	26.9
	97.3	102.0	94.9	72.8	47.5	34.8	31.6	22.9
	139.2	96.5	71.2	80.7	58.5	47.5	26.9	30.1
	109.9	75.9	82.3	79.1	68.0	42.7	30.8	38.0
	128.9	109.2	87.0	62.5	59.3	54.6	31.6	31.6
	94.1	108.4	83.1	43.5	65.7	40.3	41.9	28.5
	133.7	82.3	91.2	62.5	53.8	45.1	32.4	30.1
	199.3	94.1	111.5	84.6	50.6	45.1	41.9	26.9
	122.9	97.3	88.2	69.0	55.5	44.6	33.3	28.4

Table 8 - Mixing Time as a Function of Probe Diameter for the Conductivity Method

Impeller Diameter: 72 mm

Impeller Speed: 2000 rpm

Liquid Depth: 300 mm

Impeller Angle: -10

Run No.	103	90	101	102	104
d mm	2.5	4.6	7.6	12.7	20.4
	42.7	45.9	34.8	38.8	49.0
	50.6	39.6	40.0	52.2	40.3
	53.8	51.4	53.8	50.6	45.9
	42.7	34.8	31.6	33.2	32.4
	34.8	47.5	37.2	30.8	38.8
	47.5	42.7	38.0	41.9	40.3
	48.3	54.6	40.3	41.1	45.9
	49.8	40.3	48.3	31.6	23.7
	44.3	45.1	47.5	49.8	46.7
	46.7	45.1	49.8	45.9	59.3
	43.5	-	41.1	41.9	41.1
	35.6	-	52.2	38.0	34.0
	45.9	-	39.6	33.2	46.7
	53.8	-	38.8	45.1	53.0
	39.6	-	40.3	35.6	40.3
	41.1	-	40.3	35.6	38.0
	39.6	-	44.3	45.9	37.2
	39.6	-	41.9	39.6	42.7
	40.3	-	36.9	40.3	49.0
	38.8	-	30.1	50.6	35.6
	44.0	44.7	41.4	41.1	42.0

Table 9 - Conductivity as a Function of Time for Full-Scale Trials on 31 m Diameter Tank

Liquid Depth: 3.59 m

Time mins	Cond pS/m	Time mins	Cond pS/m	Time mins	Cond pS/m	Time mins	Cond pS/m
0	148	6	250	12	310	18	310
1	148	7	410	13	330	19	312
2	148	8	390	14	330	20	314
3	148	9	350	15	312	21	318
4	148	10	260	16	326	22	316
5	163	11	275	17	318	23	316

Liquid Depth: 7.24m

0.0	125	4.5	135	9.0	265	13.5	260
0.5	125	5.0	360	9.5	290	14.0	265
1.0	125	5.5	310	10.0	270	14.5	270
1.5	125	6.0	360	10.5	295	15.0	275
2.0	125	6.5	380	11.0	310	15.5	270
2.5	125	7.0	235	11.5	330	16.0	275
3.0	125	7.5	190	12.0	305	16.5	280
3.5	125	8.0	200	12.5	270	17.0	280
4.0	125	8.5	200	13.0	260	17.5	280

Table 10 - Simulation of Full-Scale Trials

Impeller Diameter: 44.8 mm

Impeller Speed: 3000 rpm

Run No.	71	70
Y mm	140	280
	27.6	24.0
	14.6	25.6
	18.1	18.9
	24.8	25.6
	23.6	26.8
	27.6	25.2
	24.4	29.6
	18.9	22.5
	15.8	26.8
	20.1	26.0
H.M.	24.8	20.6

Table 11 - Mixing Time as a Function of Impeller Speed for the 70 mm Tank.

N rpm	700	800	1000	1200	1400	1700	2000	2500	3000
	1.82	2.02	1.30	1.16	0.85	0.97	0.63	0.67	0.51
	1.99	1.95	1.74	1.11	0.90	1.12	0.81	0.68	0.62
	1.89	1.65	1.49	1.34	0.99	0.89	0.68	0.64	0.52
	1.67	2.05	1.35	1.34	1.27	0.92	0.65	0.58	0.59
	1.65	1.85	1.75	1.23	1.07	1.04	0.80	0.67	0.57
	1.67	2.07	1.48	1.10	1.09	0.92	0.80	0.65	0.50
	2.34	1.63	2.00	1.01	1.20	1.10	0.69	0.58	0.57
	2.07	1.96	1.48	1.36	1.35	0.93	0.79	0.58	0.53
	2.24	1.82	1.64	1.38	1.23	0.88	0.72	0.78	0.62
	2.26	2.08	1.60	1.21	0.78	1.27	0.64	0.63	0.56
H.M.	1.93	1.89	1.56	1.21	1.04	0.99	0.71	0.64	0.56

Table 12 - Mixing Time as a Function of Viscosity for 70 mm Tank

Impeller Speed: 3000 rpm

ν cS	1.01	1.19	1.41	1.67	1.95	2.32	2.83	3.31	4.00
	0.51	0.46	0.60	0.62	0.68	0.61	0.63	0.51	0.54
	0.62	0.58	0.47	0.55	0.59	0.62	0.50	0.63	0.68
	0.52	0.50	0.59	0.58	0.49	0.56	0.66	0.63	0.72
	0.59	0.51	0.58	0.73	0.65	0.62	0.58	0.52	0.50
	0.57	0.64	0.73	0.61	0.44	0.68	0.60	0.63	0.49
	0.50	0.53	0.58	0.59	0.57	0.73	0.53	0.63	0.60
	0.57	0.57	0.61	0.61	0.49	0.54	0.78	0.52	0.69
	0.53	0.74	0.59	0.49	0.62	0.77	0.60	0.75	0.48
	0.62	0.65	0.51	0.56	0.66	0.57	0.71	0.66	0.68
	0.56	0.50	0.56	0.60	0.64	0.55	0.71	0.51	0.57
H.M.	0.56	0.56	0.58	0.59	0.57	0.62	0.62	0.59	0.58

Table 13 - Mixing Time as a Function of Impeller Speed for 70 mm Tank with Buffered Ammonium Acetate System.

N rpm	700	800	1000	1200	1400	1700	2000	2500	3000
	1.56	1.44	1.24	0.98	0.89	0.62	0.61	0.58	0.46
	1.59	1.23	1.18	0.94	0.80	0.68	0.65	0.47	0.51
	1.45	1.49	1.14	0.99	0.85	0.97	0.66	0.50	0.48
	1.48	1.47	1.11	0.90	0.83	0.69	0.57	0.43	0.48
	1.67	1.26	1.34	0.89	0.86	0.84	0.69	0.55	0.52
	1.64	1.30	1.13	1.20	0.94	0.92	0.66	0.54	0.52
	1.40	1.30	1.18	0.97	0.83	0.70	0.56	0.46	0.45
	1.67	1.23	1.32	1.12	1.01	0.78	0.72	0.53	0.53
	1.68	1.39	1.18	0.95	0.80	0.76	0.61	0.62	0.46
	1.48	1.46	1.24	1.10	0.94	0.75	0.61	0.64	0.54
H.M.	1.56	1.35	1.20	1.00	0.87	0.76	0.64	0.52	0.49

Table 14 - Mixing Time as a Function of Impeller Speed for 70 mm Tank with Benzylamine Phenylbutyrate System.

N rpm	700	800	1000	1200	1400	1700	2000	2500	3000
	1.74	1.41	1.40	0.90	1.20	0.71	0.51	0.58	0.48
	1.78	1.60	1.16	1.15	1.13	0.81	0.70	0.56	0.52
	1.54	1.29	1.13	1.10	0.83	0.78	0.56	0.57	0.48
	1.68	1.69	1.28	0.88	0.92	0.90	0.63	0.68	0.57
	1.64	1.86	1.13	0.94	1.06	0.69	0.78	0.61	0.53
	1.59	1.48	1.13	0.89	0.85	0.75	0.69	0.51	0.50
	1.90	1.29	1.36	0.89	0.98	0.92	0.64	0.55	0.49
	1.67	1.51	1.14	0.89	0.92	0.65	0.69	0.49	0.58
	1.84	1.50	1.38	1.07	1.09	0.76	0.62	0.58	0.44
	1.60	1.37	1.21	1.17	0.80	0.84	0.60	0.52	0.48
H.M.	1.69	1.48	1.22	0.98	0.96	0.77	0.63	0.56	0.50

Table 15 - Mixing Time as a Function of Impeller Speed for 70 mm Tank with Various Criteria for Terminal Mixing

X = 0.10

N rpm	700	800	1000	1200	1400	1700	2000	2500	3000
	0.69	0.37	0.50	0.31	0.32	0.18	0.24	0.13	0.13
	0.74	0.52	0.53	0.46	0.41	0.16	0.25	0.10	0.18
	0.62	0.39	0.48	0.37	0.38	0.17	0.24	0.16	0.12
	0.59	0.43	0.45	0.31	0.33	0.22	0.18	0.13	0.16
	0.85	0.47	0.48	0.38	0.33	0.18	0.25	0.12	0.15
	0.80	0.41	0.37	0.38	0.34	0.18	0.22	0.12	0.18
	0.79	0.50	0.57	0.44	0.24	0.17	0.28	0.14	0.16
	0.62	0.48	0.48	0.31	0.30	0.19	0.20	0.16	0.20
	0.61	0.56	0.48	0.32	0.27	0.15	0.28	0.13	0.14
	0.69	0.40	0.45	0.37	0.34	0.17	0.18	0.18	0.19
H.M.	0.69	0.45	0.47	0.36	0.32	0.18	0.23	0.13	0.16
N	8.04	5.94	7.89	7.16	7.44	4.97	7.55	5.56	7.85

X = 0.30

N rpm	700	800	1000	1200	1400	1700	2000	2500	3000
	1.10	0.90	0.85	0.56	0.55	0.48	0.37	0.27	0.22
	1.30	0.95	0.87	0.79	0.68	0.48	0.46	0.25	0.31
	1.02	0.79	0.81	0.68	0.66	0.37	0.50	0.27	0.26
	1.16	0.94	0.75	0.64	0.61	0.47	0.30	0.31	0.27
	1.46	0.92	0.77	0.58	0.52	0.47	0.44	0.27	0.35
	1.33	1.09	0.70	0.70	0.65	0.37	0.34	0.29	0.25
	1.27	0.89	0.86	0.73	0.53	0.51	0.47	0.28	0.29
	1.14	0.94	0.81	0.55	0.60	0.40	0.37	0.28	0.37
	1.05	1.02	0.78	0.60	0.55	0.42	0.49	0.42	0.24
	1.15	0.83	0.72	0.64	0.63	0.64	0.35	0.36	0.36
H.M.	1.18	0.92	0.79	0.64	0.59	0.45	0.40	0.29	0.28
NT	13.8	12.3	13.1	12.8	13.8	12.7	13.3	12.2	14.2

X = 0.40

N rpm	700	800	1000	1200	1400	1700	2000	2500	3000
	1.14	1.20	0.95	0.65	0.59	0.58	0.46	0.38	0.27
	1.39	1.12	0.93	0.86	0.74	0.59	0.55	0.38	0.34
	1.12	0.95	0.90	0.88	0.74	0.47	0.57	0.34	0.29
	1.31	1.16	0.83	0.79	0.69	0.58	0.42	0.34	0.30
	1.56	1.10	0.80	0.72	0.57	0.63	0.49	0.37	0.44
	1.39	1.29	0.82	0.77	0.72	0.47	0.40	0.36	0.29
	1.43	0.97	0.97	0.77	0.68	0.68	0.57	0.33	0.33
	1.30	1.06	1.08	0.73	0.72	0.51	0.48	0.34	0.45
	1.15	1.16	0.86	0.83	0.70	0.49	0.58	0.48	0.29
	1.24	1.14	0.79	0.73	0.67	0.77	0.43	0.40	0.48
H.M.	1.30	1.11	0.89	0.77	0.68	0.56	0.49	0.37	0.33
NT	15.0	14.8	14.8	15.3	15.8	16.0	16.2	15.3	16.7

X = 0.50

N rpm	700	800	1000	1200	1400	1700	2000	2500	3000
	1.22	1.33	1.25	0.72	0.65	0.67	0.53	0.44	0.34
	1.49	1.26	1.00	0.89	0.80	0.70	0.60	0.45	0.39
	1.22	1.05	0.96	0.97	0.79	0.57	0.65	0.42	0.31
	1.40	1.33	0.87	0.89	0.71	0.64	0.48	0.39	0.35
	1.66	1.26	0.87	0.90	0.62	0.72	0.52	0.46	0.52
	1.52	1.45	0.95	0.88	0.79	0.61	0.43	0.46	0.33
	1.46	1.07	1.04	0.84	0.76	0.77	0.60	0.41	0.37
	1.41	1.26	1.21	0.89	0.81	0.60	0.55	0.37	0.49
	1.25	1.23	0.96	0.98	0.78	0.55	0.61	0.57	0.34
	1.35	1.41	0.86	0.82	0.72	0.85	0.52	0.44	0.51
H.M.	1.39	1.25	0.98	0.87	0.73	0.65	0.54	0.44	0.38
NT	16.2	16.7	16.4	17.4	17.0	18.4	18.1	18.2	19.1

X = 0.70

N rpm	700	800	1000	1200	1400	1700	2000	2500	3000
	1.37	1.64	1.51	0.90	0.74	0.81	0.65	0.57	0.41
	1.74	1.53	1.11	0.96	0.92	0.91	0.78	0.56	0.44
	1.40	1.27	1.07	1.17	0.94	0.70	0.75	0.51	0.38
	1.59	1.65	0.96	1.06	0.79	0.77	0.63	0.50	0.42
	1.86	1.47	1.05	1.07	0.68	0.84	0.59	0.55	0.58
	1.67	1.69	1.21	0.93	0.92	0.75	0.52	0.55	0.40
	1.60	1.30	1.14	0.89	0.92	0.89	0.77	0.50	0.47
	1.63	1.57	1.48	1.12	0.98	0.75	0.65	0.46	0.57
	1.40	1.55	1.12	1.13	0.97	0.66	0.72	0.67	0.40
	1.51	1.69	0.97	0.99	0.78	1.06	0.65	0.52	0.50
H.M.	1.55	1.52	1.14	1.01	0.85	0.80	0.66	0.53	0.45
NT	18.1	20.3	19.0	20.3	19.9	22.7	22.0	22.3	22.4

X = 0.90

N rpm	700	800	1000	1200	1400	1700	2000	2500	3000
	1.61	2.02	1.82	1.16	0.88	0.97	0.84	0.67	0.52
	2.13	1.95	1.28	1.11	1.09	1.12	0.90	0.68	0.53
	1.74	1.65	1.28	1.34	1.16	0.89	0.95	0.64	0.48
	1.89	2.05	1.16	1.34	0.91	0.92	0.80	0.58	0.51
	2.09	1.85	1.37	1.23	0.80	1.04	0.70	0.67	0.72
	1.83	2.07	1.42	1.10	1.12	0.92	0.65	0.65	0.56
	1.76	1.63	1.38	1.01	1.11	1.10	0.93	0.58	0.54
	1.87	1.96	1.82	1.36	1.29	0.93	0.78	0.58	0.70
	1.67	1.82	1.46	1.38	1.14	0.88	0.89	0.78	0.52
	1.80	2.08	1.20	1.21	0.94	1.27	0.81	0.63	0.72
H.M.	1.83	1.89	1.39	1.21	1.02	0.99	0.81	0.64	0.57
NT	21.3	25.3	23.2	24.2	23.9	28.1	27.1	26.7	28.4

X = 0.98

N rpm	700	800	1000	1200	1400	1700	2000	2500	3000
	1.84	2.10	2.33	1.34	1.09	1.21	1.13	0.79	0.75
	2.54	1.54	2.28	1.37	1.22	1.36	1.15	0.87	0.70
	2.08	1.57	1.92	1.55	1.36	1.05	1.20	0.79	0.57
	2.15	1.45	2.35	1.58	1.24	1.17	0.94	0.79	0.64
	2.34	1.57	2.16	1.53	1.00	1.28	0.80	0.80	0.84
	2.16	1.64	2.38	1.24	1.36	1.21	0.84	0.80	0.70
	2.12	1.60	1.90	1.15	1.35	1.33	1.13	0.78	0.75
	2.15	2.00	2.38	1.57	1.46	1.07	1.05	0.60	0.87
	1.97	1.66	2.15	1.65	1.42	1.08	1.08	0.91	0.72
	2.05	1.36	2.48	1.45	1.14	1.44	0.98	0.78	0.81
H.M.	2.13	1.62	2.22	1.43	1.25	1.21	1.01	0.78	0.72
NT	24.8	27.1	29.6	28.5	29.1	34.2	33.8	32.6	36.2

Table 16 - Variation in Dependence of Dimensionless Mixing Time on Impeller Speed with Various Criteria for Terminal Mixing.

Values of m calculated from $N\Upsilon = kN^m$

X	m	$N\Upsilon$	$mN\Upsilon$
0.30	0.01	13.1	0.01
0.40	0.07	15.5	1.09
0.50	0.11	17.5	1.93
0.70	0.14	20.6	2.88
0.90	0.16	25.1	4.02
0.98	0.22	30.3	6.67

Table 17 - Hot Film Anemometer Calibration Results

O/P V	Mass gm	Time secs	O/P V	Mass gm	Time secs
5.54	5.56	123.4	8.75	63.89	63.2
5.74	8.04	122.8	9.00	74.08	62.6
5.99	12.12	123.2	9.24	84.88	62.7
6.24	8.32	62.7	9.49	98.56	62.6
6.50	10.93	62.4	9.74	114.86	62.8
6.75	14.31	63.2	10.00	131.64	62.3
7.01	17.92	63.0	10.24	152.00	62.5
7.25	21.89	63.0	10.49	172.51	62.6
7.49	26.75	62.9	10.75	198.05	62.7
7.74	32.53	63.1	11.00	223.65	62.7
7.99	38.55	62.9	11.24	256.03	62.8
8.25	46.56	62.9	11.49	216.54	46.6
8.49	54.55	62.6	11.76	230.83	42.9

Table 18 - Boundary Layer Velocities

Liquid Depth: 300 mm
Impeller Diameter: 72 mm
Impeller Speed: 2000 rpm

D = 48 mm

x mm	O/P V	u mm s^{-1}
5.00	8.73	66.3
3.50	8.68	64.2
3.00	8.63	62.2
2.50	8.52	58.0
2.25	8.46	55.7
2.00	8.38	52.8
1.75	8.28	49.4
1.50	8.21	47.2
1.25	8.03	41.7
1.00	7.85	36.7
0.75	7.50	28.3
0.50	7.11	20.7

D = 30 mm

x mm	O/P V	u mm s^{-1}
5.25	6.73	14.8
4.25	6.66	13.9
3.25	6.50	11.8
2.75	6.47	11.5
2.25	6.26	9.1
1.75	6.11	7.6
1.25	5.93	6.0
0.75	5.67	4.0

Table 19 - Circulation Velocity as a Function of Impeller Reynolds Number

D mm	N rpm	O/P V	u mm s^{-1}
30	1500	6.22	8.7
30	2000	6.71	14.5
30	3000	7.37	25.6
60	500	6.65	13.7
60	600	6.88	17.0
60	800	7.43	26.9
60	1000	7.77	34.7
60	1200	8.12	44.4
60	1600	8.67	63.8
60	2000	9.12	84.3
60	2400	9.47	103.7
60	3000	9.94	135.4
72	1500	9.07	81.7
72	2000	9.96	136.9
72	2400	10.27	162.1
72	3000	10.69	202.2

Notation

A	Constant
B	Constant
C	Function of X
D	Impeller Diameter
$\mathcal{D}$	Molecular Diffusivity
F	Faraday's Constant
K_A	Acid Dissociation Constant
K_B	Base Dissociation Constant
N	Impeller Speed
Q	Impeller Pumping Capacity
R	Gas Constant
T	Tank Diameter
T_o	Temperature
U	Fluid Velocity
V	Volume of Tank
X	Colorimeter Reading
$\overline{X}$	Degree of Homogeneity
$\overline{X}_o$	Initial Value of X
Y	Liquid Depth

α	Constant
β	Constant
δ	Boundary Layer Thickness
δ_{ij}	Substitution Tensor
η	Dynamic Viscosity
λ°	Equivalent Conductivity at Infinite Dilution
ν	Kinematic Viscosity
ρ	Density
$\Delta\rho$	Density Difference
σ_{ij}	Rate-of-strain Tensor
ε	Rate of Dissipation of Energy
ε_{ijk}	Cyclic Tensor
τ	Terminal Mixing Time
τ_c	Terminal Mixing Time measured by Conductivity Method
τ_T	Time for Turbulent Dispersal
$\bar{\tau}'$	Harmonic Mean Mixing Time

Fr	Froude No. = N^2D/g
Ho	Simultaneity No. = $N\tau$
Pe	Péclet No. = ND^2/D
Re	Impeller Reynolds No. = ND^2/ν
Re_B	Boundary Layer Reynolds No. = $\delta u/\nu$

$\underline{a},\underline{b},\underline{c},\underline{d}$	Vectors Defined in Appendix 1
a_i, b_i etc	Components of $\underline{a},\underline{b}$ etc.
c	Tracer Concentration
c_a	Concentration of Material a
c_b	Concentration of Material b
c_F	Final value of c
c_I	Initial Value of c
c_T	Tracer Concentration before Addition
d	Probe Diameter
g	Acceleration Due to Gravity
k	Function of Time
k_1	Constant
k_2	Constant
l	Half-width of Probe Tip
$\underline{\delta l}$	Vector Joining Points A & B
l_c	Scale of Concentration Fluctuations
m	Slope of Curve
n	Constant
q	Ratio of Fluid Velocity to Blade Tip Velocity
r	Radius
r_H	Hub Radius
r_I	Impeller Radius
r_T	Tube Radius

s	Impeller Pitch at Radius r
t	Time
t'	Transformed Value of t
δt	Difference of Times
u	Fluid Velocity
u_c	Velocity on Centre-line of Tube
u_x	Velocity in x-direction
v	Voltage
v_T	Volume of Tracer
w	Width of Turbine Blade
x	Distance Normal to Surface of Constant Concentration
x'	Transformed value of x
x_o	Initial Value of x
y	Defined in Appendix 1
y_o	Initial Value of y
z	Charge on Ion

References

1. Rushton, J.H.; Pet. Ref. 33 (1954) 101.
2. Van der Vusse, J.G.; Chem. Ing. Tech. 31 (1959) 583.
3. Voncken, R.M.; Brit. Chem. Eng. 10 (1965) 12,179.
4. Wood, J.C., Whittemore, E.R. & Badger, W.L.; Chem. Met. Eng. 27 (1922) 1176.
5. Fossett, H. & Prosser, L.E.; Proc. Inst. Mech. Eng. 160 (1949) 224.
6. Kramers, H., Baars, G.M. & Knoll, W.H.; Chem. Eng. Sci. 2 (1953) 35.
7. Gluz, M.D. & Pavlushenko, I.S.; Zh. Prikl. Khim. 39 (1966) 2719.
8. Oldshue, J.Y., Hirschland, H.E. & Gretton, A.T.; Chem. Eng. Prog. 52 (1956) 481.
9. Macdonald, R.W. & Piret, E.L.; Chem. Eng. Prog. 47 (1951) 363.
10. Gray, J.B.; Chem. Eng. Prog. 59 (1963) 55.
11. Stead, B., Page, F.M. & Denbigh, K.G.; Faraday Soc. (Disc.) 2 (1947) 263.
12. Fox, E.A. & Gex, V.E.; A.I.Ch.E.J. 2 (1956) 539.
13. Landau, J. & Prochazka, J.; Coll. Czech. Chem. Comm. 26 (1961) 1976.

14. Tomicek, O.; Chemical Indicators (1946).

15. Rice, A.W., Toor, H.L. & Manning, F.S.; A.I.Ch.E.J. 10(1)(1964) 125.

16. Nagata, S., Yokoyama, T. & Yamagimoto, M.; Chem. Eng. Japan. 21 (1957) 278.

17. Sykes, P. & Gomezplata, A.; A.I.Ch.E.J. 11(1) (1965) 174.

18. Norwood, K.W. & Metzner, A.B.; A.I.Ch.E.J. 6 (1960) 432.

19. Dodd, L.E.J.; J. Phys. Chem. 31 (1927) 1761.

20. Van der Vusse, J.G.; Chem. Eng. Sci. 4 (1955) 178,209.

21. Landau, J. & Prochazka, J.; Coll. Czech. Chem. Comm. 26 (1961) 2961.

22. Marr, G.R. & Johnson, E.F.; Chem. Eng. Prog. Symp. Ser. 57 (1961) 109.

23. Landau, J., Prochazka, J., Vacklavek, V. & Fort, I.; Coll. Czech. Chem. Comm. 28 (1963) 279.

24. Hoogendoorn, C.J. & den Hartog, A.P.; Chem. Eng. Sci. 22 (1967) 1689.

25. Moo-Young, M., Tichar, K. & Dullien, F.A.L.; A.I.Ch.E.J. 18 (1972) 178.

26. Corrsin, S.; A.I.Ch.E.J. 3 (1957) 329.

27. Cutter, L.A.; A.I.Ch.E.J. 12 (1966) 35.

28. Evangelista, J.J., Katz, S. & Shinnar, R.; A.I.Ch.E.J. 15 (1969) 843.

29. Batchelor, G.K.; Proc. Roy. Soc. Lond. 213A (1952) 349.

30. Reid, W.H.; Proc. Camb. Phil. Soc. 51 (1955) 350.

31. Rosenhouse, H.; Diss. Abs. 25 (1964) 3458.

32. Corrsin, S.; Quart. Appl. Math. 12 (1955) 404.

33. Sachs, J.P. & Rushton, J.H.; Chem. Eng. Prog. 50 (1954) 597.

34. Schwartzberg, H.G. & Treybal, R.E.; Ind. Eng. Chem. Fundam. 7(1) (1968) 1.

35. Aiba, S.; A.I.Ch.E.J. 4 (1958) 485.

36. Rao, M.A. & Brodkey; Chem. Eng. Sci. 27 (1972) 137.

37. Kim, W.J. & Manning, F.S.; A.I.Ch.E.J. 10(5) (1964) 747.

38. Fort, I. et al.; Coll. Czech. Chem. Comm. 34 (1969) 959.

39. Blasinski, H. & Tyczkowski, A.; Int. Chem. Eng. 8 (1968) 43.

40. Mujumdar, A.S.; Can. J. Chem. Eng. 48 (1970) 475.

41. Bowers, R.H.; Proc. A.I.Ch.E. - I.Chem.E. Joint Meeting; London (1965).

42. Rushton, J.H., Mack, D.E. & Everett, H.J.; Trans. Am. Inst. Chem. Engrs. 42 (1946) 441.

43. Fort, I.; Coll. Czech. Chem. Comm. 32 (1967) 3663.

44. Porcelli, J.V. & Marr, G.R.; Ind. Eng. Chem. Fundam. 1:3 (1962) 172.

45. Folsom, R.G. & Ferguson, C.K.; Trans.A.S.M.E. 71 (1949) 73.

46. Nagata, S., Yamamoto, K., Hashimoto, K. & Naruse, Y.; Mem. Fac. Eng. Kyoto 22 (1960) 68.

47. Holmes, D.B., Voncken, R.M. & Dekker, J.A.; Chem. Eng. Sci. 19 (1964) 201.

48. Manning, F.S. & Wilhelm, R.H.; A.I.Ch.E.J. 9(1) (1963) 12.

49. Batchelor, G.K.; Camb. Phil. Soc. Proc. 43 (1947) 533.

50. Batchelor, G.K.; J. Fluid Mech. 5 (1959) 113.

51. Toor, H.L.; A.I.Ch.E.J. 8 (1962) 70.

52. Biggs, R.D.; A.I.Ch.E.J. 9 (1963) 636.

53. Duncan, W.J., Thom, A.S. & Young, A.D.; Mechanics of Fluids. E.Arnold (1970).

54. Lamb, D.E., Manning, F.S. & Wilhelm, R.H.; A.I.Ch.E.J. 6 (1960) 682.

55. Bird, R.B., Steward, W.E. & Lightfoot, E.N.; Transport Phenomena. Wiley (1960).

56. Robinson, R.A. & Stokes, R.H.; Electrolyte Solutions. Butterworths (1959).

57. Steel, B.J., Stokes, J.M. & Stokes, R.H.; J. Phys. Chem. 62 (1958) 1514.

58. Handbook of Chemistry and Physics, 53rd Edition; C.R.C. Press (1972).

59. King, L.V.; Phil.Trans. Roy. Soc. 214A (1914).

60. Bulmer, M.G.; Principles of Statistics. Oliver & Boyd (1965).

61. Hayes, J.G.; Numerical Approximation to Functions and Data. Athlone Press (1970).